Comprehensive postseismic deformation model of the 2004 Sumatra-Andaman earthquake constrained by GPS data in northern Sumatra

「2004 年スマトラ―アンダマン地震の包括的余効変動モデル～スマトラ北部の GPS データを用いて～」

Endra Gunawan

A dissertation for the degree of Doctor of Science

Department of Earth and Environmental Sciences,

Graduate School of Environmental Studies,

Nagoya University

2014

Acknowledgements

In the name of God, the Most Gracious, the Most Merciful.

I bear witness that there is no God except Allah SWT, and I bear witness that Muhammad SAW is the Messenger of Allah.

I would like to express my profound gratitude and deep regards to many people who helped me to make this work possible. First and foremost is my advisor Takeshi Sagiya, for his support and encouragement to share his vast knowledge of Earth science. I am learning a lot from him in analyzing time series data carefully, sharply and intelligently. I am truly grateful that during all these years I was able to have benefits during my splendid scientific discussion with him. I am very grateful to Fumiaki Kimata and Takeo Ito, for graciously welcome me and my family, and for their support during our stay into Nagoya University. They were the first geoscientist I met who showed me the beauty of this knowledge. I owe special thanks to Irwan Meilano, Takao Tabei, and Yusaku Ohta, for setting up Aceh GPS Network for Sumatran fault System (AGNeSS) in northern Sumatra, which I indeed relied heavily in this work.

I thank Fred Pollitz for the helpful advice on the use of VISCO1D, and make this code freely available in the scientific community. I would also like to thank V.K. Gahalaut and C. Satirapod who kindly provided the GPS data in the Andaman-Nicobar and Thailand, and Wessel and Smith for Generic Mapping Tools (GMT) software to make maps and figures in this work.

I thanks to my parents, who encourage me to keep finding knowledge, support me with their care and influences. Finally, I thank to my wife, Rahma, for sharing this life together with me, and also to my children; Zahra, Akira, and ‘Little One. Indeed we do have a lot of smiles, joy and happiness in our beloved home. The world is round and big, shall we have another adventure ?

Abstract

On December 26, 2004, the M9.2 Sumatra-Andaman earthquake occurred in the Sunda subduction zone along the north Sumatra, Nicobar and Andaman Islands. This earthquake provides us with a unique opportunity to examine the postseismic deformation using GPS data. The 2004 earthquake is an important event because of various reasons. First, this earthquake is the first M9 class earthquake recorded by modern global seismic and GPS networks (Kanamori, 2006). Using these modern equipment, we can evaluate the deformation associated to this earthquake comprehensively. Second, the 2004 earthquake caused large enough postseismic deformation (e.g. Gahalaut et al., 2008; Satirapod et al., 2008; Paul et al., 2012) and a long enough time has passed after the earthquake, which provide us a great opportunity to distinguish the physical mechanisms of postseismic deformation. Third, there have already been many studies on postseismic deformation with essentially different conclusions. It is important to unravel how different assumptions and different datasets in each study led to different conclusions and to find the most probable interpretation for the observed data. This difference indicates that mechanisms of postseismic deformation are poorly understood.

Continuous GPS data in northern Sumatra clearly show temporal decays reflecting postseismic deformation. It is noticeable that horizontal displacements significantly decreased with time, while the vertical component looks almost linear in time. The difference in the temporal changes between horizontal and vertical components implies that multiple physical

mechanisms are responsible for the postseismic deformation; we assume that they are viscoelastic relaxation and afterslip. We construct two analysis strategies to investigate the postseismic deformation after the 2004 earthquake. These strategies are (1) Strategy 1 to correlate the shorter relaxation time with viscoelastic relaxation, and the longer relaxation time with afterslip, and (2) Strategy 2 to correlate the longer relaxation time with viscoelastic relaxation, and the shorter relaxation time with afterslip.

Strategy 1, which was used by previous studies, has fatal problems regarding the vertical displacement data. First, using continuous GPS data in northern Sumatra, the calculated vertical displacements of the viscoelastic relaxation and the afterslip are expected to have similar contribution (in an opposite sense), but only viscoelastic relaxation is effective in the horizontal components. Second, in the vertical component, the viscoelastic relaxation and the afterslip have similar time constant as well as similar amplitude just to cancel out each other. These problems simply indicate that the original assumption of using horizontal displacements to construct a viscoelastic relaxation model was wrong.

In order to apply Strategy 2 to the dataset, a new iterative method to estimate both the viscoelatic structure and afterslip distribution is developed. Starting from the estimation of rheological parameters based on vertical GPS data in northern Sumatra, afterslip and the rheological parameters are estimated one after another until the minimum χ^2 is obtained. By applying this method, we can decompose the postseismic deformation into the contribution of viscoelastic relaxation and that of afterslip. We assume a simple rheological model with an elastic lithosphere overlying a Maxwell viscoelastic substratum, in which the lithosphere thickness and the Maxwell viscosity are the rheological parameters. This strategy is applied to

the GPS data in northern Sumatra with four different coseismic fault models by Kreemer et al. (2006), Banerjee et al. (2007), Fujii and Satake (2007), and Rhie et al.(2007). We find that the coseismic fault model of Rhie et al. (2007) results in the least χ^2 of 104.22 and that the Maxwell viscoelastic relaxation plus afterslip model successfully explains GPS data in northern Sumatra. The estimated best rheological parameters are the lithospheric thickness of 65±5 km and η_M of 8.0±1.0 x 10^{18} Pa s, which are consistent with various previous studies. For time period between 2005.91~2006.90, the estimated maximum afterslip was 0.90 m located at 20~40 km depth and the total seismic moment released by afterslip was 1.12 x 10^{21} N m (M_w 8.2). During 2005.91~2006.90, the estimated afterslip accounts for only 15% of the observed vertical displacement at ACEH in northern Sumatra, and the contribution is only 1% during 2006.90~2007.90. This result clearly explains why the shorter relaxation time is not evident in the observed vertical displacement at continuous GPS sites in northern Sumatra.

In this study, significance of a time-dependent (Burgers) rheology, suggested by previous studies (Pollitz et al., 2006; Panet et al., 2010), is not supported. The current study suggests that the rapid transient signal at the early postseismic stage was caused mainly by afterslip, not by the viscoelastic relaxation. The vertical component in northern Sumatra is a strong evidence for this result.

This study also demonstrates that the rheology model estimated from GPS data in northern Sumatra is applicable to postseismic deformation of the 2004 Sumatra-Andaman earthquake recorded in other regions such as the Andaman Islands and Thailand. The rheology model can reproduce the long-term trends of GPS data in Thailand while the rapid transient signals in the early postseismic stage can be attributed to the afterslip in Andaman and Nicobar

region. Also, it is shown that the postseismic deformation in the Andaman region contains significant contribution of viscoelastic relaxation. Seismic moment release by the afterslip from January 2005 to February 2006 estimated in this study is 1.1 x 10^{21}N m (M_w 7.9), which is 29 % of the previous estimate by Gahalaut et al. (2008). So it should be noted that the interpretation of postseismic deformation is highly sensitive to assumptions.

This study is based on a simplified layered structure model. So the result may be changed if we take 3-dimensional structure including subducted slab into account. Also, the satellite gravity data analyzed in previous studies are not analyzed in the current study. These problems will be solved in the future.

Through this study, a model of the rheological structure and afterslip distribution is constructed for the postseismic deformation of the 2004 Sumatra-Andaman earthquake. This is a comprehensive model in that it can reproduce main features of all the available GPS data in northern Sumatra, Andaman, and Thailand. This study provides unique as well as important insights into the rheological structure of the asthenosphere and postseismic relaxation processes of great earthquakes.

.

Table of Contents

List of Tables

List of Figures

Glossary of Abbreviations

ABIC	Akaike Bayesian information criterion
AGNeSS	Aceh GPS Network for Sumatran fault System
BIG	Geospatial Information Agency of Indonesia
BPN	National Agency for Land Administration
EOS	Earth Observatory of Singapore
FES2004	Finite Element Solutions 2004
GPS	Global Positioning System
GRACE	Gravity recovery and Climate Experiment
ITRF	International Terrestrial Reference Frame
InSAR	Interferometric Synthetic Aperture Radar
LIPI	Indonesian Institute of Sciences
RINEX	Receiver Independent Exchange Format
SLR	Satellite Laser Ranging
SOPAC	Scripps Orbit and Permanent Array Center
SuGAr	Sumatran GPS Array
USGS	United States Geological Survey
VLBI	Very Long Baseline Interferometry

Chapter 1

Introduction

1.1 Backgrounds

Large earthquakes cause significant surface deformation that is detected by precise geodetic measurements such as Global Positioning System (GPS) (e.g. Lisowski et al., 1990; Tsuji et al., 1995; Johnson et al., 2001; Banerjee et al., 2007; Ozawa et al., 2011). Significant crustal deformation is also observed after large earthquakes, which is referred as postseismic deformation (e.g. Wang et al., 2012). Several physical mechanisms, such as afterslip, viscoelastic relaxation in the Earth's mantle and lower crust, and poroelastic rebound, have been proposed by these studies to explain the postseismic deformation (e.g. Thatcher and Rundle, 1984; Peltzer et al., 1996; Heki and Tamura, 1997; Pollitz, 2003; Jónsson et a l., 2003; Perfettini and Avouac, 2007).

However, it is still difficult to resolve contributions from different physical mechanisms in the observed postseismic deformation data (e.g. Freed et al., 2006, Freed, 2007). Moreover, there are different classes of models for viscoelastic relaxation. Conventional viscoelastic models are based on the Maxwell fluid in which stress and strain rate have linear relationship (e.g. Nur and Mavko, 1974; Pollitz, 1997). On the other hand, time-dependent rheology models

have been introduced to reproduce rapid postseismic transient motion (Pollitz et al., 2001; Freed and Burgmann, 2004). In those studies, either the power-law creep or the Burgers rheology model is employed to reproduce nonlinear viscous behavior in the postseismic data.

In most of these studies, physical mechanism of postseismic deformation was assumed at first and observation data were used to estimate model parameters and the model choices were rather arbitrary. Rather, we should use observation data to resolve contributions from different physical mechanisms. However, it is not always easy to distinguish contributions from different mechanisms because postseismic deformation signal is usually small and not fully detectable even with the modern geodetic techniques. In particular, vertical displacement is always noisier than horizontal ones. Generally speaking, larger earthquakes are accompanied by larger postseismic signals. Thus occurrence of a giant earthquake over magnitude 8 is a precious opportunity to challenge the difficult problem of postseismic deformation.

On December 26, 2004, the M9.2 Sumatra-Andaman earthquake occurred in the Sunda subduction zone along the north Sumatra, Nicobar and Andaman Islands. Figure 1.1 shows the tectonics background in this particular region. The 2004 Sumatra-Andaman earthquake provides us with a unique opportunity to solve the difficulties in examining the postseismic deformation using GPS data. The 2004 earthquake is an important event because of various reasons. First, this earthquake is the first M9 class earthquake recorded by modern global seismic and GPS networks (Kanamori, 2006). Using these modern equipments, we can evaluate the deformation associated to this earthquake comprehensively. Second, the 2004 earthquake caused large enough postseismic deformation (e.g. Gahalaut et al., 2008; Satirapod et al., 2008; Paul et al., 2012) and a long enough time has passed after the earthquake, which provide us a great opportunity to distinguish the physical mechanisms of postseismic deformation. Third, there have already been many studies on postseismic deformation with essentially different

conclusions. It is important to unravel how different assumptions in each study led to different conclusions and to find the most probable interpretation for the observed data. This difference indicates that mechanisms of postseismic deformation are poorly understood.

This thesis deals with GPS data after the 2004 Sumatra-Andaman earthquake. Previous studies of postseismic deformation after the 2004 earthquake used only certain part of observations, and there have been no studies focusing on GPS data in northern Sumatra. Considering limitation of previous studies, we analyze postseismic deformation of the 2004 earthquake using all the available GPS datasets in northern Sumatra, Andaman-Nicobar, and Thailand. Hence, we expect to give a clear interpretation and better understanding of postseismic deformation data after the 2004 earthquake.

1.2 Objectives

The primary objective of this thesis is to resolve and determine the physical mechanisms of postseismic deformation after the 2004 Sumatra-Andaman earthquake by taking GPS data in northern Sumatra, Andaman-Nicobar, and Thailand, into account. The GPS data in Andaman-Nicobar and Thailand were obtained from previous studies (Gahalaut et al., 2008 and Satirapod et al., 2008), while GPS data in northern Sumatra observed and maintained by the collaboration of Nagoya University, Kochi University, Tohoku University, Institute of Technology Bandung and Syiah Kuala University.

We conduct this study with the following motivations. First, we intend to improve studies of postseismic deformation of the 2004 earthquake. Many studies on postseismic deformation of the 2004 earthquake have been done. But all these previous studies failed in reproducing some part of the observation data. So the main objective of this study is to construct a

comprehensive postseismic deformation model that can reproduce all the available observation data over northern Sumatra, Andaman-Nicobar, and Thailand.

Second, we expect to improve studies of investigating the best coseismic rupture model of the 2004 earthquake. Many coseismic fault models have been postulated, and these studies were unique in term of data and method they used, also the slip distribution result. In this study, we evaluate the best coseismic fault models which best explain the postseismic deformation. During our postseismic deformation calculation, we develop a new method to construct postseismic deformation model with multiple physical mechanisms. We perform both method of grid search for finding the rheology model and inversion analysis for calculating the postseismic slip along plate interface, simultaneously. Hence, we acknowledge this new methodology to be applied for other case of postseismic deformation after large earthquake.

1.3 Dissertation outline

In this thesis, we begin with Chapter 2 with crustal deformation associated to the 2004 earthquake. In this chapter, we describe previous studies on coseismic fault models of the 2004 earthquake. We also describe theory of postseismic deformation mechanisms attributed as poroelastic rebound, afterslip and viscoelastic relaxation, and we review previous studies on postseismic deformation of the 2004 earthquake comprehensively in this chapter. Finally, we discuss the previous studies' results.

In Chapter 3, we analyze GPS data in Andaman-Nicobar, Thailand, and northern Sumatra. GPS data in Andaman-Nicobar and Thailand obtained from previous studies (Gahalaut et al., 2008; Satirapod et al. 2008). Meanwhile, the GPS data in northern Sumatra obtained from AGNeSS (Aceh GPS Network for Sumatran fault System) and SuGaR (Sumatran GPS Array),

available from continuous and campaign observations. We show the characteristic of the continuous time series data in northern Sumatra reflecting important signal from postseismic deformation. Finally, we explore the importance of AGNeSS in analyzing the physical mechanisms of postseismic deformation after the 2004 earthquake.

In Chapter 4, our analysis of postseismic deformation of the 2004 earthquake is performed. In this chapter, we also compare four coseismic fault models used in our investigation. We discuss our strategy to model the postseismic deformation using four coseismic fault models based on GPS data in northern Sumatra, and we discuss our preference of coseismic fault model that best explains the postseismic deformation after the 2004 earthquake. In addition, we discuss afterslip in northern Sumatra comprehensively.

In Chapter 5, we discuss our best-fit rheological structure model and compare to previous studies structure model. We also discuss our postseismic deformation analysis for Andaman Islands using our model. Finally, we discuss our analysis of postseismic deformation using all GPS data sets in northern Sumatra, Andaman-Nicobar, and Thailand. Additionally, we show the limitation of our current postseismic deformation model.

Finally, we present our conclusions in Chapter 6.

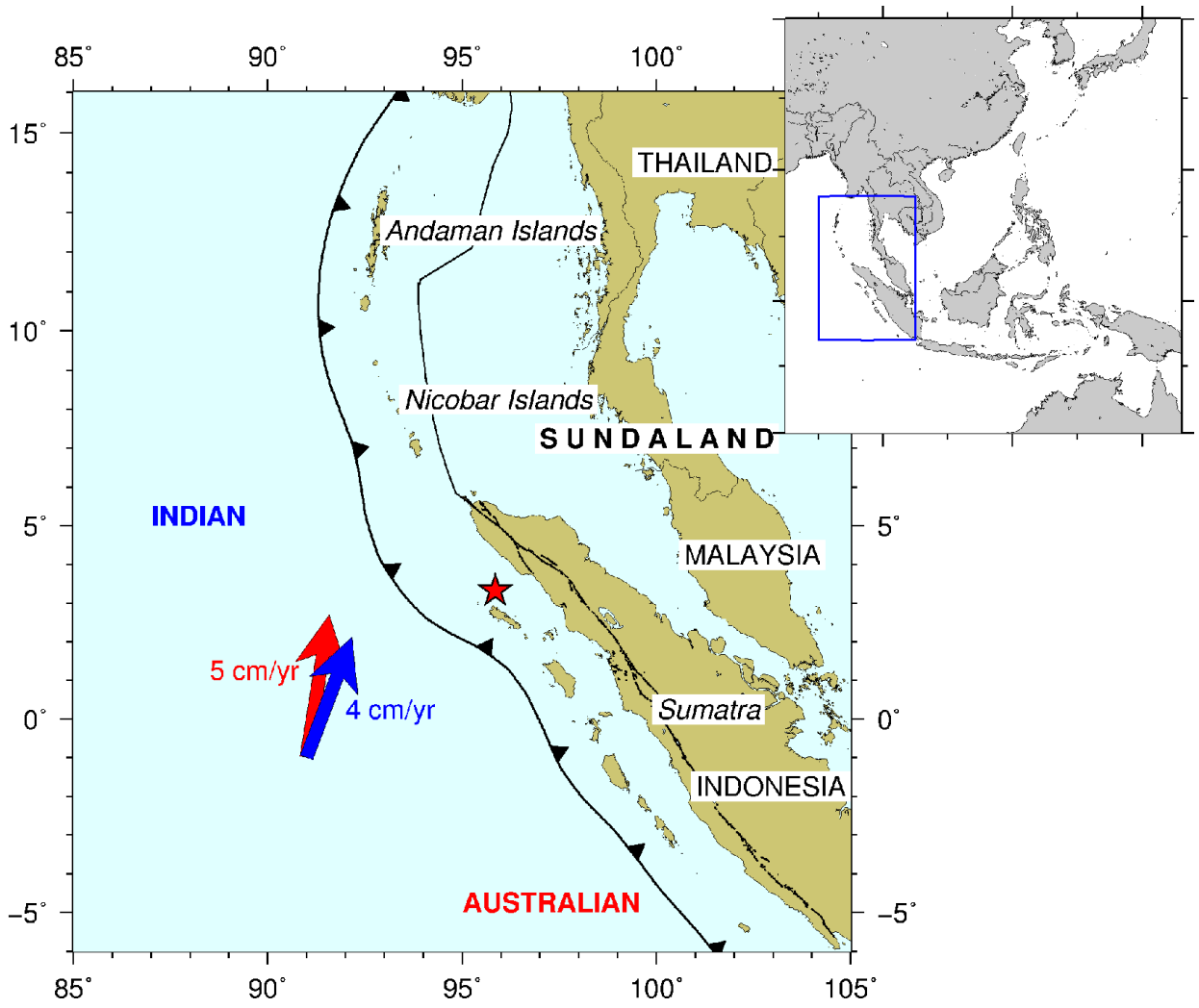

Figure 1.1. Tectonic setting in this study area. Red star indicate epicenter of the 2004 Sumatra-Andaman earthquake (located by the U.S. Geological Survey (USGS). Red arrow denotes motion of the Australian plate subduct beneath Sundaland block, while the blue arrow implies motion of the Indian plate, respectively.

Chapter 2

Coseismic and Postseismic Deformation Associated to the 2004 Sumatra-Andaman Earthquake

2.1 Coseismic fault models of the 2004 Sumatra-Andaman earthquake

Currently, various coseismic fault models of the 2004 Sumatra-Andaman earthquake have been proposed. These models were estimated based on seismological, geodetic, and/or tsunami data.

Ammon et al. (2005) presented three different coseismic fault models in order to identify the robust feature of the rupture and analyze the sensitivity of fault parameters, moment distribution and seismic data weighting choices in their models. Their model I was estimated using teleseismic surface wave polarized in the horizontal plane (SH waves) with periods shorter than 120 s. Model II was estimated using long-period seismogram in the period range from 100 to 3000 s and teleseismic surface wave with period range from 80 to 300 s. Model III was estimated using teleseismic body waves (20 to 20 s), intermediate-period three-component regional seismograms (50 to 500 s), and long-period teleseismic seismograms (250 to 2000 s). The model I has a 10 m slip near hypocenter, ~20 m slip at southeast and west of Great and Little Nicobar Islands, and 5 to 10 m of slip located near 4°N. The model II has the maximum slip of 7.5 m located between 3°N to 6°N, and slip decreased towards north into Andaman

Islands. The model III has the maximum slip of 11.4 m located between 3°N to 6°N, and slip extended northward into Andaman Islands. Ammon et al. (2005) highlighted that these models explained seismological data satisfactorily, but the coseismic slip result of these models were too small to explain GPS data in Andaman-Nicobar. Among these models, model III was the most frequently cited one by subsequent studies because it has a larger more slip in the northern part of the rupture (Figure 2.1).

Banerjee et al. (2005) used continuous GPS stations at distances of up to 4500 km from the epicenter, and campaign GPS sites located in Andaman-Nicobar to estimate a coseismic fault model. Their best-fit model suggested that coseismic slip of 6 m occurred below the Andaman Islands. Further work was done by Banerjee et al. (2007) by expanding the GPS datasets in the Andaman Islands and northern Sumatra than the previously used by Banerjee et al. (2005). Banerjee et al. (2007) compiled coseismic displacements at 150 GPS sites, consisting of 108 continuous GPS sites (Banerjee et al., 2005; Hashimoto et al., 2006; Subarya et al., 2006; Vigny et al., 2005), 12 campaign GPS sites in Andaman-Nicobar (Banerjee et. al., 2005; Jade et al., 2005; Gahalaut et al., 2006), 7 campaign GPS sites in Thailand (Vigny et al., 2005), and 23 campaign GPS sites in northern Sumatra (Subarya et al., 2006). They analyzed near- and far- field GPS data by considering vertical rigidity layering and Earth sphericity, into account. Their result of a coarser slips model includes a deep dip slip of ~20 m in the Nicobar segment from 5°N to 8°N, and 3 to 8 m of slip along Andaman Islands north of ~9°N (Figure 2.1).

Kreemer et al. (2006) used the far-field GPS sites to estimate the rupture process of the 2004 earthquake. They found a much smaller slip on the northern rupture segment than Banerjee et al. (2005), which they argued much more consistent with in the model of seismic studies (Figure 2.1). Their result suggested that GPS data detected a coherent surface motion at more than 5000 km from the epicenter.

Fujii and Satake (2007) used satellite altimetry (Jason1, TOPEX/Poseidon, and Envisat)

and tide gauge measurements to estimate a fault slip model. Their preferred model corresponds to a 900 km long fault and an average rupture velocity of 1 km/s, even though a 1400 km long fault model fits the satellite data better (Figure 2.1). They showed that slips near the Andaman Islands would overpredict amplitudes at Indian tide gauge stations. Similarly, Piatanesi and Lorito (2007) inverted tsunami observations for the fault slip model. Their best-fit model has large slip segments at the both ends of the rupture, at 8°N, and at 12°N, with an average rupture velocity of 2 km/s (Figure 2.1). This model overpredicts tide gauge amplitudes at Indian tide gauge station, as was discussed by Fuji and Satake (2007).

Rhie et al. (2007) performed joint inversions of long-period seismogram and GPS data. They found that the largest slip patch located at the west of the northern Sumatra (Figure 2.1). They preferred a steeper dip angle from the aftershock data, and they found that the average rupture velocity was between 1.8~2.6 km/s.

From the coseismic fault models mentioned above, each models obtained different slip distribution. Ones identified largest slip located around the Nicobar Islands (Kreemer et al., 2006; Banerjee et al., 2007), or at the west of the northern Sumatra (Fujii and Satake, 2007; Piatanesi and Lorito, 2007; Rhie et al., 2007), other from northern Sumatra to Nicobar Islands (Ammon et al., 2005). This slip difference attributed to the data source and method use in the calculation used by these studies.

2.2 Mechanisms of postseismic deformation

After large earthquakes with magnitude over 7, we usually detect deformation signals after the earthquake occurrence and the deformation continues for days to years with a time-dependent displacement rate. This phenomena is called postseismic deformation. With an improved measurement accuracy of space geodetic techniques, the number of postseismic deformation has been rapidly increasing during the last two decades (e.g. Wang 2007). In

general, postseismic deformation is attributed to following physical mechanisms; (1) poroelastic rebound, in which the coseismic pressure changes drive fluid flow in the upper crust causing crustal deformation (e.g. Jónsson et al., 2003); (2) afterslip on fault interface as a result of stress transfer from the mainshock rupture (e.g. Miyazaki et al., 2004; Ozawa et al., 2011); and (3) viscoelastic relaxation of the asthenosphere driven by the coseismic stress change (e.g. Wang et al., 2001; Hu et al., 2004; wang, 2007; Bürgmann and Dresen, 2008). Various studies also suggested that multiple mechanisms are responsible for postseismic deformation in many cases (e.g. Pollitz et al., 1998; Sheu and Shieh, 2004; Ryder et al., 2007; Suito and Freymueller, 2009; Wang et al., 2009). Here we briefly describe these mechanisms.

2.2.1 Poroelastic rebound

Ito and Nakashima (2002) showed that liquid-like water is always present in polycrystalline quartz grain based on infrared microspectroscopy,. When an earthquake occurs, it imposes stress changes within a certain distance from its epicenter and the Earth's crust behaves as a fluid-saturated poroelastic medium, not as purely elastic medium (e.g. Roeloffs, 1988; Piombo et al., 2005). Due to the presence of fluids in the crust, pore pressure change is induced by a sudden change of the stress field due to a large earthquake. After an earthquake, in response to elastic stress change, pore fluid diffuses to equilibrate pore pressure in the crust. As fluid flows from regions of high pressure to regions of low pressure, this poroelastic rebound results in subsidence within coseismically compressed region, and uplift in extensional region. Peltzer et al. (1998) used InSAR observations to analyze time-dependent strain of the crust subsequent to the 1992 Landers earthquake due to poroelastic rebound. Jónsson et al. (2003) modeled the postseismic deformation following two M6 earthquakes in June 2000 in south Iceland and concluded that poroelastic rebound dominated the postseismic deformation in the first few months after the earthquakes. All these studies they evaluate the transient deformation due to fluid pressure changes in the presence of fluid diffusion and can be observed for period

ranging up to times in the order of 1 year.

In poroelasticity, the body force per unit volume and fluid mass per unit time can be defined as (Wang and Kümpel, 2003):

$$(\lambda + 2\mu)\nabla(\nabla.\boldsymbol{u}) - \mu\,\nabla \times (\nabla \times \boldsymbol{u}) - \alpha\nabla p = \boldsymbol{f}(\boldsymbol{x}, t) \tag{2.1}$$

$$Q^{-1}\frac{\partial p}{\partial t} + \alpha\frac{\partial}{\partial t}\nabla.\boldsymbol{u} - \chi\,\nabla^2 p = q(x, t) \tag{2.2}$$

where $\boldsymbol{u}$ is the displacement vector, p is the pore pressure, λ and μ are Lamé coefficients, α is the dimensionless coefficient of effective stress, Q^{-1} is the bulk compressibility, χ is Darcy conductivity, $\boldsymbol{f}$ is the body force per unit volume acting on the solid matrix and q is the fluid volume injection rate, where $\boldsymbol{f}$ and q are the functions of spatial position $\boldsymbol{x}$ and time t. In this relation:

$$\lambda = \frac{2v\mu}{1-2v} \tag{2.3}$$

$$\alpha = \frac{3(v_u - v)}{(1-2v)(1+v_u)B} \tag{2.4}$$

$$Q^{-1} = \frac{9(1-2v_u)(v_u - v)}{2(1-2v)(1+v_u)^2\mu B^2} \tag{2.5}$$

$$\chi = \frac{9(1-v_u)(v_u - v)D}{2(1-2v)(1+v_u)^2\mu B^2} \tag{2.6}$$

where B is skempton's coefficient, that is the change in pore pressure per unit change in confining pressure under undrained conditions, v and v_u are Poisson's ratio governing drained (long-time) and undrained (short-time) response, and D is hydraulic diffusivity, respectively.

2.2.2 Afterslip

Afterslip is a fault slip that follows large earthquakes. Afterslip usually occurs on the fault

interface surrounding the main shock with a decreasing slip rate in time (e.g. Helmstetter and Shaw, 2009). Marone et al. (1991) proposed an afterslip based on the rate and state dependent friction law. The rate and state dependent friction law was proposed by Dieterich (1979) based on friction experiments of rocks. This friction law is described as:

$$\mu = \mu^* + A\, ln\frac{V}{V^*} + B\, ln\frac{\theta V^*}{D_C} \tag{2.7}$$

where μ and μ* are friction coefficient and reference frictional coefficient, V and V* are slip rate and reference velocity, A and B are friction parameters, D_c is the critical slip distance, and θ is the state variable.

The time dependence of state variable obeys (e.g. Liu and Rice, 2005):

$$\frac{d\theta}{dt} = 1 - \frac{V\theta}{D_c} \tag{2.8}$$

During a steady state regime, the $\theta = 0$, and the equation (2.7) becomes (e.g. Rice and Gu, 1983):

$$\mu_{SS} = \mu^* + (A - B)\, ln\frac{V}{V^*} \tag{2.9}$$

If $A - B < 0$, friction at steady state decreases with slip rate and the friction is called velocity-weakening regime. In the case of $A - B > 0$, μ_{SS} increases with V and the friction is called velocity- strengthening regime. Thus the $A - B$ is the main parameter that controls mechanical behavior of the fault .

Earthquakes are considered to occur in a velocity-weakening region. Then the surrounding velocity-strengthening region is stressed by the earthquake (e.g. Scholz, 1998).

Afterslip is interpreted as the result of stress relaxation within the velocity-strengthening region (e.g. Freed, 2005; Marone et al., 1991).

To model the afterslip time history, previous studies used a closed-form temporal decay function techniques, such as an exponential function (e.g. Savage and Prescott, 1987; Kreemer et al., 2006):

$$U_S = A\left(1 - e^{-t/T_A}\right) \qquad \text{(Exponential)} \qquad (2.9)$$

or a logarithmic function (e.g. Marone, 1991; Ohta et al., 2012):

$$U_S = A\, ln\left(1 + \frac{t}{T_A}\right) + V_o t \qquad \text{(Logarithmic)} \qquad (2.10)$$

where A is the amplitude of the decay signal, T_A is the characteristic time, V_o is the constant loading rate, and t is elapsed time after the main shock. The modified Omori law (e.g. Langbein et al., 2006; Helmstetter and Shaw, 2009) is also frequently used to fit afterslip rate:

$$U_S = \frac{AT_A}{1-p}\left[\left(1 + t/T_A\right)^{1-p} - 1\right] \qquad \text{(Ohmori)} \qquad (2.11)$$

where the index p is associated exponent associated with the slip rate decay.

2.2.3 Viscoelastic relaxation

Another important physical mechanism of postseismic deformation is viscoelastic relaxation. It is well known that there exists a viscous layer called asthenosphere below elastic lithosphere. According to the traditional definition of the lithosphere, it is 100-200 km thick, containing the whole crust and the uppermost part of the mantle (e.g. Kirby & Kronenberg,

1987). However, recent studies of postseismic deformation suggested the viscoelastic relaxation also occurs in the lower crust too (e.g. Pollitz et al., 2001). So the elastic lithosphere and the viscoelastic asthenosphere may not be well defined and the definition itself may depend on the time of spatial scale of interest. In this thesis, we assume a simple two-layered structure due to the sparsity of the available observation data. It should be noted that the conclusion can change in a smaller time- and spatial scale

Deformation at high temperature and pressure involves both elastic and viscous behavior. The stress-strain relation of a linear elastic material is defined as:

$$\sigma = \mu\varepsilon \tag{2.12}$$

where μ represents by a shear modulus. Meanwhile, the stress-strain relation of a viscous material is:

$$\sigma = \eta\dot{\varepsilon} \tag{2.13}$$

where η is viscosity and dots denote differentiation with respect to time.

Combination of two simple elements, a spring k and a dashpot at a η, in series is named Maxwell fluid (Figure 2.2). If ε_1 and ε_2 are the strains of the spring and the dashpot:

$$\varepsilon_1 = {}^{\sigma}/_{\mu} \quad ; \quad \dot{\varepsilon}_2 = {}^{\sigma}/_{\eta} \tag{2.14}$$

so the total strain satisfies:

$$\dot{\varepsilon} = {}^{\dot{\sigma}}/_{\mu} + {}^{\sigma}/_{\eta} \tag{2.15}$$

When a strain ε_0 is suddenly imposed on to this system at $t=0$, then stress rises suddenly to $k\varepsilon_0$, and gradually decreases to zero as describe by the following equation:

$$\sigma = \mu\varepsilon_0 e^{-t/\tau} \quad \text{, where} \quad \tau = \eta/\mu \tag{2.16}$$

where τ is the relaxation time.

A parallel combination of spring μ and dashpot η is called Kelvin solid. (Figure 2.2). In this case, the stress across the spring and dashpot is denoted as:

$$\sigma = \eta\dot{\varepsilon} + \mu\varepsilon \tag{2.17}$$

If constant stress S is suddenly applied at $t=0$, then equation (2.17) become:

$$S = \eta\dot{\varepsilon} + \mu\varepsilon \tag{2.18}$$

This equation is solved with $\varepsilon=0$ when $t=0$, then we obtain:

$$\varepsilon = (S/\mu)\left[1 - e^{-t/\tau}\right] \quad \text{, where} \quad \tau = \eta/\mu \tag{2.19}$$

The equation (2.19) describe a transient creep behavior and instantaneous elastic strain ε_e does not appear. Since an earthquake causes instantaneous elastic strain, Kelvin solid is not a valid representation of the Earth.

Material consisting of a Kelvin solid element and a Maxwell element in series is called Burgers body (Figure 2.2). The total strain ε of a Burgers body can be denoted as :

$$\varepsilon = \varepsilon_K + \varepsilon_M \tag{2.20}$$

where ε_K and ε_M are strain of the Kelvin and Maxwell elements, respectively. By eliminating ε_K and ε_M from equation (2.15), (2.17) and (2.20) then we obtain:

$$\eta_K \ddot{\varepsilon} + \mu_K \dot{\varepsilon} = \left(\frac{\eta_K}{\mu_M}\right) \ddot{\sigma} + \left[1 + \frac{\mu_K}{\mu_M} + \frac{\eta_K}{\eta_M}\right] \dot{\sigma} + \left(\frac{\mu_K}{\eta_M}\right) \sigma \tag{2.21}$$

If constant stress *S* is applied to a Burgers body at *t=0*, the strain follows a temporal change as follows:

$$\varepsilon = \frac{S}{\mu_M} + \frac{S}{\mu_K}\left[1 - e^{-t/\tau_K}\right] + \frac{S}{\eta_M} t \tag{2.22}$$

The deformation following an earthquake as a function of time can be explained using a linear rheology, such as Maxwell rheology (e.g. Wahr and Wyss, 1980) and Burgers rheology (e.g. Pollitz, 2003), or a non-linear power-law rheology (Freed and Bürgmann, 2004). Results of different studies suggested that different rheology models could produce similar displacement fields on a postseismic deformation case (e.g.Freed. 2007; Bruhat et al., 2011). Hence choosing the right postseismic model might be strongly related to the temporal and spatial behavior of the used data source.

2.3 Previous studies of postseismic deformation

The coseismic stress of the 2004 earthquake was large and extensive, causing significant postseismic deformation detected by GPS data in various location, such as in Andaman Islands (Gahalaut et al., 2008; Paul et al., 2012), Nicobar Islands (Gahalaut et al., 2008), or even

Thailand (Pollitz et al., 2006; Satirapod et al., 2008; Panet et al., 2010). These GPS data displacements are characterized by a trench-ward motion on the continental side of the plate boundary. There have been many studies to explain the postseismic deformation of the 2004 earthquake. These studies are different one another in both in the physical mechanism assumed and observation data analyzed. Here we review these studies comprehensively.

2.3.1 Pollitz et al. (2006) and Pollitz et al. (2008)

Pollitz et al. (2006) investigate the postseismic deformation of the 2004 earthquake assuming viscoelastic relaxation of both the upper and the lower mantle. In their calculation, they consider a spherically symmetric, laterally homogeneous viscoelastic structure that neglects the influence of the downgoing Indo-Australian slab, compressible and self-gravitational earth model for the relaxation process. They use 10 GPS data located in Thailand, North Sumatra, and Singapore (Figure 2.3). With these GPS sites, they used the horizontal components (Easting and Northing) inferred from the earliest time period GPS data (0.25 year after the 2004 earthquake) to analyze the postseismic deformation of the 2004 earthquake.

In their calculation, they consider two viscosity structures; (1) Maxwell rheology with η_1 = 5 x 10^{17} Pa s, η_{UM} = 1 x 10^{20} Pa s, η_{LM} = 1 x 10^{21} Pa s, and (2) Burgers body rheology with η_1 = 1 x 10^{19} Pa s, η_2 = 5 x 10^{17} Pa s, η_{UM} = 1 x 10^{20} Pa s, η_{LM} = 1 x 10^{21} Pa s, where η_1 is the asthenospheric steady state Maxwell viscosity, η_2 is the asthenospheric transient Kelvin viscosity, η_{UM} is the upper mantle Maxwell viscosity, and η_{LM} is the lower mantle Maxwell viscosity (Figure 2.4). The asthenosphere is assumed to exist from the depth of 62 to 220 km, the upper mantle is 220 to 670 km, and the lower mantle covers the depth range from 670 to 2891 km. They concluded that the Burgers rheology model yields better misfits to the GPS data than the Maxwell rheology model (Figure 2.5).

Another study of Pollitz et al. (2008) investigated the effect of 3-D viscoelastic structure of the 2004 earthquake. They used the compiled GPS data for 11 months from various

continuous GPS networks and campaign sites (Figure 2.3). Following their previous result (Pollitz et al., 2006), they used the Burgers rheology viscoelastic structure and a 30 km thick slab structure. They found that the horizontal and vertical displacement in the far field on the continental side reduced about ~20% because of the slab effect. To fit the data, they considered a 40% reduction of asthenosphere viscosity at the continental side of the mantle wedge and a reduction of the elastic plate thickness to 50 km were necessary. With this earth structure, they found a good agreement with the far field GPS data (CPN, BNKK, CHMI and PHKT) and fair agreement with the near field horizontal motions around the southern half of the 2004 rupture (UMLH, CAMP and KARD). However, in the near field around Andaman Islands north of 8° N, displacement model poorly fit the data. Also, the vertical component of UMLH in northern Sumatra was underpredicted with this model (Figure 2.6).

2.3.2 Paul et al. (2007) and Paul et al. (2012)

Paul et al. (2007) investigated physical mechanism of postsesimic deformation in the Andaman Islands for the first two years testing poroelastic relaxation, viscoelastic relaxation and afterslip as candidate mechanisms (Figure 2.3). Their viscoelastic structure model consists of a 70 km thick elastic layer and the upper mantle with the Maxwell viscosity of 5×10^{17} Pa s, overlaying the lower mantle with the Maxwell viscosity of 1×10^{21} Pa s.

They showed that this viscoelastic structure model do not reproduce GPS data. Poroelastic relaxation does not match the data either. They concluded that deep afterslip is the main mechanism of postseismic deformation of the 2004 earthquake in the Andaman Islands (Figure 2.7).

Paul et al. (2012) used 6 years of GPS data in the Andaman Islands to revisit the postseismic deformation in this region. They argued that in the Andaman Islands, postseismic measurements are not sensitive to fine-scale details of coseismic slip distribution. They compared the coseismic fault model of Banerjee et al. (2007) and their own coseismic model in

the previous study (Paul et al., 2007). Based on the comparison of these two models, they interpreted the difference as a representative of the uncertainties in near-field viscoelastic deformation.

They found the best-fit viscoelastic structure model consists of a 90 km thick surface elastic layer overlying the upper mantle with a viscosity of 3 x 10^{17} ~ 1 x 10^{18} Pa s. Using this model, they calculated the residual displacements and interpreted them as a result of an afterslip (Figure 2.8).

2.3.3 Gahalaut. (2008)

Using a total of one continuous and 22 campaign-mode GPS sites in Andaman-Nicobar (Figure 2.3) for a total period of 2.2 years after the 2004 earthquake, Gahalaut et al. (2008) investigated the postseismic deformation in this region. They assumed that a frictional afterslip is responsible for postseismic deformation during this time period.

Based on their analysis of afterslip using horizontal and vertical components of GPS data, they suggested that afterslip occurred at the down-dip part of the plate boundary in the Andaman region, while in Little Andaman and Nicobar, afterslip and coseismic rupture partly overlapped (Figure 2.9).

2.3.4 Panet et al. (2010)

Panet et al. (2010) investigated the postseismic deformation of the 2004 earthquake using 3.5 years of GPS data in Thailand (Figure 2.3) and gravity variations from GRACE (Gravity recovery and Climate Experiment) satellite. Following Pollitz et al. (2006), they used a 60 km thick lithosphere overlying a 160 km thick asthenosphere with a biviscous Burgers rheology. Using GRACE, they found that afterslip has to be introduced and/or they need to modify the viscoelastic relaxation model of Pollitz et al. (2006).

Their viscoelastic structure model result consists of η_1 = 8 x 10^{18} Pa s, η_2 = 4 x 10^{17} Pa s,

η_{UM} = 8 x 10^{18} Pa s, η_{LM} = 8 x 10^{20} Pa s, where η_1 is the asthenospheric steady state Maxwell viscosity, η_2 is the asthenospheric transient Kelvin viscosity, η_{UM} is the upper mantle Maxwell viscosity, and η_{LM} is the lower mantle Maxwell viscosity (Figure 2.4(b)). With an addition of afterslip of 30 cm/yr, they showed their model fits the GPS data located in Thailand very well (Figure 2.10).

2.3.5 Hoechner et al. (2011)

Using the same GPS data as Paul et al. (2007) with an addition of GRACE data, Hoechner et al. (2011) investigated viscoelastic relaxation and afterslip of the 2004 Sumatra-Andaman earthquake. Following previous result of Pollitz et al. (2006), they used the Burgers rheology. By fitting GPS data to the displacement model, they found that the surface elastic layer is 40 km thick, and that Burgers rheology in the asthenosphere with the transient Kelvin viscosity of 1 x 10^{18} Pa s and the steady state Maxwell viscosity of 1 x 10^{19} Pa s reproduces the observation data very well. Then they investigated viscoelastic relaxation using Maxwell rheology, and found the best-fit rheology model of surface elastic layer with 40 km thick and steady state Maxwell viscosity of 2 x 10^{18} Pa s. They showed that the combined mechanisms of afterslip and viscoelastic relaxation using Maxwell rheology fit the data too.

To obtain the best model between these two results, they used an additional independent observation GRACE. They concluded that viscoelastic relaxation with Burgers rheology produce postseismic geoid change better than the combined afterslip and viscoelastic relaxation using Maxwell rheology (Figure 2.11).

2.3.6 Hu and Wang (2012)

Using a spherical finite element earth model with incorporating realistic slab and fault geometry, Hu and Wang (2012) analyzed a short-term postseismic deformation model using ~1 year GPS displacements in the Andaman Islands and northern Sumatra, and ~3 year GPS time

series in Thailand. These GPS data sets are the same as those used by Pollitz et al. (2008) (Figure 2.3). They constrained the short-term postseismic deformation model using horizontal GPS data and used the vertical components for qualitative validation due to large uncertainties.

In their study, they investigate the combined mechanisms of viscoelastic relaxation and afterslip. They used a 30 km slab thickness and a 40 km elastic thickness. They employed a smaller elastic thickness than previous studies (e.g. Panet et al. 2010) because the postseismic deformation occurred in the arc and back-arc where heat flow is higher than continental average. In their calculation, they tested Maxwell rheology and Burgers rheology. In their preferred model, the observed deformation is best explained with a model that includes both the afterslip and Burgers rheology, with transient and steady state viscosities of the continental mantle of 5 x 10^{17} Pa s and 1 x 10^{19} Pa s with transient and steady state viscosities of the oceanic mantle of 5 x 10^{17} Pa s and 1 x 10^{20} Pa s, respectively (Figure 2.12).

2.4 Discussion on previous studies' results

We summarize the previous result on postseismic deformation of the 2004 earthquake in Table 2.1. As we see, previous studies reached different conclusions. Discrepancies are mainly attributed to different assumptions on postseismic deformation mechanisms. Some studies assumed only afterslip (Paul et al., 2007; Gahalaut et al., 2008), or viscoelastic (Pollitz et al., 2006; Pollitz et al., 2008; Hoechner et al., 2011), is the main mechanism responsible for the postseismic deformation process, while others argued that combined model of viscoelastic relaxation and afterslip (Panet et al., 2010; Paul et al., 2012; Hu and Wang, 2012) is the main mechanism.

Another problem is that previous studies used only a certain part of observations, such as GPS data in Andaman Islands (Paul et al., 2007; Hoechner et al., 2011; Paul et al., 2012), Andaman-Nicobar (Gahalaut et al., 2008), Thailand (Pollitz et al., 2006; Panet et al., 2010).

Some studies used independent GRACE data to overcome this limitation (Hoechner et al., 2011; Panet et al., 2010). Instead of using three components (easting, northing and height) of GPS data, most of previous studies used only horizontal GPS data (easting and northing) to constrain their postseismic model (Pollitz et al., 2006; Pollitz et al., 2008; Hu and Wang, 2012).

Horizontal GPS data in Andaman-Nicobar and Thailand showed transient deformation that some of the previous studies inferred as a result of afterslip (e.g. Gahalaut et al., 2008), or viscoelastic relaxation with the Burgers rheology (e.g. Pollitz et al., 2006), or a steady state Maxwell rheology (Paul et a., 2012). Clearly, the interpretation of this transient deformation is not clear and thus can be argued.

Finally, in their attempt of investigating the postseismic deformation of the 2004 earthquake, except Pollitz et al. (2008) and Hu and Wang (2012), previous studies did not analyze the postseismic deformation in northern Sumatra. Although Pollitz et al. (2008) used the data in northern Sumatra, their model could not fit the data at UMLH site (Figure 2.6). Based on the previous studies of the 2004 coseismic rupture, the largest coseismic slip was located in west off northern Sumatra (e.g. Rhie et al., 2007) (Figure 2.1). The largest and probably the most important signal of postseismic deformation was recorded in this region. We should be able to explain the deformation observed in this region, together with all available GPS datasets. In this study, we tackle and answer all those problems mention above comprehensively.

Table 2.1. Previous studies on postseismic deformation of the 2004 Sumatra-Andaman earthquake

Source	Time Period	Preferred Postseismic Mechanisms	Afterslip Moment	Viscoelastic Parameter		
				Rheology Model	Assumed	Best-Fit
Pollitz et al. (2006)	Early 3 months after the earthquake	Viscoelastic relaxation	-	Burgers body	$d_{elastic}$ = 62 km d_{UM} = 220 km d_{LM} = 670 km η_{UM} = 1 x 10^{20} Pa s η_{LM} = 1 x 10^{21} Pa s	η_1 = 1 x 10^{19} Pa s η_2 = 5 x 10^{17} Pa s
Paul et al. (2007)	Two years after the earthquake	Afterslip	~M_w 7.5	-	-	-
Pollitz et al. (2008)	January 2005 ~ November 2005	Viscoelastic relaxation	-	Burgers body	d_{UM} = 220 km d_{LM} = 670 km η_{UM} = 1 x 10^{20} Pa s η_{LM} = 1 x 10^{21} Pa s	$d_{elastic}$ = 50 km η_1 = 1 x 10^{19} Pa s η_2 = 5 x 10^{17} Pa s η_{MW} = 4 x 10^{19} Pa s
Gahalaut et al. (2008)	January 2005 ~ February 2007	Afterslip	~M_w 8.5	-	-	-
Panet et al. (2010)	January 2005 ~ June 2008	Viscoelastic relaxation + Afterslip	~M_w 8.2	Burgers body	$d_{elastic}$ = 60 km d_{UM} = 220 km	η_1 = 8 x 10^{18} Pa s η_2 = 4 x 10^{17} Pa s η_{UM} = 8 x 10^{18} Pa s η_{LM} = 8 x 10^{20} Pa s
Hoechner et al. (2011)	Two years after the earthquake	Viscoelastic relaxation	-	Burgers body	d_{UM} = 210 km d_{LM} = 660 km η_{UM} = 1 x 10^{20} Pa s η_{LM} = 1 x 10^{21} Pa s	$d_{elastic}$ = 40 km η_1 = 1 x 10^{19} Pa s η_2 = 1 x 10^{18} Pa s
Paul et al. (2012)	Six years after the earthquake	Viscoelastic relaxation + Afterslip	-	Maxwell	d_{LM} = 670 km η_{LM} = 1 x 10^{21} Pa s	$d_{elastic}$ = 90 km η_1 = 3 x 10^{17} ~ 1 x 10^{18} Pa s
Hu and Wang (2012)	January 2005 ~ June 2008	Viscoelastic relaxation + Afterslip	-	Burgers body	$d_{elastic}$ = 40 km	η_1 = 1 x 10^{19} Pa s η_2 = 5 x 10^{17} Pa s

η_1 and η_2 are the Maxwell and Kelvin viscosity

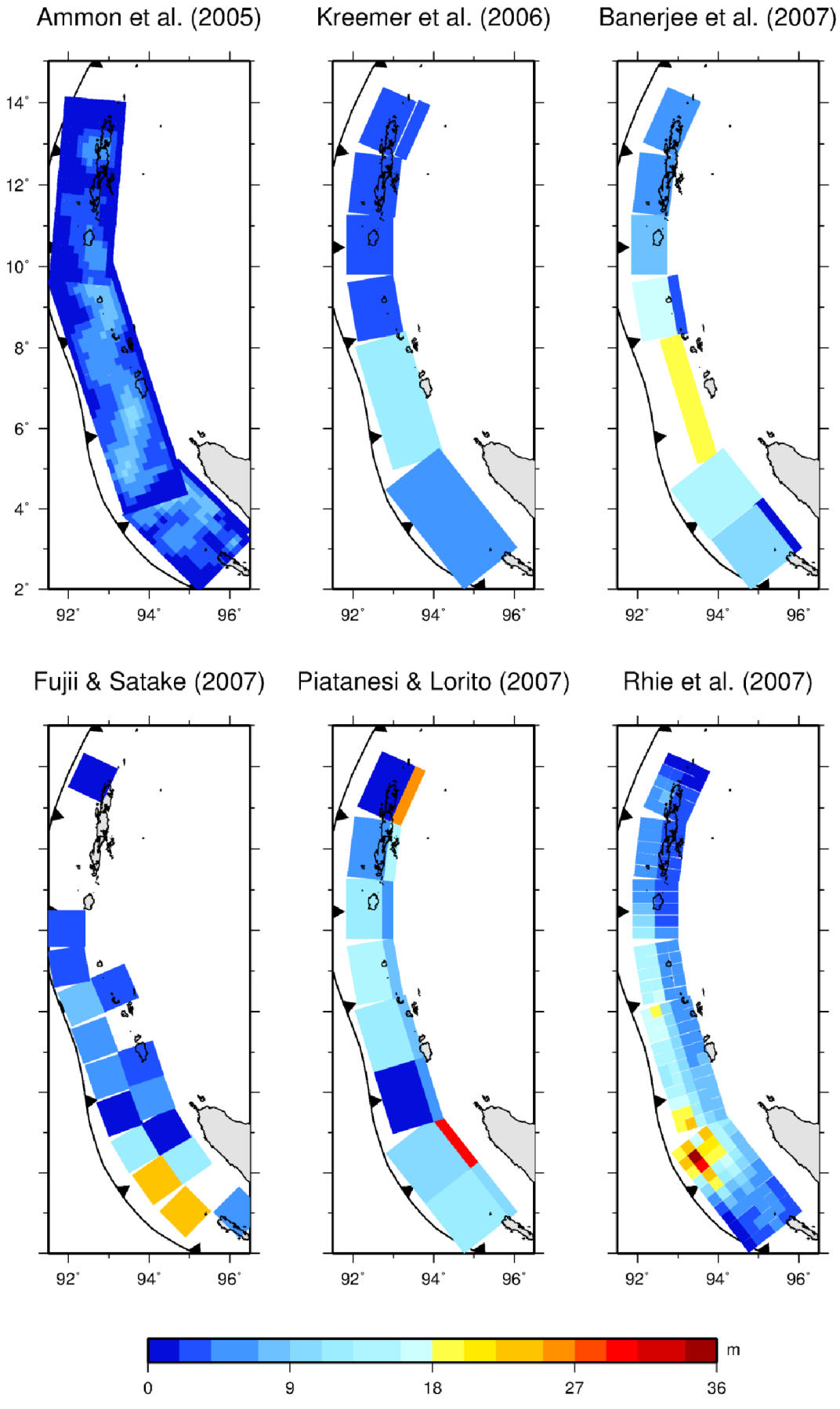
Ammon et al. (2005)
Kreemer et al. (2006)
Banerjee et al. (2007)
Fujii & Satake (2007)
Piatanesi & Lorito (2007)
Rhie et al. (2007)
14°
12°
10°
8°
6°
4°
2°
92°
94°
96°
m
0
9
18
27
36

Figure 2.1. Coseismic fault models from various studies.

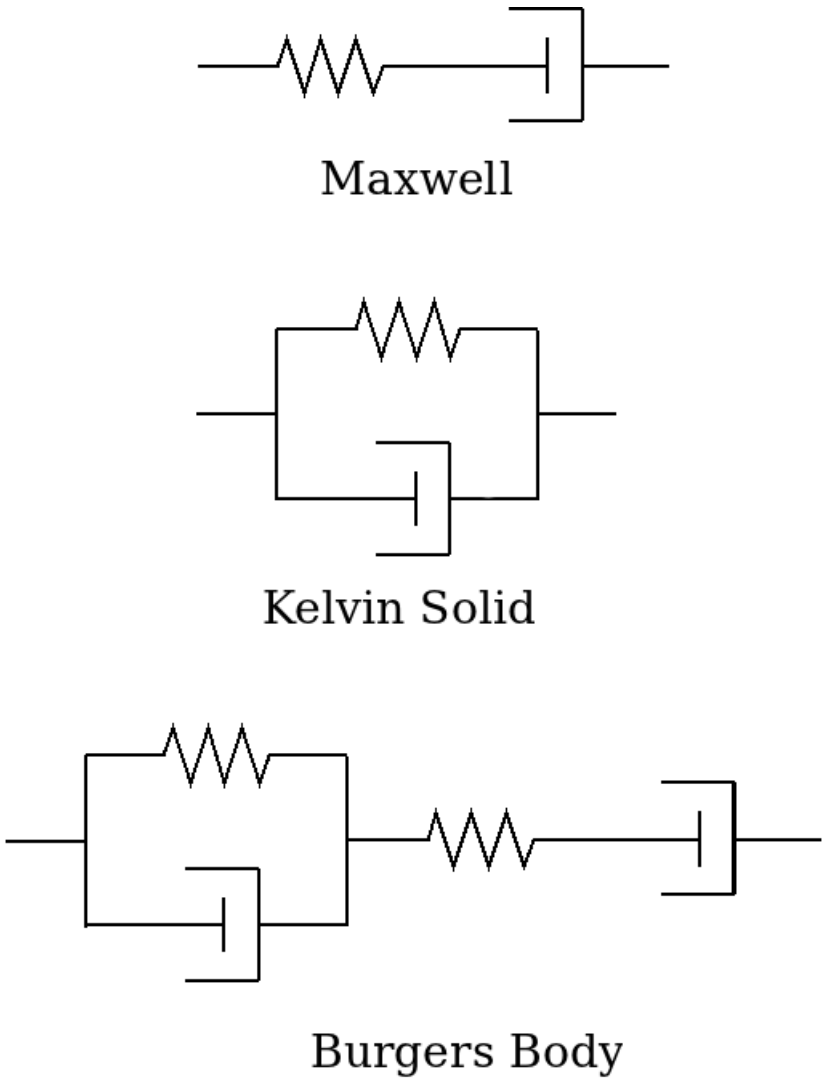

Figure 2.2. Composition of Maxwell, Kelvin solid, and Burgers body material.

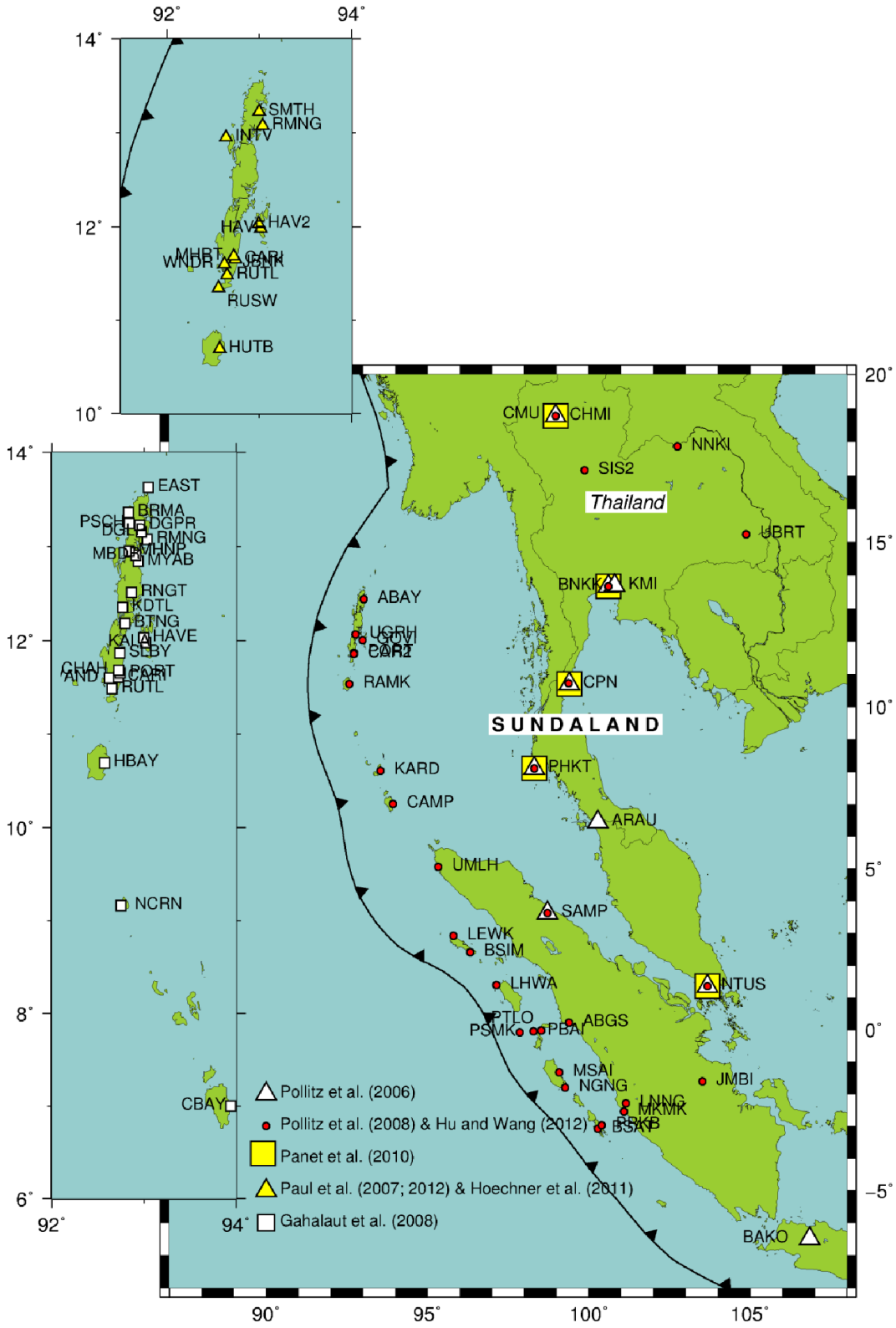

Figure 2.3. Location of GPS sites used by previous studies on postseismic deformation of the 2004 Sumatra-Andaman earthquake.

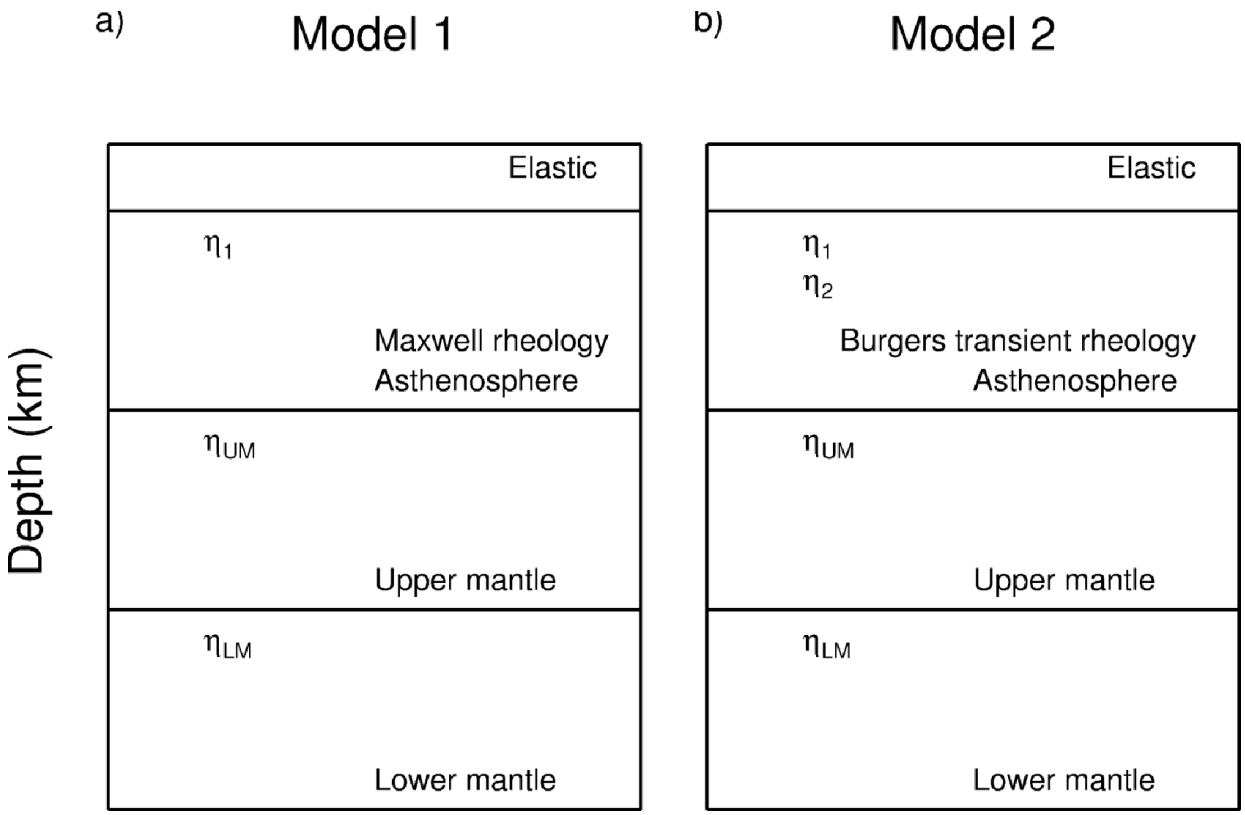

Figure 2.4. Two-dimensional viscoelastic structure used by previous studies. η_1 indicates asthenospheric steady state Maxwell viscosity, η_2 represents asthenospheric transient Kelvi viscosity, η_{UM} denotes upper mantle Maxwell viscosity and η_{LM} implies lower mantle Maxwell viscosity.

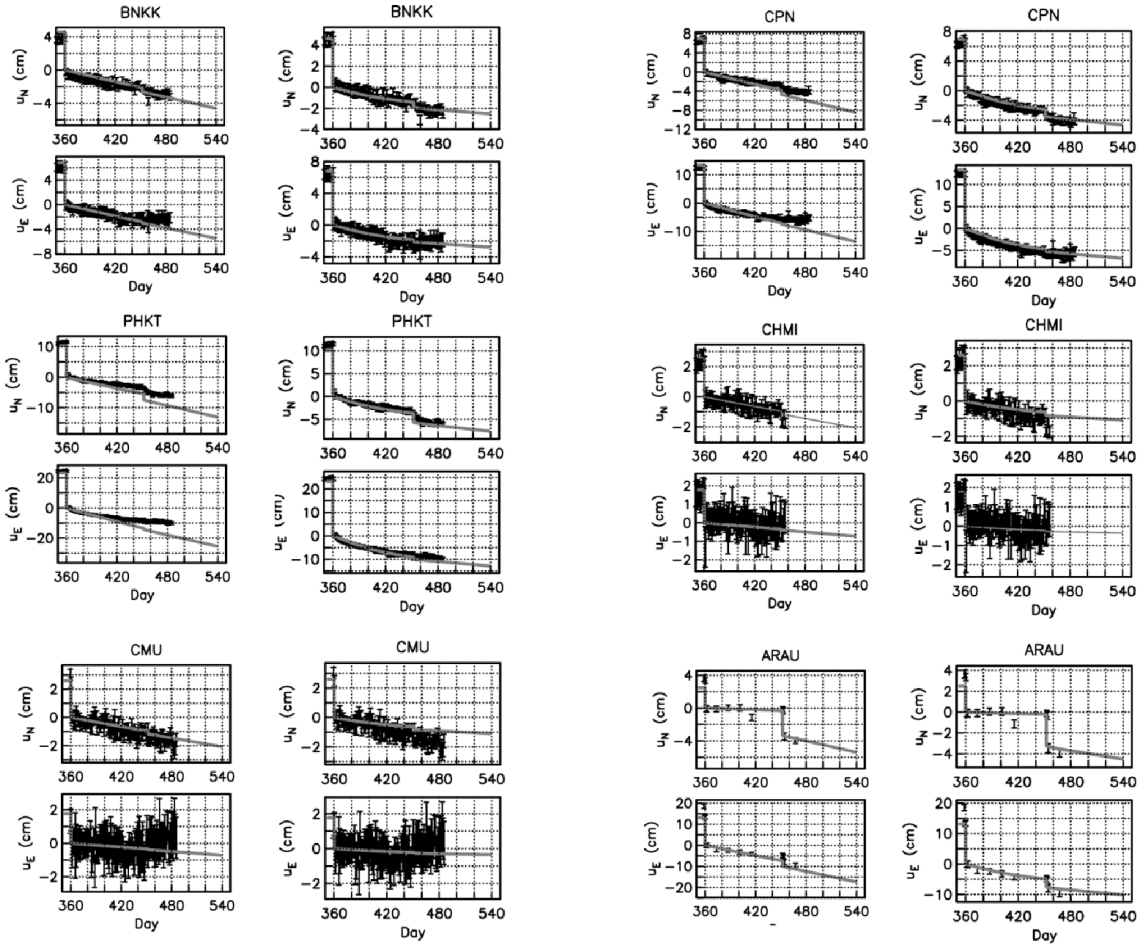

Figure 2.5. (Similar to Figure 12 and Figure 13 of Pollitz et al., 2006) Comparison between observed GPS data and model (left-hand side panel) predicted displacement on Maxwell rheology model (right-hand side panel) predicted displacement on Burgers body rheology.

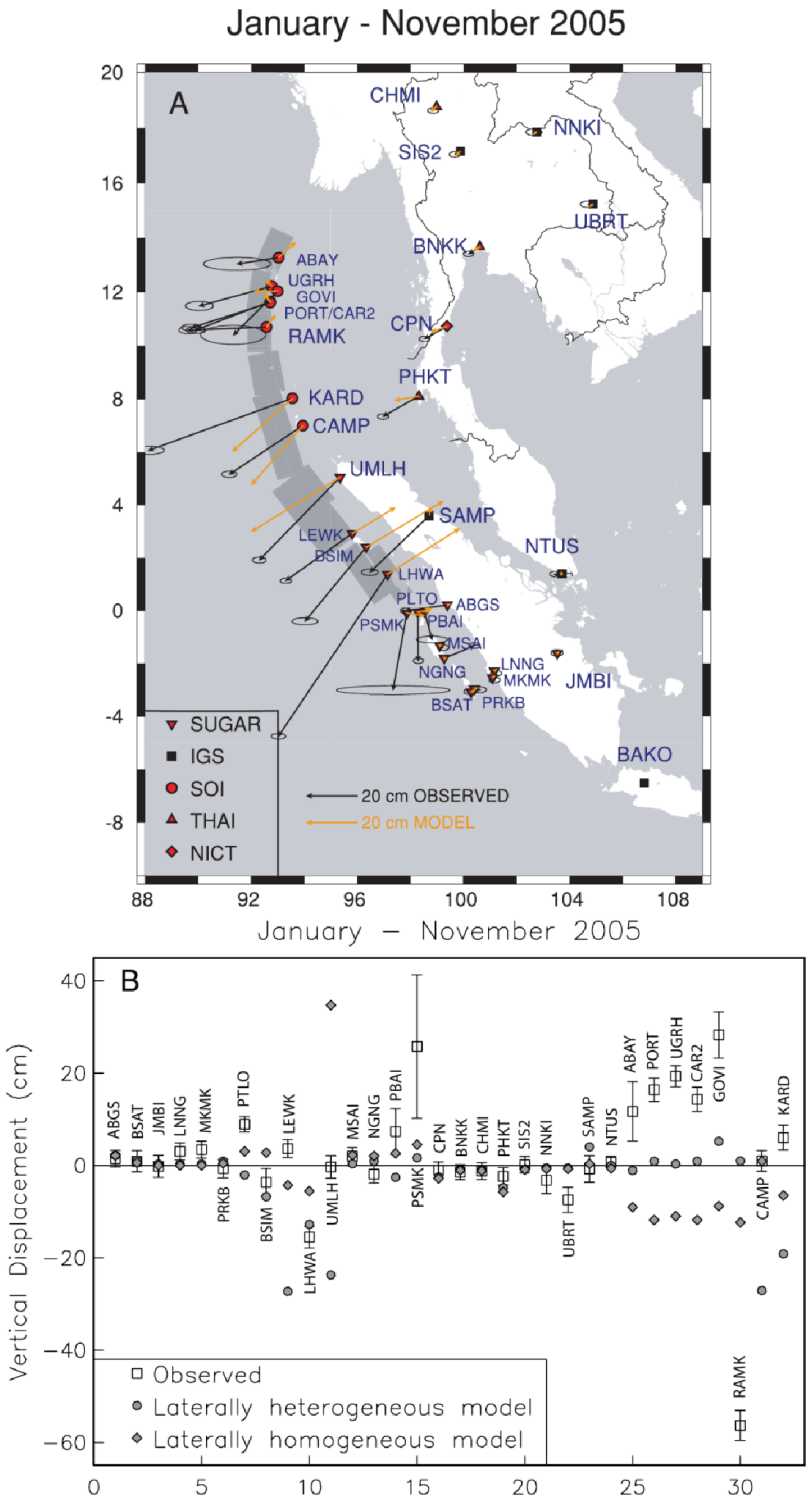

Figure 2.6. (Similar to Figure 15 of Pollitz et al., 2008) Horizontal (a) and vertical (b) postseismic deformation at GPS sites during 11 months after the 2004 earthquake. Heterogeneous model indicates the model that was use in the Pollitz et al. (2008), while homogeneous model implies the model that was use in Pollitz et al. (2006).

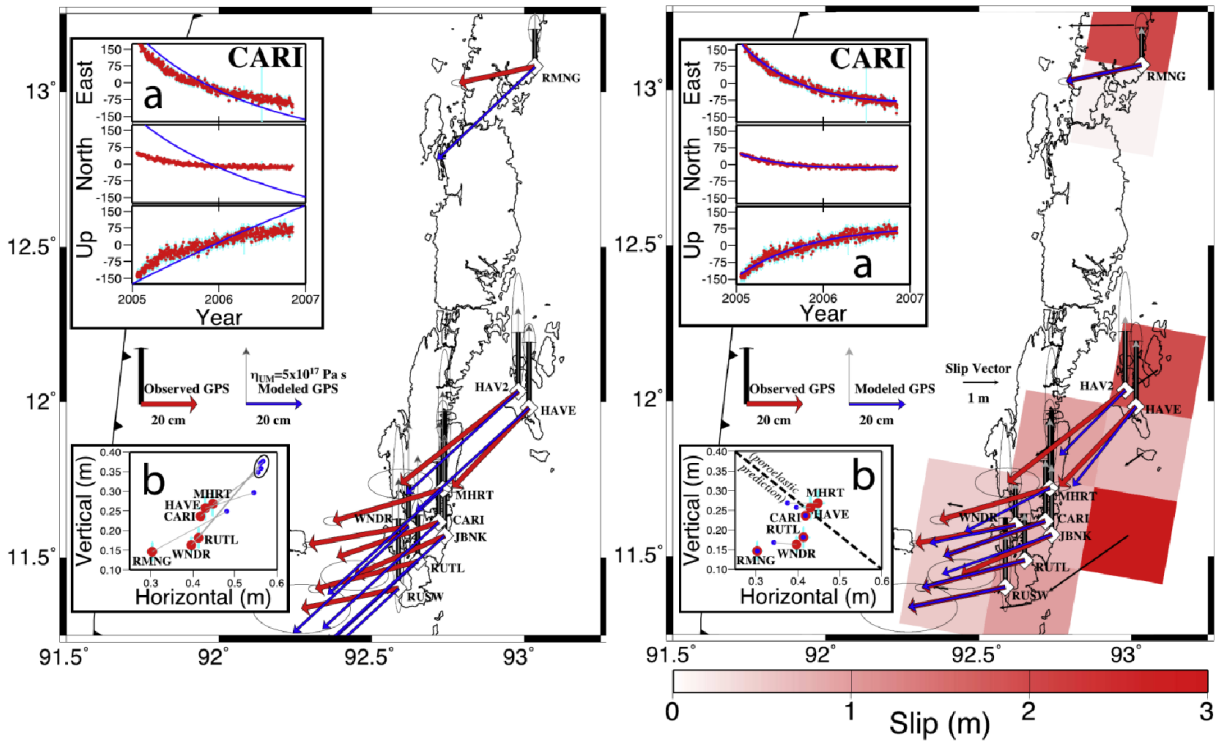

Figure 2.7. (Similar to Figure 3 and Figure 4 of Paul et al., 2007) (Left-hand side panel) GPS data comparison to predicted displacement due to viscoelastic relaxation of Maxwell rheology (Right-hand side panel) GPS data comparison to predicted displacement due to afterslip.

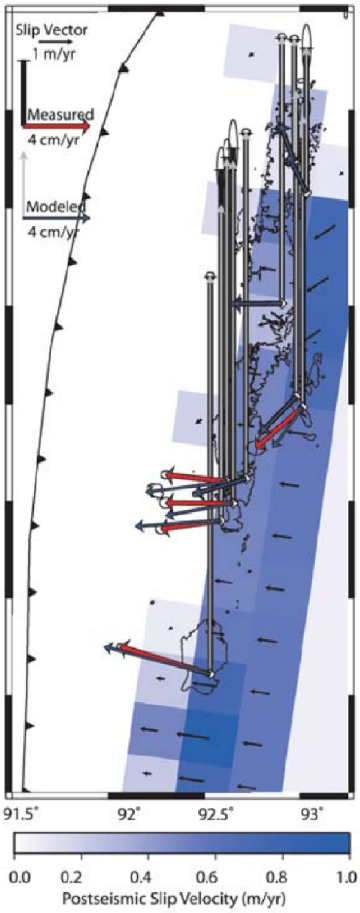

Figure 2.8. (Similar to Figure 3 of Paul et al., 2012) Afterslip distribution in Andaman Islands using residual velocities after subtracting the best-fit of viscoelastic relaxation.

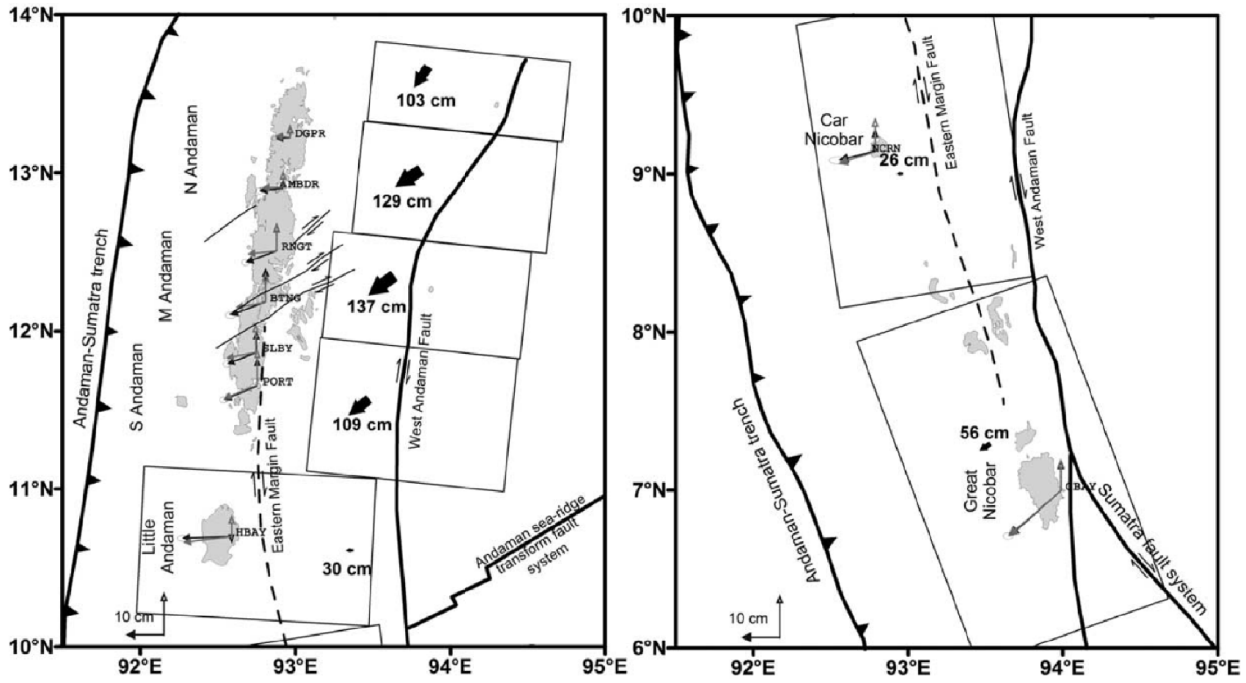

Figure 2.9. (Similar to Figure 3 of Gahalaut et al., 2008) Afterslip distribution in Andaman-Nicobar during February 2006 to February 2007. Gray arrows show the predicted displacement at each sites due to the estimated afterslip.

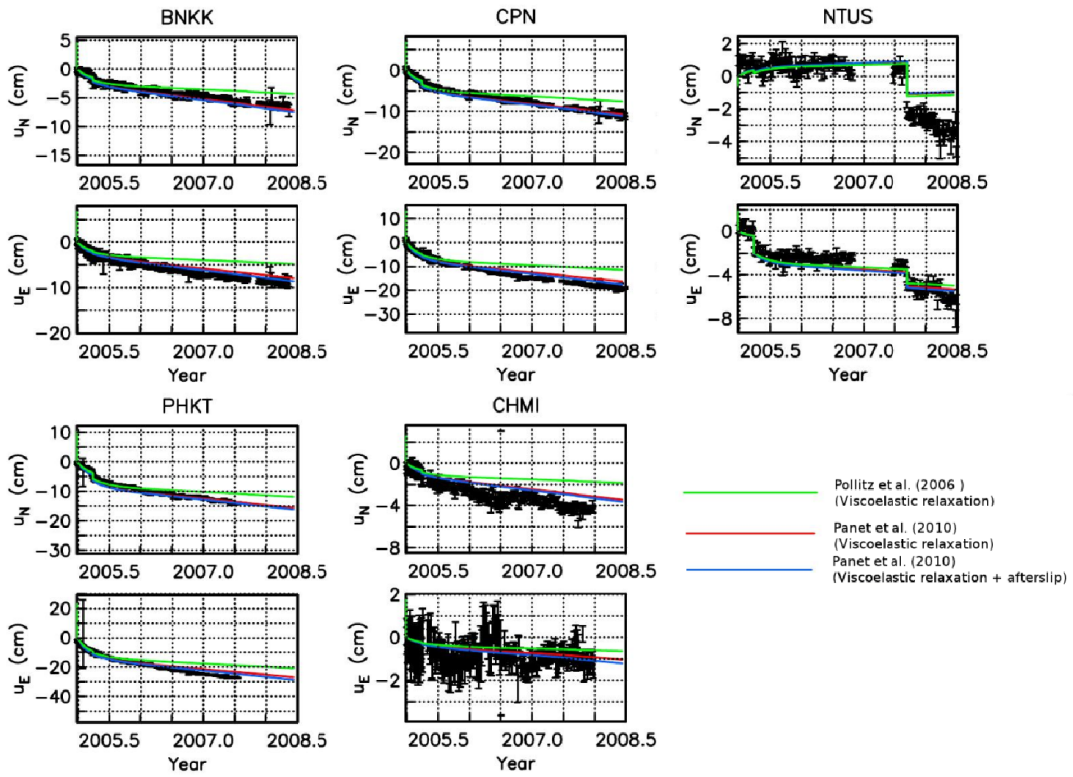

Figure 2.10. (Similar to Figure 10. of Panet et al., 2010) Horizontal displacements from GPS data compared to various postseismic deformation models for 3.5 years after the 2004 Sumatra-Andaman earthquake.

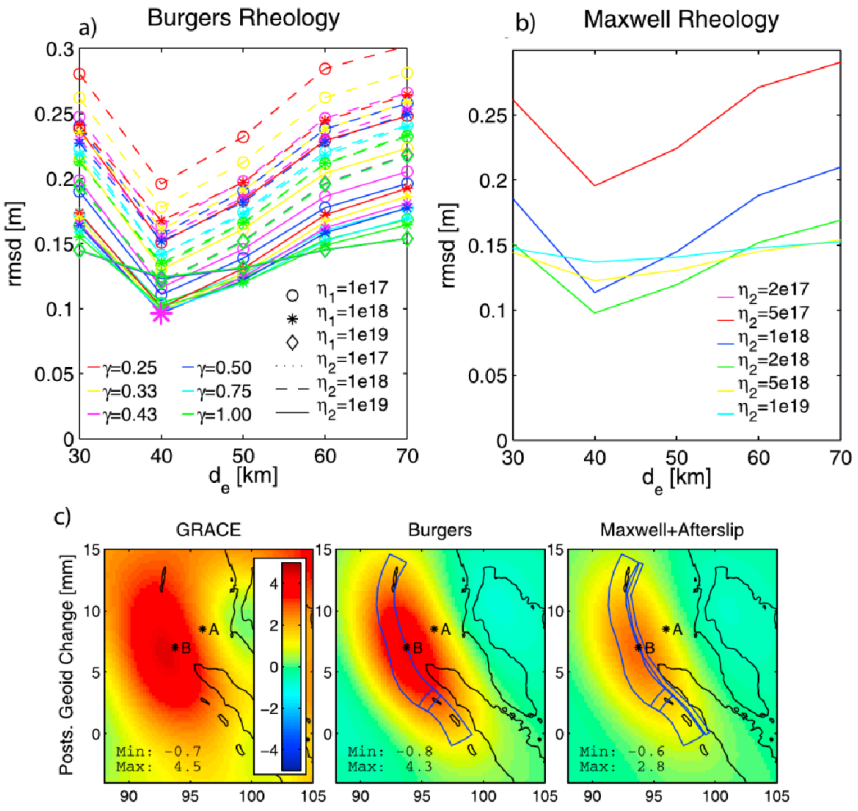

Figure 2.11. (Similar to Figure 1 and Figure 9 of Hoechner et al., 2011) (a) Minimum misfit calculation between modeled and GPS data for various rheological parameters of Burgers body rheology (b) Minimum misfit calculation between modeled and GPS data for various rheological parameters of Maxwell rheology (c) Postseismic geoid change comparison, shown as average of fourth year minus first year after the 2004 earthquake.

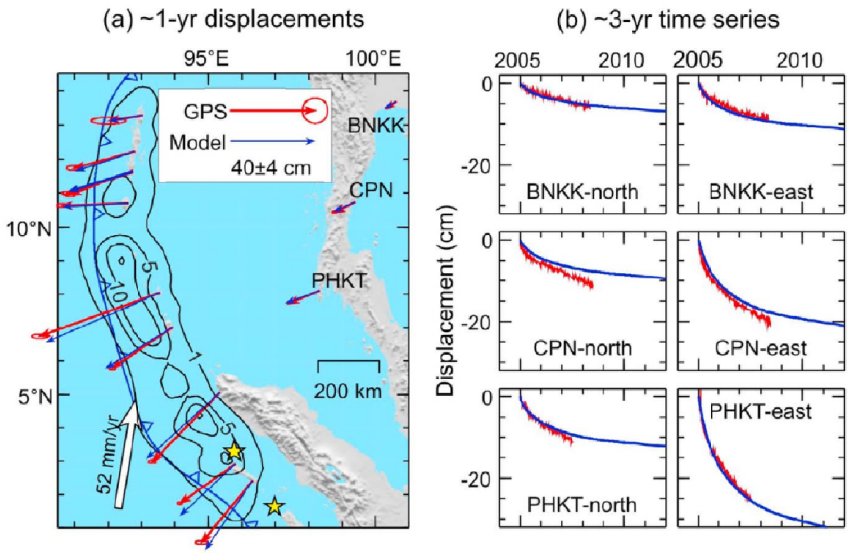

Figure 2.12. (Similar to Figure 7 of Hu and Wang, 2012) Comparison between displacement from GPS data and calculated model of Burgers body rheology with afterslip. (Left-hand side panel) ~1 year displacement, with contour are total slip including coseismic slip and afterslip (Right-hand side panel) ~3 year time series data in Thailand.

Chapter 3

Global Positioning System Data

3.1 Introduction

The development of GPS in the late 1980's has made a great impact on a wide range of geophysical studies. GPS has become an indispensible geodetic tool for studying various geophysical phenomena. Three dimensional position obtained from GPS measurements has a high precision of millimeters level. Also, GPS measurements can be operated essentially under any weather condition, without intervisibility between antennas, and by a small number of team members with a modest budget. Furthermore, GPS receivers and antennas are portable and easy to carry, make scientific research using GPS became enormously increase in numbers (Leick, 2004).

With these enormous advantages, GPS has successfully succeeded the Very Long Baseline Interferometry (VLBI) and Satellite Laser Ranging (SLR) for the study of plate motions and plate boundary deformation. In comparison to strainmeters, GPS offers a better spatial coverage and long term stability. For the study of earthquakes and volcanoes, GPS and Interferometric Synthetic Aperture Radar (InSAR) are complementary each other as GPS provides long-term stability, and better temporal coverage than the extensive spatial coverage of InSAR. GPS also successfully replaced trilateration and leveling (Segall and Davis, 1997).

The M6.2 1987 Superstition Hills earthquake and the M7.1 1989 Loma Prieta earthquake were the early events in which GPS was used to analyze the coseismic deformation (Larsen et al., 1992; Lisowski et al., 1990; Williams et al., 1993). In term of postseismic deformation, the Loma Prieta earthquake and the M7.3 1992 Landers earthquake were considered as the first earthquake events that postseismic signal was well recorded using GPS (Savage et al., 1994; Bürgmann et al., 1997; Shen et al., 1994; Savage and Svarc, 1997).

The continuous GPS network in Japan, now called GPS Earth Observation Network (GEONET) (Sagiya, 2004) successfully detected coseismic and postseismic signal of the M7.5 1994 Sanriku-Haruka-Oki earthquake (Heki et al, 1997) and many other earthquakes with magnitude over 6 in and around Japan (e.g. Sagiya, 2004). Moreover, GEONET showed its capability by detecting coseismic and postseismic signal of the M9.0 2011 Tohoku-oki earthquake (e.g. Ozawa et al. 2012). Further examples of GPS network in Taiwan (e.g. Chen et al., 2006; Hsu et al., 2009), Turkey (e.g. Reilinger et al., 2000; Dogan et al., 2014;), New Zealand (e,g, Beavan et al., 2012), Chile (e.g. Bedford et al., 2013), and other places around the world (e.g. Árnadóttir et al., 2005; Diao et al., 2011; Kogan et al., 2011) indicated that GPS plays a major role in the study of crustal deformation and earthquakes.

The 2004 Sumatra-Andaman earthquake provides us with a great opportunity to investigate postseismic deformation considering its large scale deformation and long time duration since its occurrence. As the 2004 earthquake was the first M9 class recorded by GPS, we can analyze the longest GPS time series data than any other M9 earthquake.

Shortly after the 2004 earthquake, GPS measurements were started in northern Sumatra, Andaman-Nicobar and Thailand. In this chapter, we describe the GPS sites in these regions comprehensively. First, we describe the GPS data located in Andaman-Nicobar and Thailand, obtained from previous studies. Then we describe our GPS measurements in northern Sumatra, processing strategy of these GPS data, and characteristics of these GPS data regarding the postseismic deformation after the 2004 earthquake. Finally, we discuss importance of the GPS

network in northern Sumatra for the study on postseismic deformation of the 2004 earthquake.

3.2 GPS data in Andaman-Nicobar and Thailand

The 2004 earthquake was accompanied by a very large scale deformation, affecting Andaman Islands, and Thailand, more than 1000 km apart from the epicenter. Here, we describe the GPS data located in Andaman-Nicobar and Thailand obtained from previous studies (Gahalaut et al., 2008; Satirapod et al., 2008).

3.2.1 GPS data in Andaman-Nicobar

Gahalaut et al. (2008) reported GPS observations in Andaman-Nicobar. The network consisted of 22 campaign-mode sites and 1 continuous-mode site. Some of these sites were built by Survey of India (SOI) before the 2004 earthquake, while others were newly constructed. These GPS sites are located either on a hard rock, or on a deeply buried cement pillar. Figure 3.1 shows the location of GPS sites in Andaman-Nicobar.

Soon after the 2004 earthquake, Gahalaut et al. (2006) conducted GPS measurements in Andaman-Nicobar between January-February 2005. They repeated the measurements on February 2006, and February 2007. Gahalaut et al. (2008) processed these GPS data using GAMIT/GLOBK, and the time series results were estimated in the International Terrestrial Reference Frame 2005 (ITRF2005) reference frame (Altamimi et al., 2007).

Here, we translated the daily displacements into the Sundaland block reference frame Simons et al., 2007) to make the time series appropriate for tectonic discussion and represent the actual displacements. First, we transform the coordinates from ITRF2005 to ITRF2000 (Altamimi et al., 2007) using equation (3.1), that is:

$$\begin{bmatrix} X_S \\ Y_S \\ Z_S \end{bmatrix} = \begin{bmatrix} X \\ Y \\ Z \end{bmatrix} + \begin{bmatrix} T_X \\ T_Y \\ T_Z \end{bmatrix} + \begin{bmatrix} D & -R_Z & R_Y \\ R_Z & D & -R_X \\ -R_Y & R_X & D \end{bmatrix} \begin{bmatrix} X \\ Y \\ Z \end{bmatrix} \quad (3.1)$$

where X, Y, Z are the coordinates in ITRF2005 frame, and Xs, Ys, Zs are the coordinates in ITRF2000. Table 3.1 shows the transformation parameters from ITRF2005 to ITRF2000. Then from ITRF2000, we transform the coordinate into the Sundaland block reference frame by using the following formula.

$$v = \varpi R \sin \{ \cos^{-1}[\sin\lambda_X \sin\lambda_P + \cos\lambda_X \cos\lambda_P \cos(\phi_P - \phi_X)] \} \quad (3.2)$$

$$\beta = 90 + \sin^{-1}\left(\frac{\cos\lambda_P \sin(\phi_P - \phi_X)}{\sin a}\right) \quad (3.3)$$

with v and β are magnitude and azimuth at point X relative to Sundaland block, λ_x and ϕ_x are latitude and longitude of point X, R is the radius of the Earth, while ϖ, λ_P and ϕ_P are angular velocity, latitude and longitude of the rotation pole. Following Simons et al. (2007), the parameters for λ_P, ϕ_P and ϖ are 49.0°N, -94.2°E, and 0.336/Ma, respectively. Figure 3.2 shows the postseismic displacements in Andaman-Nicobar in the Sundaland block reference frame.

3.2.2 GPS data in Thailand

Satirapod et al. (2008) reported GPS observations that were measured after the 2004 earthquake in Thailand. In total, six or more measurements were performed during two years after the 2004 earthquake. These GPS sites were occupied by the Royal Thai Survey Department (RTSD) with campaign-mode surveys. Figure 3.3 shows the location of GPS sites in Thailand.

They processed the GPS data using GIPSY-OASIS II, and their final solution result was obtained in ITRF2000 (Altamimi et al., 2002). We then transform their time series solution to the Sundaland block reference frame using equations (3.2) and (3.3). Figure 3.4 shows the

time series of GPS sites in Thailand with respect to Sundaland block reference frame.

3.3 GPS data in northern Sumatra

Northern Sumatra is located about 100 km northward from the epicenter of the 2004 earthquake. Here, we discuss the GPS network observed in this region.

3.3.1 GPS sites overview

The GPS network in northern Sumatra was constructed under the collaboration of Nagoya University, Kochi University, Tohoku University, Institute of Technology Bandung and Syiah Kuala University. This GPS network was named AGNeSS (Aceh GPS Network for Sumatran fault System) (Ito et al., 2012). Figure 3.5 shows the location of GPS sites in northern Sumatra.

AGNeSS consists of both continuous and campaign sites. Every GPS site is equipped with a dual-frequency GPS antenna and a GPS receiver. The first continuous site, ACEH located in Banda Aceh, was installed in March 5th, 2005. The antenna for ACEH site is permanently installed on the top of a concrete roof of a building (Ito et al., 2012).

Later, on November 2005, more continuous sites were constructed. At these continuous sites, a GPS receiver and a recording device stored in a steel box embedded in the foundation of a 1.5 m high concrete pillar. We equipped our continuous sites with solar controller and a battery as a backup power. During the observations, we also conduct campaign GPS measurements using a tripod. Figure 3.6 shows the typical GPS measurements for continuous sites and campaign sites in northern Sumatra.

Until the end of 2009, 7 continuous sites were constructed and 20 campaign sites were repeatedly occupied in AGNeSS. Among the AGNeSS sites, PIDI, BIRN and SKTN benchmark belongs to Geospatial Information Agency of Indonesia (*BIG*), KEMA benchmark belongs to

National Agency for Land Administration (*BPN*), and other sites were newly constructed. Table 3.2 shows description of the AGNeSS GPS sites.

Besides AGNeSS, a GPS site of the SuGAr (Sumatran GPS Array) network named UMLH (www.tectonics.caltech.edu/sumatra/sugar.html) is present in northern Sumatra. This GPS site is currently operated by the Earth Observatory of Singapore (EOS) and the Indonesian Institute of Sciences (*LIPI*). GPS data of UMLH site is available in time periods between April 2005 to July 2008 from SOPAC (Scripps Orbit and Permanent Array Center),. Figure 3.7 shows the availability of UMLH and AGNeSS GPS data in northern Sumatra.

3.3.2 GPS data processing

We process the Receiver Independent Exchange Format (RINEX) data using Bernese 5.0 software (Dach et al., 2007). CODE final ephemeris, earth rotation parameters, ionosphere model parameters and differential code biases for satellites and receivers are downloaded from the ftp site of the University of Bern (ftp://ftp.unibe.ch/aiub/). Meanwhile, ocean tide model coefficients are calculated based on Finite Element Solutions 2004 (FES2004) (Lyard et al., 2006) from website of the Onsala Space Observatory (http://holt.oso.chalmers.se/loading/). A standard Bernese routine RNX2SNX.PCF was used to produce an integrated daily solution with a consistent reference frame in the International Terrestrial Reference Frame 2008 (ITRF2008).

We transform coordinates from ITRF2008 to ITRF2000 (Altamimi et al., 2011) using equation (3.1). Transformation parameters from ITRF2008 to ITRF2000 can be found in Table 3.1. We conduct another coordinate transformation from ITRF2000 reference frame to Sundaland block reference frame using equations (3.2) and (3.3).

3.3.3 Characteristics of the displacement data

We show the time series of horizontal and vertical components on continuous GPS sites and horizontal components on the campaign GPS sites in Figure 3.8. For campaign GPS sites

we do not use vertical information in this study because antenna height records during the campaign GPS observations are missing.

Observed GPS displacements in northern Sumatra clearly show a temporal decay, most likely reflecting postseismic deformation. We fit a linear trend to the postseismic motion at ACEH GPS site for every one year time period. During 2005.19~2006.19, horizontal motion was 41.0±0.1 cm/yr to the southwest, directing the 2004 earthquake rupture. During the period 2006.19~2007.19, the velocity significantly decreased by about 56%, to 18.0±0.1 cm/yr. On the other hand, the vertical displacement rate during 2005.19~2006.19 and 2006.19~2007.19 were 1.3±0.5 cm/yr and 1.9±0.5 cm/yr, and the whole time series looks almost linear in time. We find similar characteristics for the displacement rate of another continuous GPS data at UMLH. The horizontal displacement rate of the first year periods between 2005.32~2006.32 was 39.1±0.2 cm/yr, and then significantly decreased to 13.4±0.2 cm/yr during 2006.32~2007.32. Meanwhile, the vertical displacement rate was 2.4±0.4 cm/yr and 1.3±0.4 cm/yr during these time periods. Similar tendency is found for campaign GPS sites, horizontal displacement rate during 2005.91~2006.90 at MBMG, JERM, GEUM, CALA and BEUN were 10.7±0.1 cm/yr, 12.7±0.1 cm/yr, 14.43±0.2 cm/yr, 16.8±0.2 cm/yr, 15.6±0.2 cm/yr, respectively, and they significantly decreased to 6.1±0.1 cm/yr, 6.6±0.1 cm/yr, 8.9±0.1 cm/yr, 11.4±0.1 cm/yr, and 13.8±0.2 cm/yr during 2006.90~2007.90. These results clearly indicate that GPS horizontal components in northern Sumatra showed a rapid decay with a decay time less than 1 year, while the vertical component had a much longer relaxation time.

3.3.4 Importance of AGNeSS in the study of postseismic deformation of the 2004 Sumatra-Andaman earthquake

In this study, we tackle the postseismic deformation of the 2004 earthquake by taking GPS data in northern Sumatra, AGNeSS, into account. AGNeSS data are important due to the

following reasons: (1) The network is located in the near-field of the main slip patch of the 2004 earthquake. The main slip patch of the 2004 earthquake is located just west off northern Sumatra, with a distance of about ~150 km. Hence, significant postseismic deformation is expected in this region; (2) GPS measurements started a few months after the main shock. The ACEH site has been measured since March 2005, thus it provides information of early postseismic deformation after the 2004 earthquake; (3) Availability of continuous GPS measurements. In northern Sumatra, there are two continuous GPS stations, ACEH and UMLH, which provide a good control on both horizontal and vertical components; (4) These GPS data have not been used in analyzing postseismic deformation comprehensively. As we mentioned in Chapter 2, previous studies on postseismic deformation of the 2004 earthquake (Pollitz et al., 2008; Hu and Wang et al., 2012) could not reproduce GPS displacement data in northern Sumatra. Ito et al. (2012) analyzed these data to estimate afterslip distribution on the plate interface, in order to estimate slip rate of the Great Sumatran Fault. In our study, instead of interpreting with a single physical mechanism of afterslip, we take two physical mechanisms of afterslip and viscoelastic relaxation into consideration.

In order to give a clear interpretation of postseismic deformation of the 2004 earthquake, we include both horizontal and vertical components in our analysis from continuous GPS sites. Vertical GPS data in northern Sumatra provide valuable information to find an optimum rheology model. We also introduce a new strategy of postseismic calculation which takes two physical mechanisms, afterslip and viscoelastic relaxation, into account.

Table 3.1. Transformation parameters from ITRF2008 and ITRF2005 to ITRF2000

Solution	**T_x (mm) (mm/yr)**	**T_y (mm) (mm/yr)**	**T_z (mm) (mm/yr)**	**D (ppb) (ppb/yr)**	**R_x (0.001″) (0.001″/yr)**	**R_x (0.001″) (0.001″/yr)**	**R_x (0.001″) (0.001″/yr)**
ITRF2005	0.1 -0.2	-0.8 0.2	-5.8 -1.8	0.40 0.08	0 0	0 0	0 0
ITRF2008	-1.9 0.1	-1.7 0.1	-10.5 -1.8	1.34 0.08	0 0	0 0	0 0

Table 3.2. Description of AGNeSS GPS sites

Site	Monument Type	Receiver type	Organization
ACEH	Fix on top of roof	Trimble 4000	Newly constructed
BEUN	Benchmark	Trimble 5700	Newly constructed
CELA	Benchmark	Trimble 5700	Newly constructed
GEUM	Benchmark	Trimble 5700	Newly constructed
JERM	Benchmark	Trimble NetRS	Newly constructed
KAWA	Benchmark	Trimble 5700	Newly constructed
KEMA	Benchmark	Trimble 5700	BPN
MBMG	Benchmark	Trimble NetRS	Newly constructed
PIDI	Benchmark	Trimble 5700	BIG
BIRN	Benchmark	Trimble 5700	BIG
CALA	Benchmark	Trimble 5700	Newly constructed
BTAT	Pillar	Trimble 4000	Newly constructed
BTBW	Pillar	Trimble 4000	Newly constructed
KLMJ	Benchmark	Trimble NetRS	Newly constructed
MNYK	Pillar	Trimble 5700	Newly constructed
PTRA	Pillar	Trimble NetRS	Newly constructed
UJNG	Benchmark	Trimble 5700	Newly constructed
SARP	Benchmark	Trimble NetRS	Newly constructed
SGMT	Benchmark	Trimble NetRS	Newly constructed
SKTN	Benchmark	Trimble 5700	BIG
TNDP	Pillar	Trimble 5700	Newly constructed
TANG	Pillar	Trimble 4000	Newly constructed
MALO	Pillar	Trimble 4000	Newly constructed
UGDN	Pillar	Trimble 4000	Newly constructed

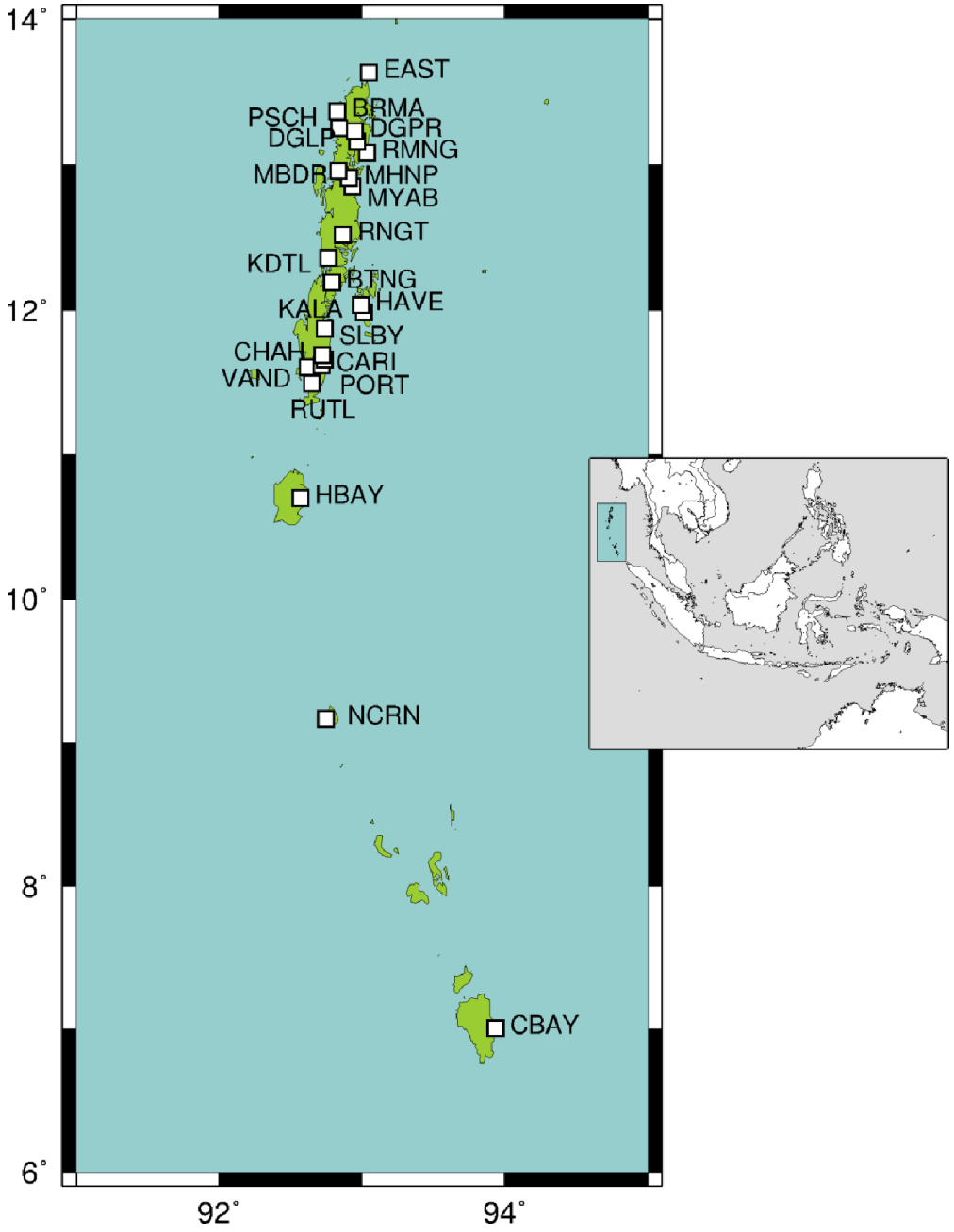

Figure 3.1. Location of GPS sites in Andaman Islands and Nicobar obtained from Gahalaut et al. (2008) indicates by white squares.

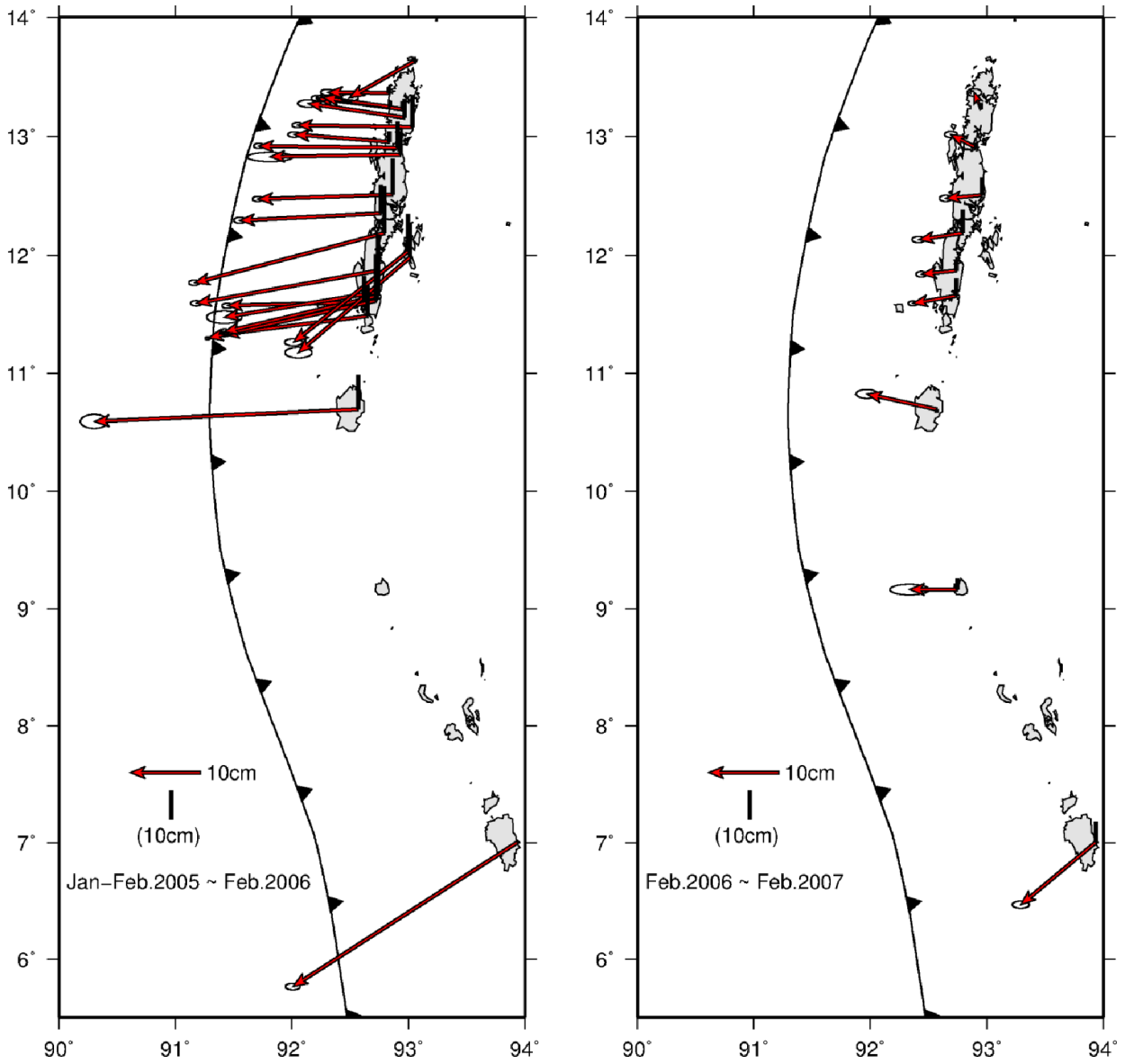

Figure 3.2. Horizontal (red arrows) and vertical (black bars) displacements in Andaman-Nicobar for time periods of January-February 2005 to February 2006 (left figure) and February 2006 to February 2007 (right figure) with reference to Sundaland block.

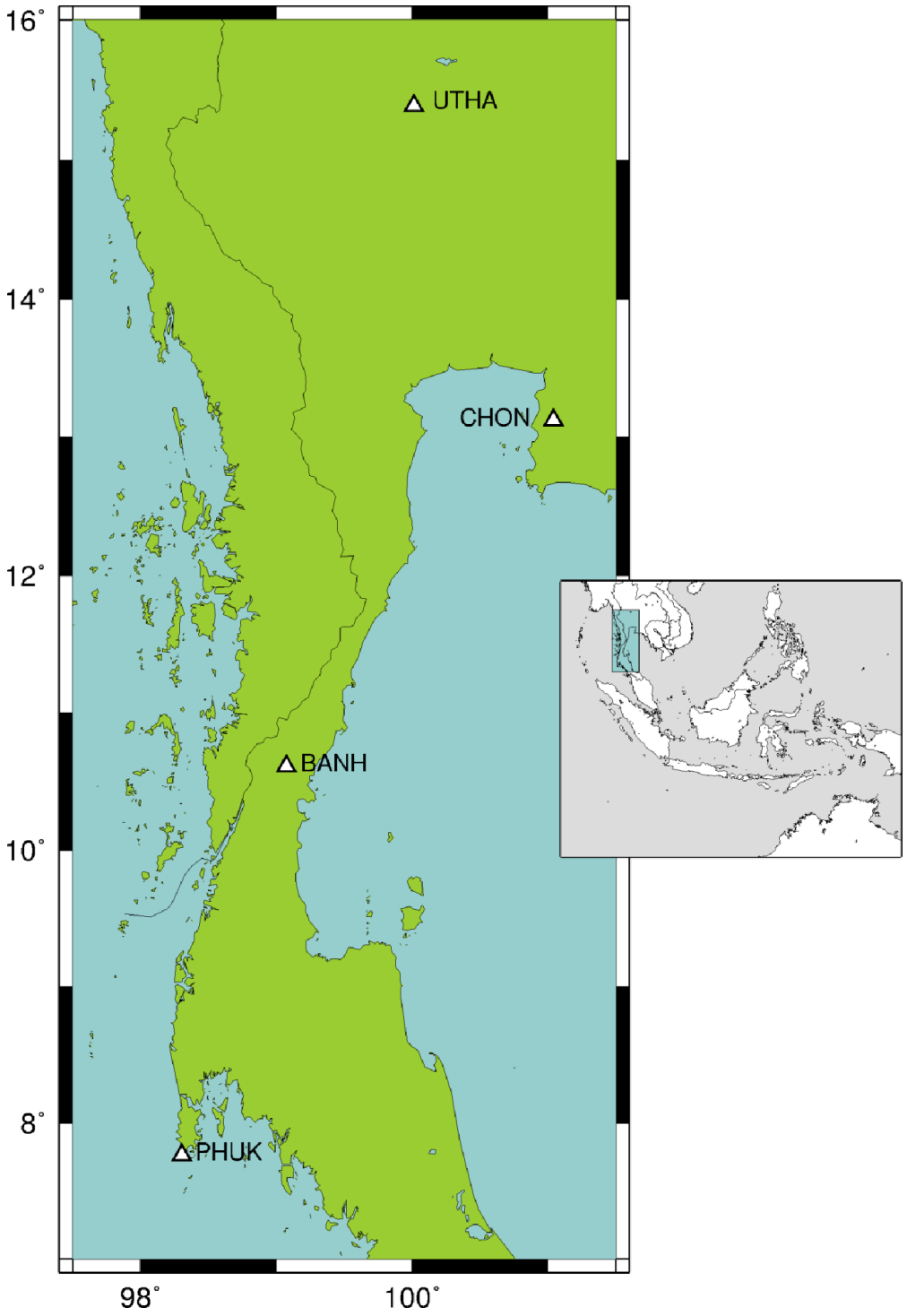

Figure 3.3. Location of GPS sites in Thailand obtained from Satirapod et al. (2008) indicates by white triangles.

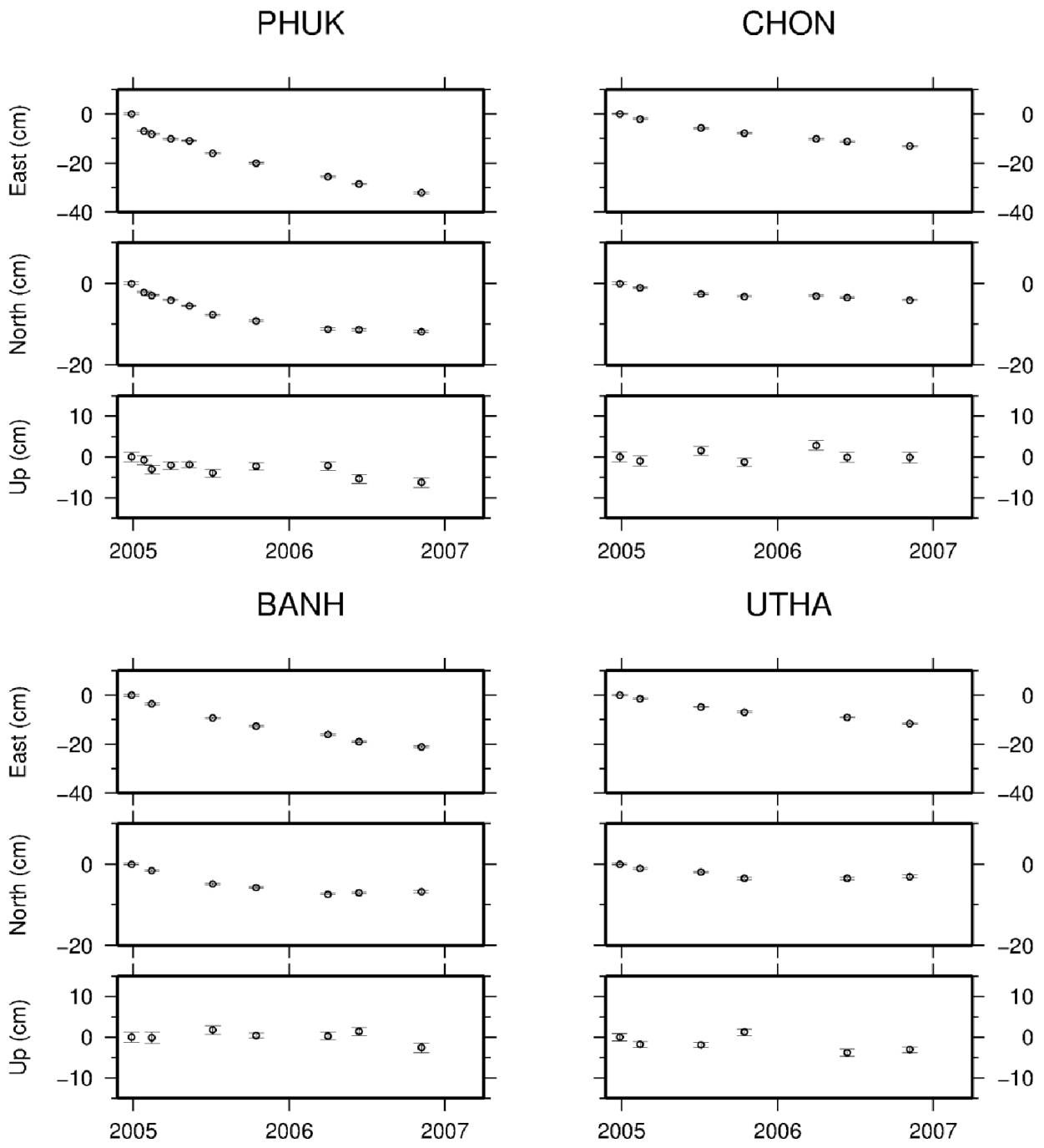

Figure 3.4. GPS time series of campaign sites in Thailand

Figure 3.5. Location of AGNeSS sites in northern Sumatra. White triangles denote continuous GPS sites, while white squares imply campaign sites and white hexagonal indicates SUGaR site. Continuous solid line represents the trace of great Sumatran fault (Sieh and Natawidjaja, 2000).

Figure 3.6. Typical GPS measurements in northern Sumatra. (Left-hand side picture) A concrete pillar type for continuous GPS sites. (Right-hand side picture) Campaign GPS measurements using tripod.

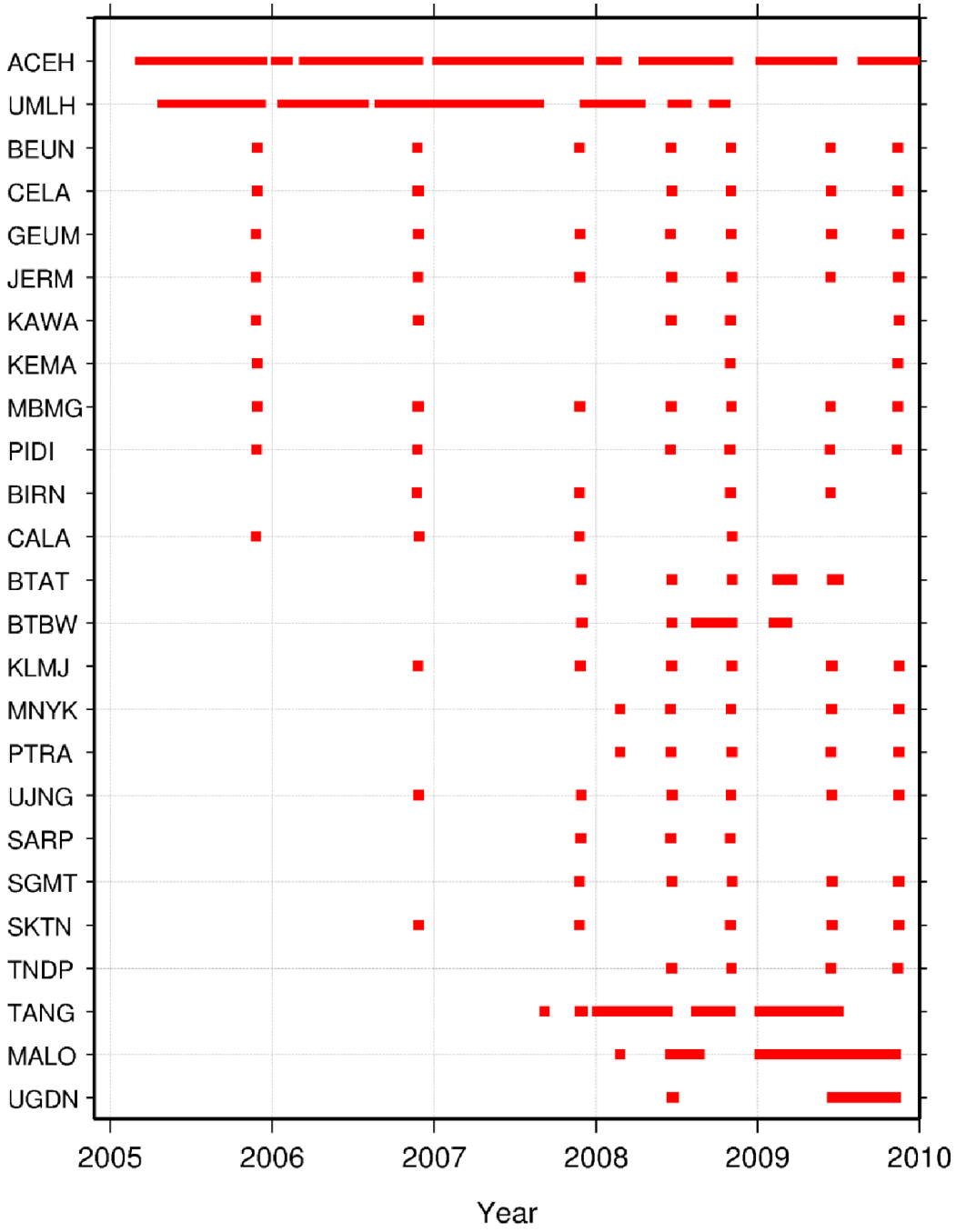

Figure 3.7. Data availability at every GPS sites in northern Sumatra.

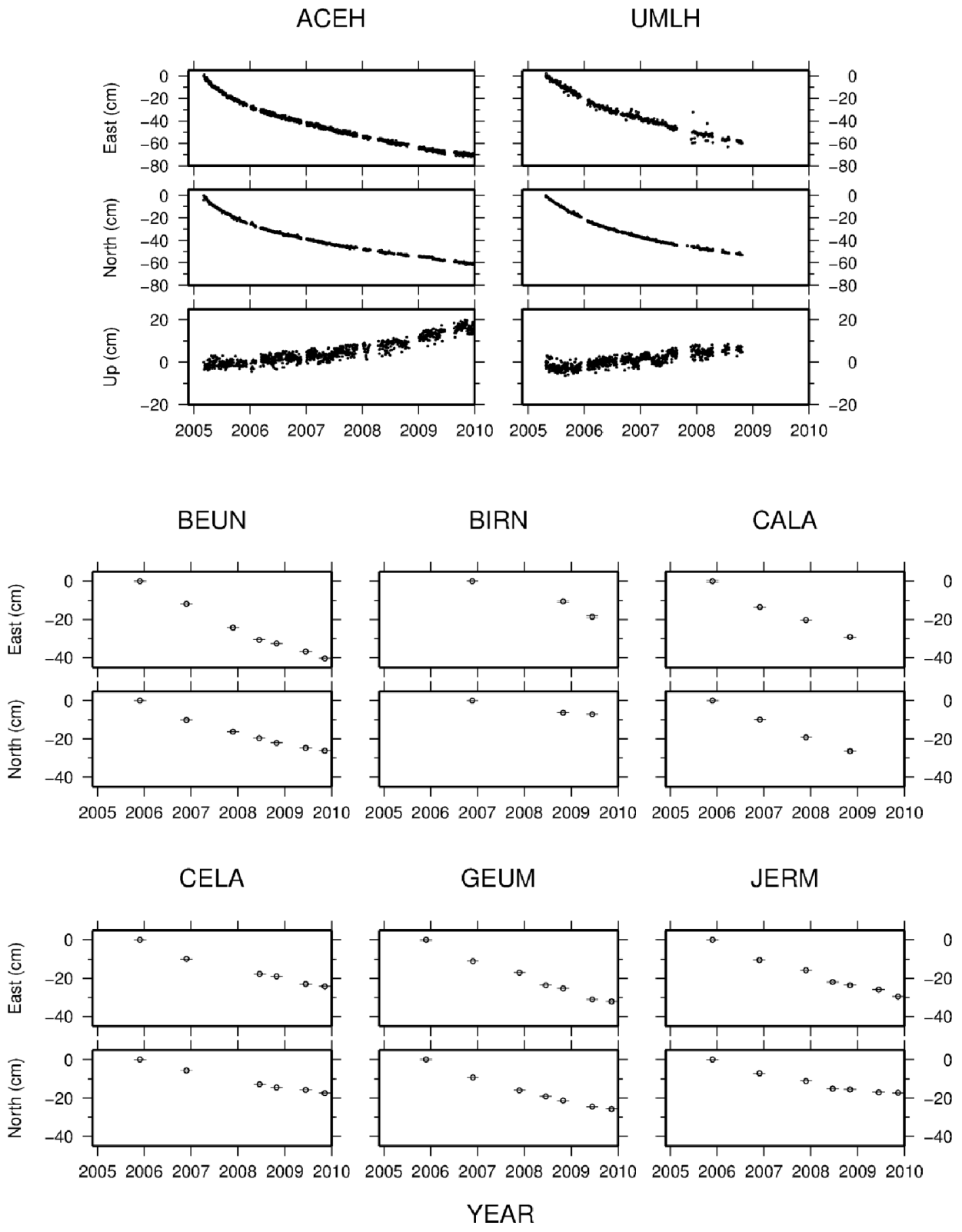

Figure 3.8. GPS time series of continuous sites and campaign sites in northern Sumatra.

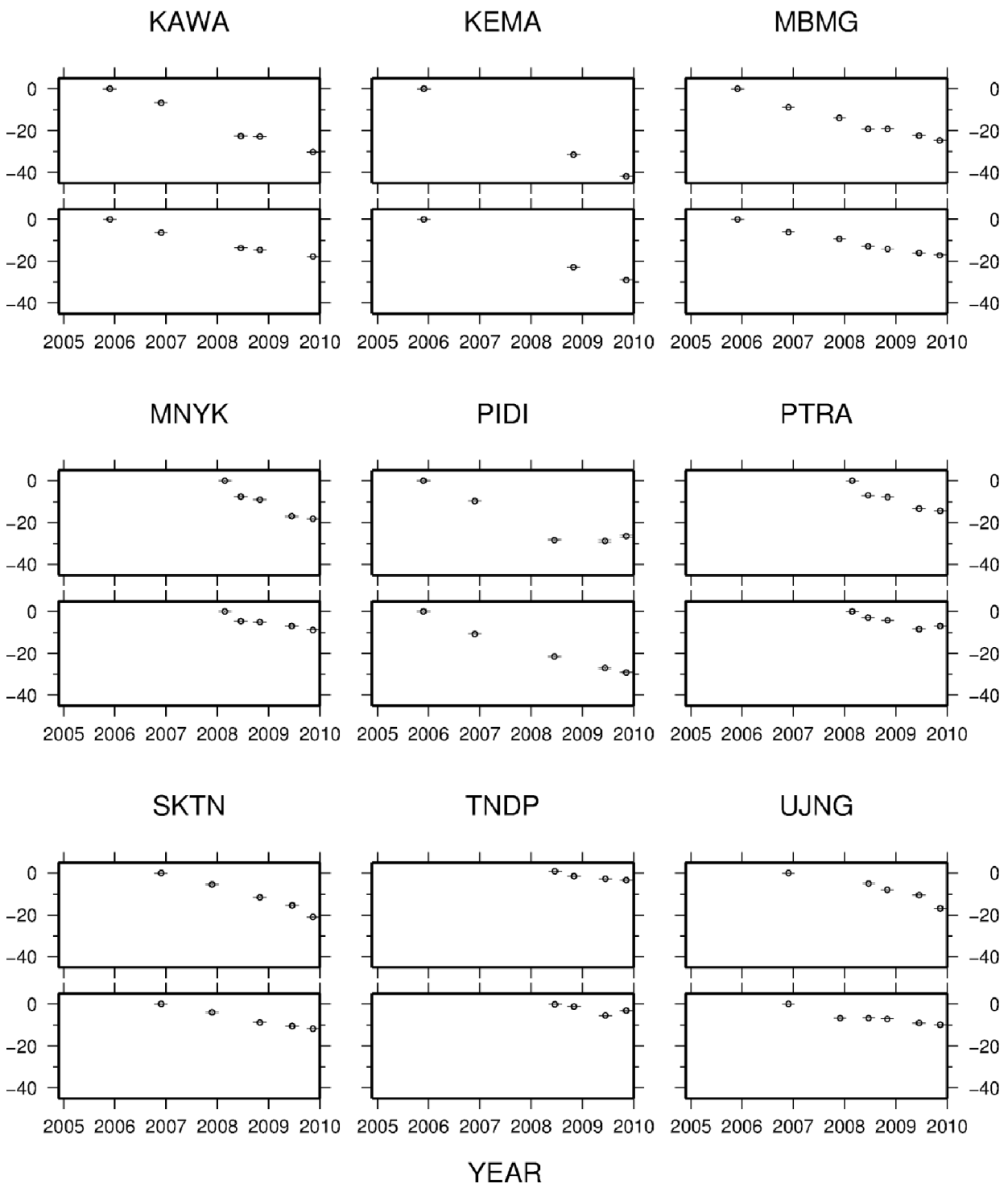

Figure 3.8. *(continued)*

Chapter 4

Analysis of Postseismic Deformation

4.1 Introduction

GPS data in northern Sumatra play an important role in our attempt to investigate postseismic deformation after the 2004 earthquake. Moreover, the availability of continuous GPS data within just a few months after the 2004 earthquake provides a good control on both horizontal and vertical displacements. Using these continuous GPS data, we find different relaxation times for horizontal and vertical components in northern Sumatra. We show that the relaxation time of the vertical component is longer than that of the horizontal ones (see Chapter 3.3.3).

The aim of this chapter is to describe our analysis on postseismic deformation using GPS data in northern Sumatra using four coseismic fault models comprehensively. First, we compare previous studies of coseismic fault models we used for investigating the postseismic deformation. Second, we analyze previous postseismic deformation studies result based on GPS data in northern Sumatra. Third, we discuss our strategy to model the postseismic deformation. Finally, in the last section, we summarize our analysis result.

4.2 Comparison of coseismic fault models

In this study we investigate postseismic deformation using four different coseismic fault models of the 2004 earthquake. These fault models are Kreemer et al. (2006) (hereinafter referred to as Kreemer model), Banerjee et al. (2007) (hereinafter referred to as Banerjee model), Fujii and Satake (2007) (hereinafter referred to as Fujii model), and Rhie et al. (2007) (hereinafter referred to as Rhie model). The coseismic fault parameters for each model are listed in Appendix A. We chose these fault models among many others models as they represented a result obtained from a certain data sets used in their investigation.

Far-field GPS data were used in the Kreemer model, while in Banerjee model, both GPS data of near-field and far-field were used. Fujii model was obtained using tide gauge and satellite altimetry data, while Rhie model used teleseismic and near-field GPS data. Thus, between four coseismic fault models we use in our study, two models were derived from geodetic observations, one model derived from joint seismic and geodetic observation, and one model derived from tsunami data.

Among these coseismic fault models, location and magnitude of the maximum slip is different one another. While in the Kreemer model and Banerjee model, the maximum slip distribution is located north of 5° N, in the Fujii model the maximum slip is located at about 3° N. Meanwhile, in the Rhie model, the maximum slip distribution is located at about 4.5° N, slightly north of the maxium slip of the Fujii model (Figure 2.1).

Comparing the maximum coseismic slip of these models, the Rhie model has the largest slip of 35.3 m, while the Kreemer model has the smallest maximum slip of 11.3 m. Meanwhile, the Banerjee model has the maximum slip of 19.4 m, and the Fujii model has the maximum slip of 24.6 m. Since these models have similar total seismic moment (Kreemer model is 6.11×10^{22} N m (M_w 9.13), Banerjee model is 7.62×10^{22} N m (M_w 9.22), Fujii model is 6.00×10^{22} N m

(M_w 9.1), and Rhie model is 7.12 x 10^{22} N m (M_w 9.20), the largest slip differences is attributed to the different spatial resolution of each analysis. The Rhie model has the finest fault resolution, followed by Fujii model, while both Banerjee model and Kremer model have the coarse fault resolution. The finest fault resolution used in Rhie model corresponds to the lower cutoff period of seismic waveform data to produce a smooth kinematic rupture model. The Fujii model did not mentioned a specific reason to use a 100 km × 100 km, instead just to follows previous study of Hirata et al. (2006). The Banerjee model used aftershock distribution and seismic source studies (Lay et al., 2005) and subdivided each segment into two sub-segments to simulate the dip increase with depth following the slab model (Gudmundsson and Sambridge, 1998). The Kreemer model followed previous study used in the Banerjee model. Table 4.1 shows the comparison of coseismic fault models used in this study.

4.3 Analysis strategy of postseismic deformation

We showed the displacement rate of horizontal components in northern Sumatra significantly decreased from the first year to the second year after the 2004 earthquake. On the other hand, the vertical displacement rate looks almost linear in time (see Chapter 3.3.3). This difference implies that multiple physical mechanisms are responsible for the postseismic deformation. Considering its large spatial extent and the long duration over years, we do not consider poroelastic rebound as a responsible physical mechanism of postseismic deformation in this case. Thus, there are two main candidate postseismic mechanisms: (1) viscoelastic relaxation of the asthenosphere driven by coseismic stress changes produced by the 2004 Sumatra-Andaman earthquake, and (2) afterslip on the subducting plate interface. With these two possible physical mechanisms in mind, in order to construct a model for postseismic deformation, we develop a new methodology to distinguish contributions from viscoelastic

relaxation and afterslip. Our basic assumption is that two different time constants found in postseismic deformation time series corresponds to the different physical mechanisms. Thus there are two possibilities. In the first case, the short time constant is associated with the viscoelastic relaxation and the long time constant with the afterslip. In the second case, the opposite correspondences are assumed. In the following, we refer the analysis strategies with the above assumptions as Strategy 1 and 2, respectively. Detailed analysis results with these strategies are discussed in the following sections.

4.3.1 Strategy 1

The first strategy, named Strategy 1, is to correlate the shorter relaxation time with viscoelastic relaxation, and the longer relaxation time with afterslip. In this Strategy 1, we try to interpret horizontal displacements as a result of viscoelastic relaxation then the residual displacements are analyzed to estimate afterslip. Previous studies such as Panet et al. (2010) and Paul et al. (2012) followed the same assumption. In their attempt to investigate postseismic deformation of the 2004 earthquake, they analyzed only the horizontal components to estimate their rheology models.

Here, instead of analyzing the horizontal GPS data to estimate rheology structure, we apply the rheology model of Panet et al. (2010) and Paul et al. (2012) to GPS data in northern Sumatra. In our procedure to calculate viscoelastic relaxation, we use Visco1D (Pollitz et al., 1997). The program calculate viscoelastic relaxation in a layered spherical earth, and in our calculation, we include the gravitational viscoelastic response. Figure 4.1 shows a comparison of GPS time series of ACEH and the calculated viscoelastic displacements using the rheological models of Panet et al. (2010) and Paul et al. (2012). The model of Paul et al. (2012) predicts horizontal displacement at ACEH successfully. However, there are problems in the vertical components. Based on our assumption that viscoelastic relaxation and afterslip are the main causes of postseismic deformation, we subtract viscoelastic relaxation effect from observed

GPS data to obtain “afterslip” displacements. We use the term “afterslip” displacements as displacements that should be attributed to afterslip on the subducting plate interface. The relationship is defined as follows:

$$\nu_{afterslip} = \nu_{observation} - \nu_{viscoelastic} \tag{4.1}$$

where ν represents a displacements vector.

In Figure 4.1(b), we show observed as well as calculated “afterslip” vertical displacements. Calculated curves are drawn for two cases corresponding to model of Panet et al. (2010) and Paul et al. (2012). In this plot, contribution of the viscoelastic relaxation (solid curves) and “afterslip” (dashed curve) have similar relaxation time and amplitude, but in the opposite sense. On the other hand, in horizontal components, afterslip effects are not allowed to exist since the viscoelastic relaxation of Paul et al. (2012) has already fit the observation data almost perfectly. Meanwhile, the model of Panet et al. (2010) cannot fit horizontal displacement at ACEH. We expect afterslip to fit the residual. In the vertical component, however, viscoelastic relaxation and “afterslip” contribution have similar relaxation time and amplitude, but in an opposite sense, just like the case of Paul et al. (2012)’s model.

Result of Strategy 1 has mainly two fatal problems. First, although the viscoelastic relaxation and the afterslip are expected to have similar contribution (in an opposite sense) in the vertical component, only viscoelastic relaxation is effective in the horizontal components. Second, in the vertical component, the viscoelastic relaxation and the afterslip have similar time constant as well as similar amplitude just to cancel out each other. These problems simply indicate that the original assumption of using horizontal displacements to construct a viscoelastic relaxation model was wrong. To find a much better hypothesis, we construct second strategy describe below.

4.3.2 Strategy 2

The second strategy, named Strategy 2, is to correlate the longer relaxation time as viscoelastic relaxation, and the shorter relaxation time as afterslip. In this Strategy 2, the viscoelastic relaxation model is first applied to reproduce the vertical displacement, and residual displacements are analyzed to estimate afterslip.

Since GPS data in northern Sumatra clearly indicate that the relaxation time in the vertical component is longer than the horizontal ones, we adopt the Strategy 2 in our investigation by using the vertical component to reproduce the viscoelastic relaxation model. First we fit the vertical component of daily coordinates at ACEH (2005.16~2009.87) and UMLH (2005.31~2008.56) with the viscoelastic relaxation model. In our first initial estimation process, we search for the optimum rheology model to minimize the chi-squared defined as:

$$\chi^2 = \sum_{i=1}^{n} \left(\frac{obs_i - pred_i}{\sigma_i} \right)^2 \qquad (4.2)$$

where obs_i is the observed displacement, $pred_i$ is the calculated displacement from a viscoelastic relaxation model, and σ_i is the standard deviation.

In the estimation of a rheology model, we employ VISCO1D software to calculate gravitational Maxwell viscoelastic response of a spherical Earth model (Pollitz, 1997). Elastic properties such as rigidity, bulk modulus, and density are defined following PREM (Dziewonski and Anderson, 1981).

In our viscoelastic model, we search for the thicknesses of the elastic layer (*D1*), and the steady state Maxwell viscosity in the asthenosphere (η_M) (Figure 4.2) using a grid search algorithm to minimize χ^2. In our grid search, we test *D1* for every 5 km from 40 to 140 km, and η_M with values for (0.1, 0.2, 0.3, 0.4, 0.5, 0.6, 0.7, 0.8, 0.9, 1.0) x (10^{18}, 10^{19}) Pa s. We use this grid interval as the error for our elastic thickness and viscosity.

Using the first result of rheology model, we can calculate horizontal and vertical

displacements due to viscoelastic relaxation at any point. Then, the estimated "afterslip" displacements are derived by subtracting predicted viscoelastic displacements from observed GPS data.

For our afterslip inversion analysis procedure in northern Sumatra, we divide the plate interface into rectangular subfaults with a size of 30 km × 30 km. To reduce the number of parameters, we fixed the rake angles to 90° following the coseismic slip estimation result in northern Sumatra (e.g. Rhie et al., 2007). We use a fault geometry obtained from a previous study (Rhie et al., 2007) and extend it to the depth of 150 km, following the Slab 1.0 model in northern Sumatra (Hayes et al., 2012).

In order to calculate afterslip distribution on the subducting plate interface, we conduct a linear inversion to estimate slip amount for each sub fault. Green's function for elastic half space by Okada (1985) is used. We construct a linear observation equation for afterslip distribution (m) and "afterslip" displacement (d) as follows.

$$\boldsymbol{d} = \boldsymbol{G}\boldsymbol{m} \tag{4.3}$$

where $\boldsymbol{d}$ is the surface displacements, $\boldsymbol{G}$ is the Green's functions, and $\boldsymbol{m}$ is the afterslip amounts. Applying a smoothness constraint ($\boldsymbol{S}$) on the slip distribution and by weighting it with a smoothness parameter (α^2), then the equation (4.3) in matrix form become:

$$\begin{pmatrix} \boldsymbol{d} \\ \boldsymbol{0} \end{pmatrix} = \begin{pmatrix} \boldsymbol{G} \\ \alpha^2 \boldsymbol{S} \end{pmatrix} \boldsymbol{m} \tag{4.4}$$

The solution for equation (4.4) is given by:

$$\boldsymbol{m} = (\boldsymbol{G}^T \boldsymbol{E}^{-1} \boldsymbol{G} + \alpha^2 \boldsymbol{S})^{-1} \boldsymbol{G}^T \boldsymbol{E}^{-1} \boldsymbol{d} \tag{4.5}$$

then, denoting

$$s(\boldsymbol{m}) = (\boldsymbol{d} - \boldsymbol{Gm})^T \boldsymbol{E}^{-1}(\boldsymbol{d} - \boldsymbol{Gm}) + \alpha^2 \boldsymbol{m}^T \boldsymbol{Sm} \quad (4.6)$$

To determine the appropriate smoothness parameter (α^2) for the observed data, we use the Akaike Bayesian information criterion (ABIC) (Akaike, 1980). Following Yabuki and Matsu'ura (1992), we can express ABIC in the form:

$$ABIC(\alpha^2) = (N + P - M)\, log\, s(\boldsymbol{m}) - P log \alpha^2 + log\|\boldsymbol{G}^T \boldsymbol{E}^{-1} \boldsymbol{G} + \alpha^2 \boldsymbol{S}\| + C \quad (4.7)$$

where N is the total number of data points, P is the number of subfaults, M is the number of model parameters and C is a constant. Search for the value of α^2 is carried as an iterative process, in which α^2 that gives the minimum ABIC is regarded as the optimal value. Once the optimum value of α^2 is determined, denoted as $\hat{\alpha}^2$, we can obtain the best estimate of $\boldsymbol{m}$ using equation (4.5). Using the afterslip distributions results, we re-calculate the "afterslip" displacements by assuming a homogeneous elastic half-space (Okada, 1985).

In the first result of the rheology model, analyzed displacement data contain afterslip effects too. So we correct the afterslip contribution from the original deformation data to obtain the calculated "afterslip" displacements, and then we estimate the rheology model again by subtracting this calculated "afterslip" displacements from observed GPS data. We define the relationship as:

$$v_{estimated\ viscoelastic} = v_{observation} - v_{calculated\ afterslip} \quad (4.8)$$

In this estimation of rheology model, we use the viscoelastic relaxation displacements for

certain time periods of 2005.91~2006.90, 2006-90~2007.90, 2007.90~2008.92 and 2008.92~2009.87. We iterate this procedure until we obtain the minimum χ^2. Figure 4.3 summarizes the analysis procedure utilized in this study.

4.4 Analysis result of Strategy 2

The estimated rheology model depends on the coseismic fault model used in the calculation. Following our analysis procedure of Strategy 2 (Figure 4.3), in our first attempt to calculate the rheological structure model, we estimate a rheology model to fit vertical component of continuous GPS data in northern Sumatra. Here we describe our analysis result of Strategy 2 using various coseismic fault models describe below.

4.4.1 Kreemer model

In our first trial to fits the vertical GPS data in northern Sumatra, estimated rheology parameters based on Kreemer model are *D1* of 75±5 km and η_M of 6.0±1.0 x 10^{18} Pa s. Following our procedure shown in Figure 4.3, we use this rheological structure to calculate afterslip distribution on the fault plane in northern Sumatra. We then correct the afterslip contribution from the original deformation data and estimate the rheology model again. For time period between 2005.91~2006.90, the maximum afterslip amount was 0.72 m located between 20~40 km depth (Figure 4.4(a)). In this time period, the afterslip distribution and the coseismic rupture were compensatory each other (Figure 4.5(a)). In the next consecutive year, the maximum afterslip amount significantly reduced to 0.28 m during 2006.90~2007.90, and slightly reduced to 0.27 m and 0.19 m between 2007.90~2008.92, and 2008.87~2009.87 (Figure 4.4(a)). The total seismic moment released by afterslip during these consecutive time periods were 0.87 x 10^{21} N m (M_w 7.9), 0.39 x 10^{21} N m (M_w 7.7), 0.37 x 10^{21} N m (M_w 7.6), and 0.27 x

10^{21} N m (M_w 7.5), respectively (Table 4.2).

The final solution of rheological structure model of Kreemer model has *D1* of 75±5 km and η_M of 6.0±1.0 x 10^{18} Pa s (Figure 4.6(a)). This model is considered to be best-fit one because the later result of rheology structure model yields similar result with the previous one. The best-fit rheological structure parameters used in VISCO1D for Kreemer model can be found in the Appendix B. Table 4.3(a) summarizes the χ^2 result of each calculation process for Kreemer model.

4.4.2 Banerjee model

The initial estimated rheology parameters based on Banerjee model are *D1* of 70±5 km and η_M of 8.0±1.0 x 10^{18} Pa s. During the next consecutive process of 1st, 2nd, and 3rd, the rheology parameter are *D1* of 75±5 km and η_M of 1.0±1.0 x 10^{19} Pa s, *D1* of 70±5 km and η_M of 1.0±1.0 x 10^{19} Pa s, *D1* of 65±5 km and η_M of 1.0±1.0 x 10^{19} Pa s. Because the 3rd process results in a larger χ^2 value than the 2nd one, we conclude the rheology parameters of the 2nd process are the best-fit ones (Table 4.3(b); Figure 4.6(b); Appendix B).

The maximum afterslip amount from the best-fit model during 2005.91~2006.90 was 0.67 at 20~40 km depth, where the afterslip distribution and the coseismic rupture were compensatory each other (Figure 4.5(b)). The total seismic moment of afterslip was 0.94 x 10^{21} N m (M_w 7.9). The maximum afterslip significantly reduced to 0.27 m with total seismic moment was 0.43 x 10^{21} N m (M_w 7.7) during 2006.90~2007.90. For time periods between 2007.90~2008.92, and 2008.87~2009.87, a small change in afterslip moments of 0.38 x 10^{21} N m (M_w 7.6) and 0.29 x 10^{21} N m (M_w 7.6) with the maximum afterslip amount of 0.20 m and 0.20 m (Figure 4.4(b); Table 4.2).

4.4.3 Fujii model

Using Fujii model, the initial estimated rheology parameters are *D1* of 45±5 km and η_M of

4.0±1.0 x 10^{18} Pa s. In the current calculation, the 1st process produced similar result of rheology model to the preliminary model. Hence, these parameters are the best-fit model (Table 4.3(c); Figure 4.6(c); Appendix B).

From this model, the maximum afterslip of 0.35 m at 15~40 km depth (Figure 4.5(c)) with total seismic moment of afterslip was 0.29 x 10^{21} N m (M_w 7.6) calculated during 2005.91~2006.90. During 2006.90~2007.90, the maximum slip was 0.14 m with total seismic moment was 0.13 x 10^{21} N m (M_w 7.3). From 2007.90~2008.92 onwards, based on GPS displacements, afterslip did not observed in northern Sumatra (Figure 4.4(c); Table 4.2).

.

4.4.4 Rhie model

In this model, the initial estimated rheology parameters are *D1* of 75±5 km and η_M of 8.0±1.0 x 10^{18} Pa s, the 1st process are *D1* of 70±5 km and η_M of 8.0±1.0 x 10^{18} Pa s, the 2nd process are *D1* of 65±5 km and η_M of 8.0±1.0 x 10^{18} Pa s, and the 3rd process are *D1* of 60±5 km and η_M of 8.0±1.0 x 10^{18} Pa s. In the calculation, the 3rd process resulted in a larger χ^2 value than the 2nd one, so we conclude the rheology parameters of the 2nd process is the best-fit model (Table 4.3(d); Figure 4.6(d); Appendix B).

During 2005.91~2006.90, the seismic moment of afterslip was 1.12 x 10^{21} N m (M_w 8.0) with the maximum afterslip amount was 0.90 m located at 20~40 km depth. During this time period, the afterslip distribution concentrated in the deeper extension of the coseismic rupture (Figure 4.5(d)). The seismic moment significantly decreased to 0.52 x 10^{21} N m (M_w 7.7) with the maximum afterslip amount of 0.37 m during 2006.90~2007.90. During 2007.90~2008.92, and 2008.87~2009.87, the seismic moment was estimated to be 0.45 x 10^{21} N m (M_w 7.7) and 0.36 x 10^{21} N m (M_w 7.6), with maximum afterslip amount of 0.28 m and 0.22 m, respectively (Figure 4.4(d); Table 4.2).

4.5 The best coseismic fault models

Our χ^2 results show that the best χ^2 of Kreemer model, Banerjee model, Fujii model , and Rhie model have 114.75, 132.57, 749.25, and 104.22, respectively (Table 4.3). We perform a chi-squared statistical test for each best-fit model using a probability critical value of 1% based on the chi-square distribution table (Appendix C).The degree of freedom (*dof*) of all best-fit model is 74, which obtained from number of data in the matrix **d** subtracts rank of matrix **G** in the equation (4.4), which include the smoothing matrix, times number of time periods used in the afterslip inversion analysis in addition to model parameters in the viscoelastic relaxation calculation. Because the calculated χ^2 of Rhie model is less than the critical value of 105.202 (Appendix C), we accept the hypothesis that the Rhie model is better than other models to explain the postseismic deformation after the 2004 earthquake.

In another study of investigating the best coseismic fault of the 2004 earthquake, Poisson et al. (2011) used a different approach to our study. They examined the simulated tsunami from various coseismic fault models and compare the results with the satellite altimetry data. In their analysis, they employed the coseismic fault models of Banerjee et al. (2007), Fujii et al. (2007), Piatanesi et al. (2007), Rhie et al. (2007), and Chlieh et al. (2007). Their conclusion of the best coseismic fault model which explains simulated tsunami very well is the Rhie model.

4.6 Afterslip in northern Sumatra

In Figure 4.5(d) we compare the estimated afterslip distribution during 2005.91~2006.90 with the coseismic slip by Rhie et al. (2007) in northern Sumatra. It is clearly shown that the distributions of the afterslip and the coseismic slip are compensatory each other. Similar characteristics have been found for other interplate megathrust events (e.g. Yagi et al., 2003;

Miyazaki et al., 2004). Such a compensatory distribution between coseismic and postseismic slip is consistent with the idea that afterslip is driven by the change in stress due to the mainshock (e.g. Marone et al., 1991).

In the time period between 2005.91~2006.90, one of the estimated afterslip patches calculated using Rhie model is located at 100~120 km depth (Figure 4.5d). Our deep afterslip result indicates that afterslip occurred at the transition zone between elastic crust and asthenosphere. There are two possible arguments for deep afterslip in northern Sumatra.

First, the extrapolation of laboratory-derived flow laws suggested the melting of the mantle begins at depth of ~120 km at temperatures of 700~1200°C, and so it is possible that the mantle rock at the depth of 100-120km holds significant strength (e.g . Hirth and Kohlsteadt, 1996; Kessel et al., 2005). Second, the deep afterslip is a kinematic solution to fit the displacements data in northern Sumatra. In our afterslip calculation, we obtain large error of afterslip result because of GPS data limitation. During time period 2005.91~2006.90, our calculated result for Rhie model is showing significant amount of afterslip where the magnitude of afterslip larger than the estimation error (Figure 4.7). We test the spatial resolution test of our current analysis using a checkerboard test. We assign a synthetic afterslip of 0.75 cm and no afterslip, and compare this to the afterslip distribution result. We calculate four different scenarios shown in Figure 4.8. The resolution test indicate that our analysis cannot resolve afterslip near trench at shallower than 20 km depth. However, we can distinguish existence of afterslip at 100 km depth. So from this checkerboard test, our result of deep afterslip indicate a kinematic solution and the fault's strength at deeper fault to slip asseismically during 2005.91~2006.90.

According to our calculations, afterslip at depth generates a very limited contribution to the vertical displacement at the ground surface. Based on displacements results, the afterslip accounts for only 15% and 13% of the observed vertical displacement at ACEH and UMLH during 2005.91~2006.90 (Table 4.4). For time period of 2006.90~2007.90, relative afterslip

contribution was significantly reduced to 1% at ACEH, but increased to 22% at UMLH. This happened because the large afterslip distribution patch at deeper fault between 100~120 km depths in northern Sumatra was significantly reduced from the maximum afterslip amount of 0.62 m to 0.26 m. On the other hand, the large afterslip distribution patch at the depth between 20~40 km still exist during 2006.90~2007.90 with maximum afterslip amount of 0.38 m just west-off UMLH site (Figure 4.4(d)). The large afterslip patch during 2006.90~2007.90 at west-off UMLH site generates large subsidence at this site. During time period of 2007.90~2008.92, the relative contribution of afterslip to the vertical displacements at UMLH was similar to previous one, in the sense of vertical displacement was increasing from -1.5 cm to -1.1 cm. On the other hand, the vertical displacement at ACEH was very small, for less than 1mm. This result clearly explains why the shorter relaxation time feature is not evident in the observed vertical displacement at ACEH.

Relative contribution of viscoelastic horizontal displacement contribution at GPS sites in northern Sumatra increases in time (Table 4.4). This result is confirmed by the reduction of afterslip distribution during 4 years time period of 2005.91~2009.87 in northern Sumatra (Figure 4.4(d)).

4.7 Summary

Difference in the displacement rate between horizontal and vertical components implies that multiple physical mechanisms are responsible for the postseismic deformation; they are viscoelastic relaxation and afterslip. We construct two analysis strategies to investigate the postseismic deformation after the 2004 earthquake. These strategies are (1) Strategy 1, that correlates the shorter relaxation time with viscoelastic relaxation, and the longer relaxation time with afterslip, and (2) Strategy 2, that correlates the longer relaxation time with viscoelastic

relaxation, and the shorter relaxation time with afterslip.

Strategy 1, which was used by previous studies but has fatal problems regarding the vertical displacement data. First, calculated vertical displacements of the viscoelastic relaxation and the afterslip are expected to have similar contribution (in an opposite sense), but only viscoelastic relaxation is effective in the horizontal components. Second, in the vertical component, the viscoelastic relaxation and the afterslip have similar time constant as well as similar amplitude just to cancel out each other. These problems simply indicate that the original assumption of using horizontal displacements to construct a viscoelastic relaxation model was wrong.

On the other hand, the Strategy 2 we used in this study solves the problem of the Strategy 1. Our rheology model with the Maxwell viscoelastic relaxation plus afterslip, is more appropriate to explain GPS data in northern Sumatra than any other models previously proposed. Different coseismic fault models used to calculate the best-fit rheology model generate different rheological structure, thus create different afterslip amount in northern Sumatra. The calculated afterslip displacements result on four coseismic fault models looks reasonable too. We discuss our analysis of our investigation result in Chapter 5.

Table 4.1. Comparison of coseismic fault models used in this study.

Model	Data Source	Maximum Slip (m)	Seismic Moment	Fault Resolution (Length x Width)
Kreemer model	Far-field GPS	11.3 at ~5°N	6.11 x 10^{22} N m (M_w 9.13)	Coarse (largest size are 355 km x 116 km)
Banerjee model	Near- & Far- field GPS	19.4 at ~5°N	7.62 x 10^{22} N m (M_w 9.22)	Coarse (largest size are 355 km x 116 km)
Fujii model	Tide gauge and satellite altimetry	24.6 at ~3°N	6.00 x 10^{22} N m (M_w 9.10)	Fine (100 km x 100 km)
Rhie model	Seismic & Near-field GPS	35.3 at ~4.5°N	7.12 x 10^{22} N m (M_w 9.20)	Finest (30 km x 30 km)

Table 4.2. Calculated afterslip moment in northern Sumatra

Remarks		Kreemer model	Banerjee model	Fujii model	Rhie model
2005.91~2006.90	Seismic moment (N m)	0.87 x 10^{21} (M_w 7.9)	0.94 x 10^{21} (M_w 7.9)	0.29 x 10^{21} (M_w 7.6)	1.12 x 10^{21} (M_w 8.2)
	Max slip (m)	0.72	0.67	0.35	0.9
2006.90~2007.90	Seismic moment (N m)	0.39 x 10^{21} (M_w 7.7)	0.43 x 10^{21} (M_w 7.7)	0.13 x 10^{21} N m (M_w 7.3)	0.52 x 10^{21} (M_w 7.7)
	Max slip (m)	0.28	0.27	0.14	0.37
2007.90~2008.92	Seismic moment (N m)	0.37 x 10^{21} (M_w 7.6)	0.38 x 10^{21} (M_w 7.6)	-	0.45 x 10^{21} (M_w 7.7)
	Max slip (m)	0.27	0.2	-	0.28
2008.87~2009.87	Seismic moment (N m)	0.27 x 10^{21} (M_w 7.5)	0.29 x 10^{21} (M_w 7.6)	-	0.36 x 10^{21} (M_w 7.6)
	Max slip (m)	0.19	0.2	-	0.22

Table 4.3. The χ^2 result of best-fit rheology model at each calculation process calculated using (a) Kreemer model (b) Banerjee model (c) Fujii model (d) Rhie model.

a) Kreemer model

Process	Best Fit Rheology Parameter D1 (km)	η_H (Pa s)	χ^2	Description
0	75	6.0×10^{18}	80.28	Fitting to vertical component only
1	75	6.0×10^{18}	114.75	Fitting to horizontal and vertical component

b) Banerjee model

Process	Best Fit Rheology Parameter D1 (km)	η_H (Pa s)	χ^2	Description
0	70	8.0×10^{18}	53.55	Fitting to vertical component only
1	75	1.0×10^{19}	656.21	Fitting to horizontal and vertical component
2	70	1.0×10^{19}	132.57	Fitting to horizontal and vertical component
3	65	1.0×10^{19}	173.88	Fitting to horizontal and vertical component

c) Fujii model

Process	Best Fit Rheology Parameter D1 (km)	η_H (Pa s)	χ^2	Description
0	45	4.0×10^{18}	140.80	Fitting to vertical component only
1	45	4.0×10^{18}	749.25	Fitting to horizontal and vertical component

d) Rhie model

Process	Best Fit Rheology Parameter D1 (km)	η_H (Pa s)	χ^2	Description
0	75	8.0×10^{18}	66.60	Fitting to vertical component only
1	70	8.0×10^{18}	120.42	Fitting to horizontal and vertical component
2	65	8.0×10^{18}	104.22	Fitting to horizontal and vertical component
3	60	8.0×10^{18}	109.62	Fitting to horizontal and vertical component

Table 4.4. Displacement percentage due to viscoelastic relaxation and afterslip at every GPS sites in northern Sumatra using Rhie model.

Site	Viscoelastic Relaxation				Afterslip				Component
	2005.91~2006.90	2006.90~2007.90	2007.90~2008.82	2008.92~2009.87	2005.91~2006.90	2006.90~2007.90	2007.90~2008.82	2008.92~2009.87	
ACEH	36%	47%	55%	62%	64%	53%	45%	38%	Horizontal
UMLH	29%	47%	50%	-	71%	53%	50%	-	
BEUN	41%	42%	50%	60%	59%	58%	50%	40%	
CELA	38%	-	-	60%	62%	-	-	40%	
GEUM	39%	58%	-	58%	61%	42%	-	42%	
JERM	34%	60%	-	58%	66%	40%	-	42%	
KAWA	53%	-	-	50%	47%	-	-	50%	
MBMG	40%	65%	49%	57%	60%	35%	51%	43%	
ACEH	85%	99%	98%	97%	15%	1%	2%	3%	Vertical
UMLH	87%	78%	74%	-	13%	22%	26%	-	

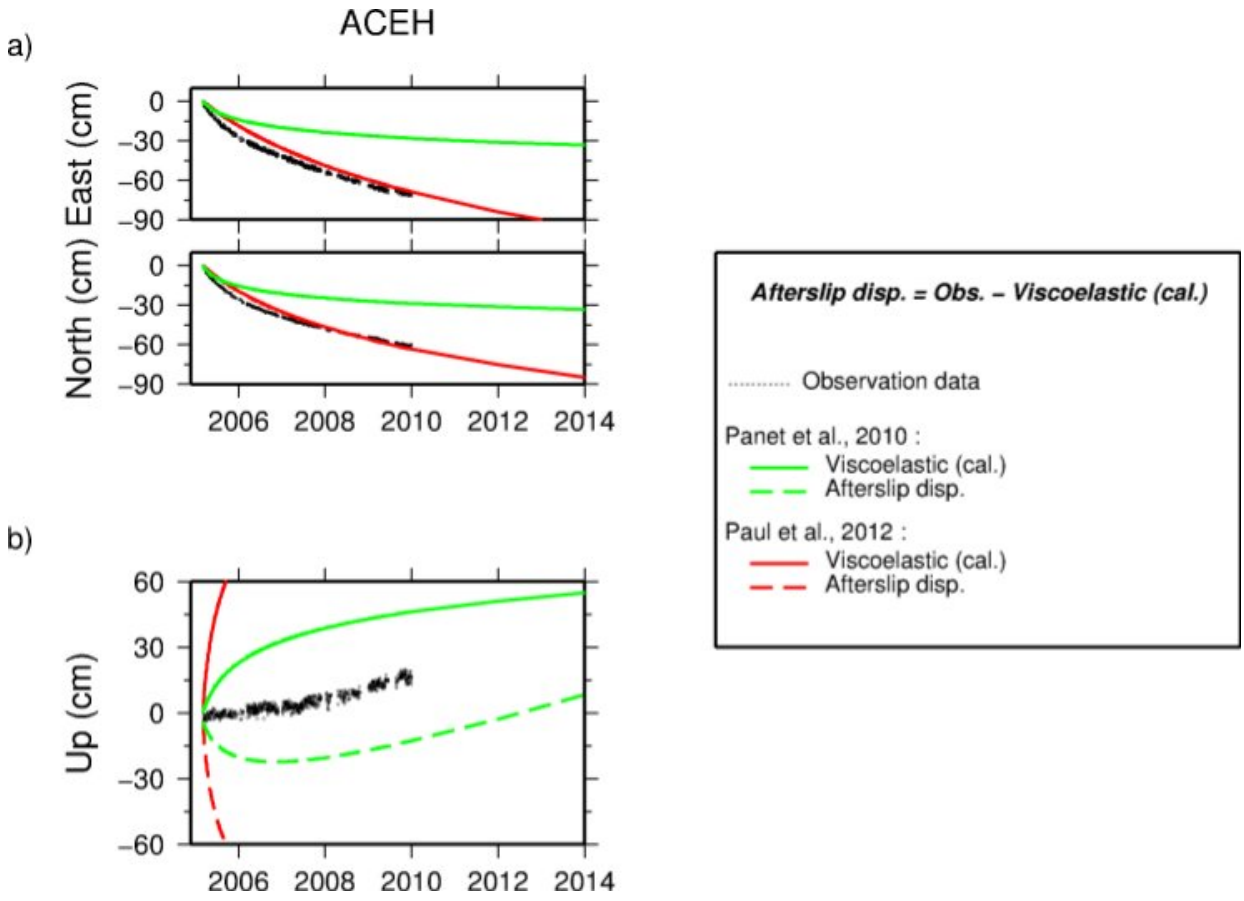

Figure 4.1. Time series of continuous GPS data in northern Sumatra, ACEH. (a) Horizontal components. (b) Vertical component. Dashed black dots in each figure imply the observation data. Green line indicates viscoelastic displacement of Panet et al. (2010) model. Red line denotes viscoelastic displacement of Paul et al. (2012) model. Dashed red line and dashed green line represent expected afterslip displacement of each viscoelastic model, respectively.

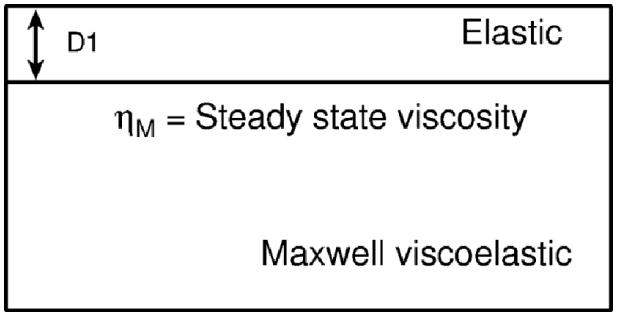

Figure 4.2. Two dimensional viscoelastic structure used in this study, constructed on elastic upper crust and Maxwell viscoelastic asthenosphere. Two parameters to describe this model are the depth of elastic layer ($D1$) and steady state viscosity (η_M).

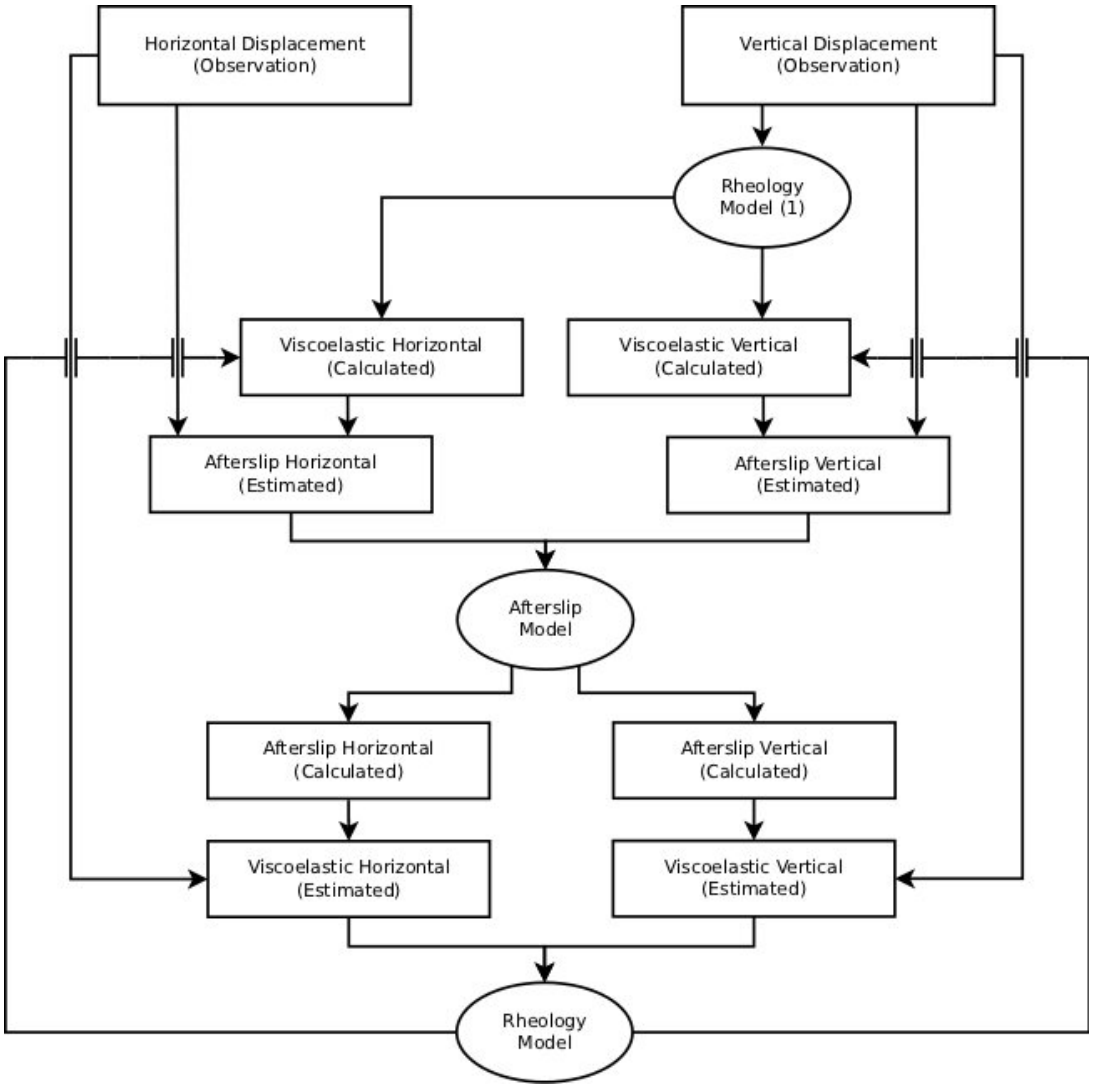

Figure 4.3. Flowchart method of Strategy 2 used in this study. In this procedure, vertical displacement will be use as preliminary information to find the rheology model, and obtained the calculated horizontal and vertical displacements of viscoelastic relaxation. Using this calculated of viscoelastic relaxation, we estimate the "afterslip" displacements by subtracting the calculated viscoelastic displacements from observed GPS data. The "afterslip" displacement will be utilized to invert afterslip distributions on the plate interface, and these afterslip distributions will account for the calculated "afterslip" displacement. By subtracting these calculated "afterslip" displacements from observed GPS data, we obtained the estimated displacement of viscoelastic relaxation to re-produce the rheology model structure. This iteration process will be continuously calculated until minimum χ^2 obtained.

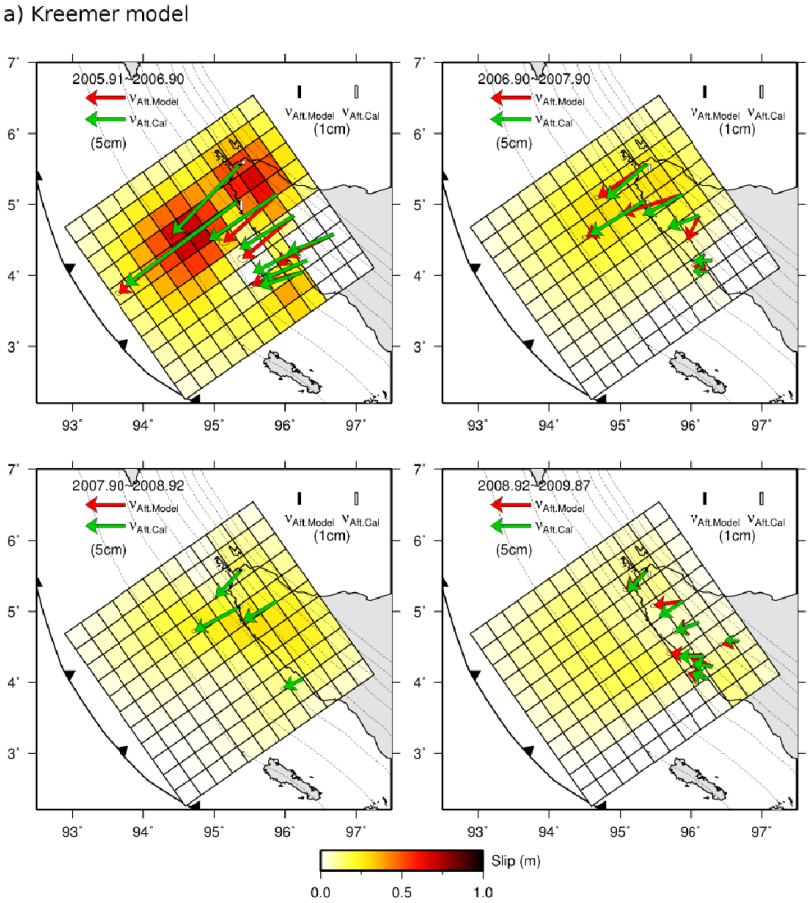

Figure 4.4. Afterslip inversion analysis of four time periods in northern Sumatra; 2005.91~2006.90, 2006.90~2007.90, 2007.90~2008.92, and 2008.92~2009.87. Red arrows and black bars ($v_{\text{Aft. Est.}}$) denote estimated "afterslip" displacements of horizontal and vertical components, while green arrows and white bars ($v_{\text{Aft. Cal.}}$) indicate calculated "afterslip" displacements of horizontal and vertical components. Black square box represents fault area used in the inversion analysis, which is discretized into 30 km × 30 km rectangular patches. Inverted apparent cumulative afterslip in northern Sumatra shown by gradient color. Dashed black lines denote Slab 1.0 model every 20 km (Hayes et al., 2012). (a) Kreemer model. (b) Banerjee model. (c) Fujii model. (d) Rhie model.

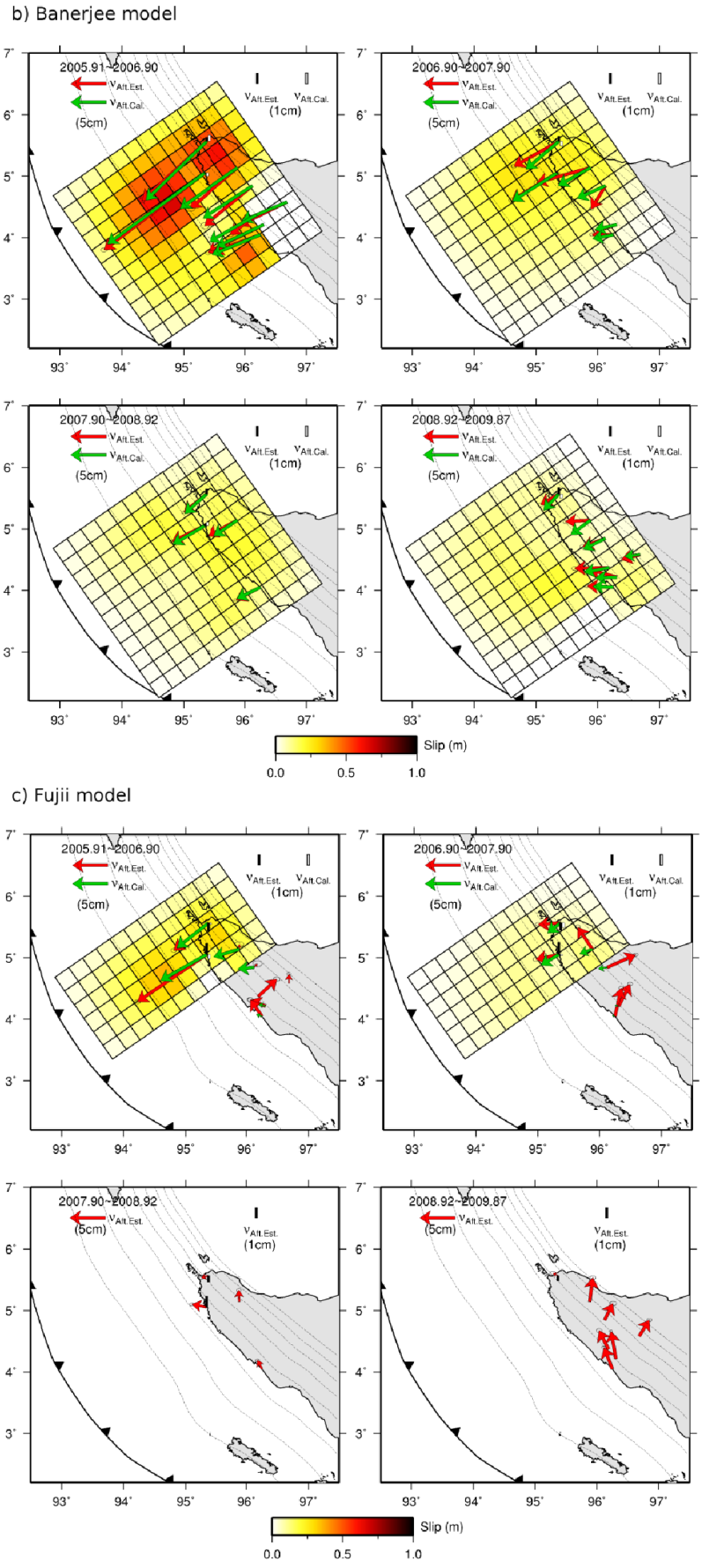

Figure 4.4. (*continued*)

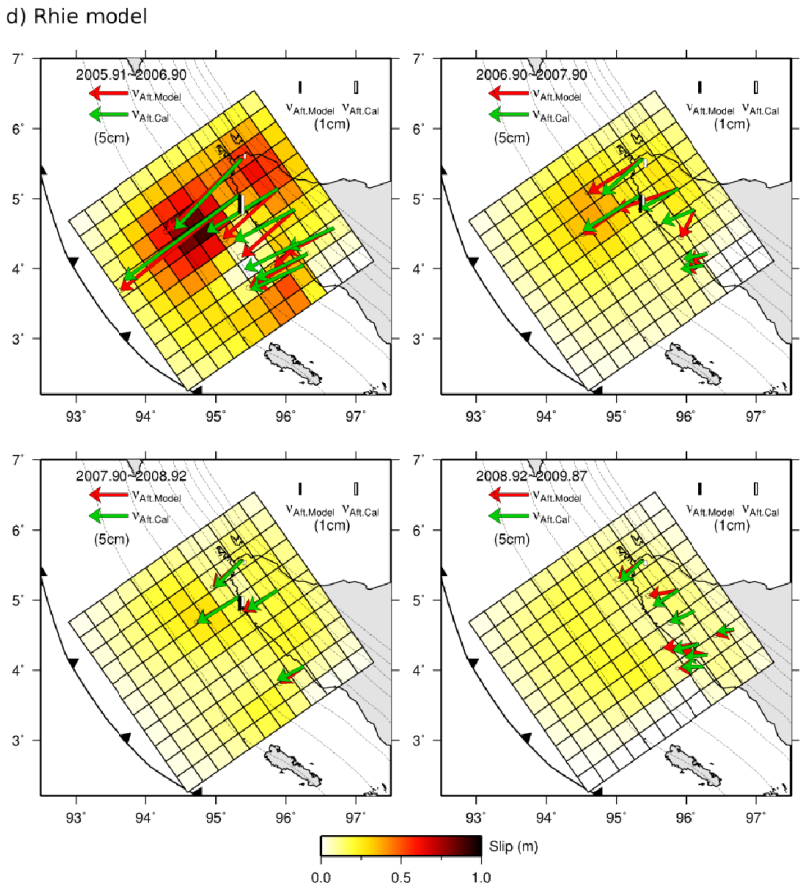

Figure 4.4. (*continued*)

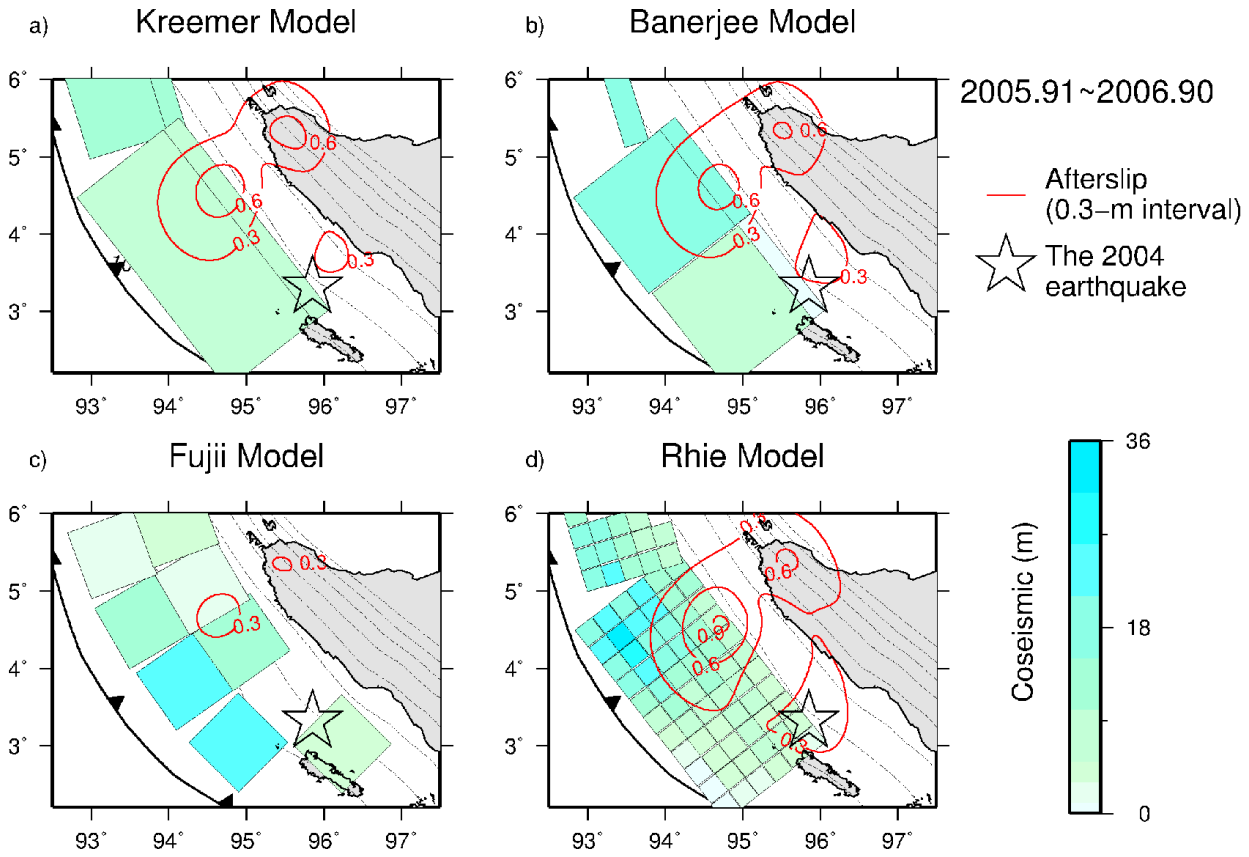

Figure 4.5. Coseismic slip rupture and afterslip contour in northern Sumatra in northern Sumatra between 2005.91~2006.90 for various coseismic fault models. (a) Kreemer model. (b) Banerjee model. (c) Fujii model. (d) Rhie model. In each figures, dashed black lines denotes Slab1.0 model every 20 km (Hayes et al., 2012). Red contour indicates afterslip with 0.3 m intervals. White star identifies the epicenter of the 2004 earthquake.

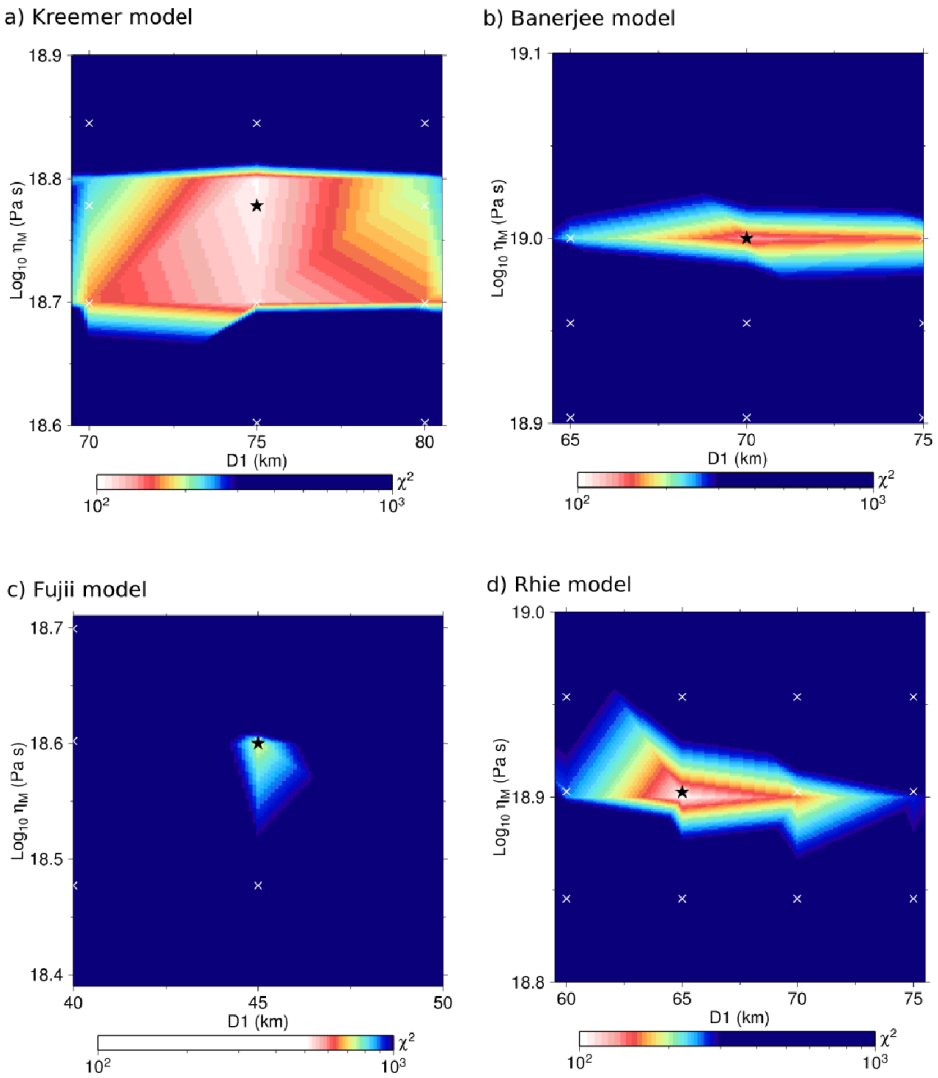

Figure 4.6. Best misfit (χ^2) calculated using grid search. Black star indicates the minimum χ^2 value, and white crosses mark the location of calculated model. (a) Kreemer model. (b) Banerjee model. (c) Fujii model. (d) Rhie model.

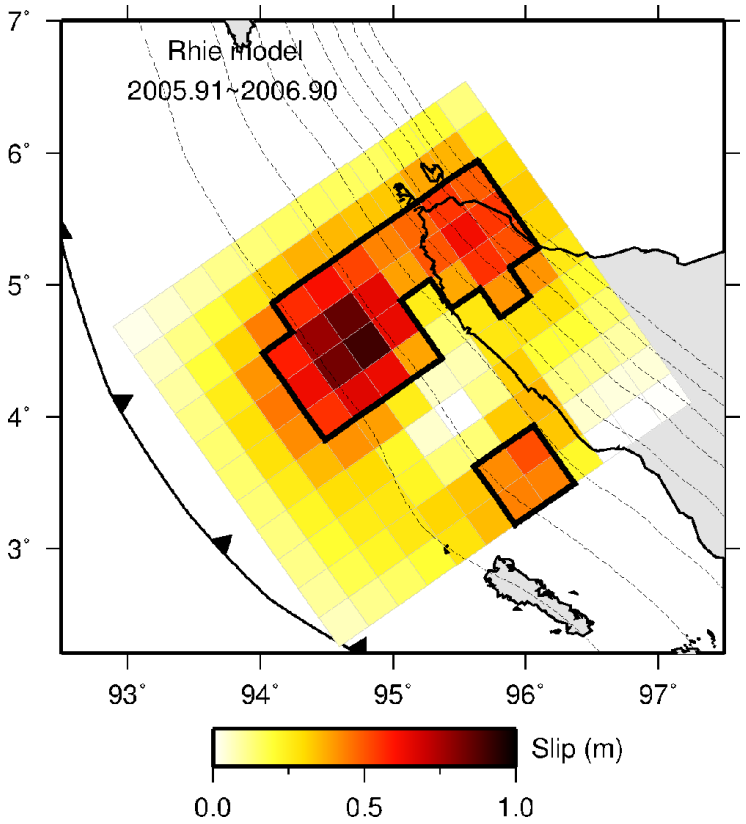

Figure 4.7. Significant afterslip where slip magnitude larger than the estimation error marked by thick black lines calculated for Rhie model during time period of 2005.91~2006.90.

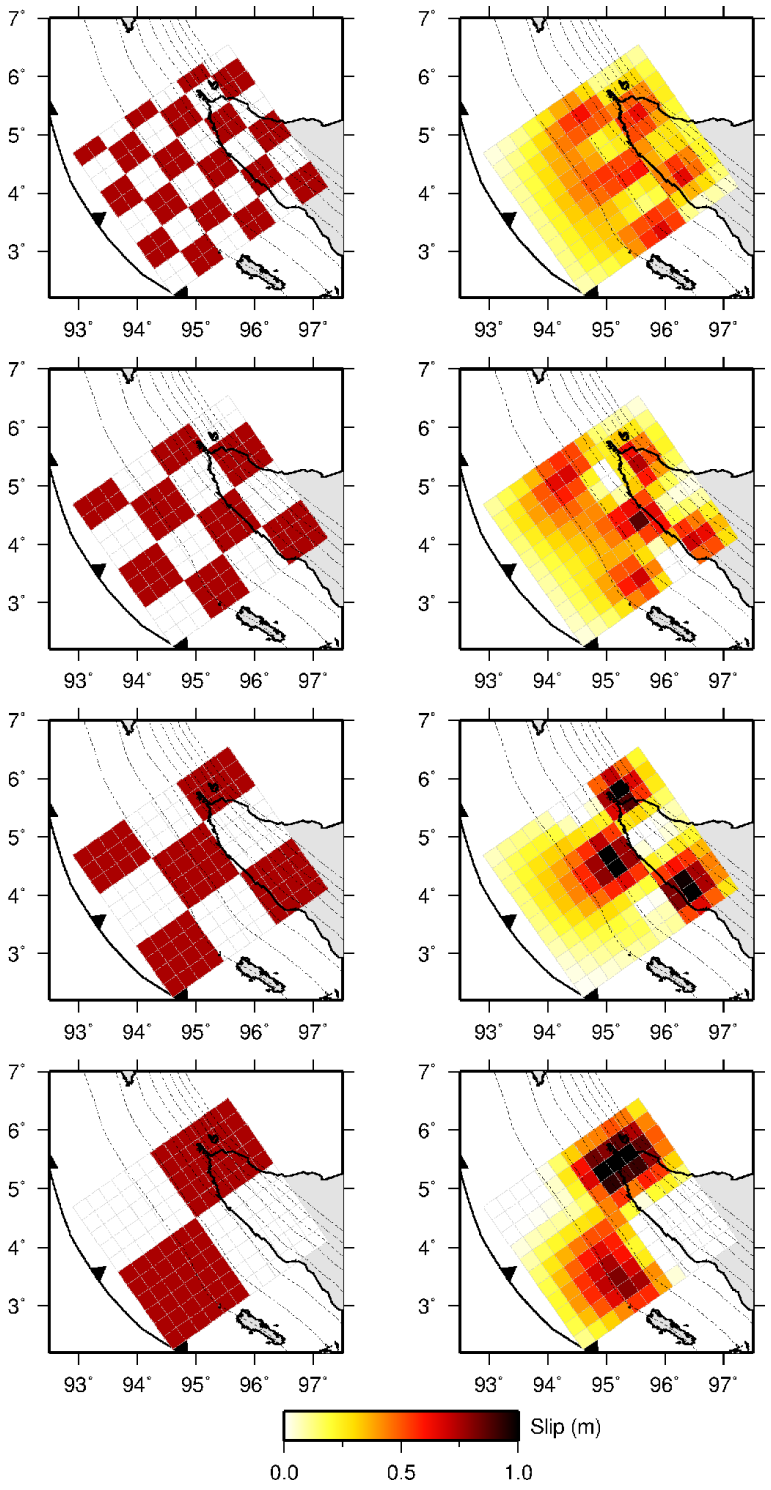

Figure 4.8. Checkerboard test for a synthetic afterslip at four different scenarios. Red color indicates a synthetic afterslip of 0.75 cm, while white implies no afterslip.

Chapter 5

Discussion

5.1 Rheological structure model

We showed that assumptions of previous studies on postseismic deformation were invalid (see Chapter 4.3.1). Therefore their result of viscoelastic structure, such as elastic thickness, is questionable. Using a different approach from previous studies, our postseismic calculation indicates reasonable result. We showed that vertical displacements in northern Sumatra with a longer time constants is attributed to viscoelastic relaxation. Also, the residual displacements are attributed to afterslip showing a time-dependent decay during 4 years time period of 2005.91~2009.87 (Table 4.4).

Our best-fit rheology of Rhie model yields an elastic thickness of 65 km (Table 4.3(d)). In comparison to different studies using 3-D shear wave velocity structure in South China Sea and surrounding region, Wu et al. (2004) estimated the thickness the lithosphere in this particular region. They found that the lithosphere thickness varies in the range of 45~65 km depth. In northern Sumatra, their result of lithosphere thickness is similar to our elastic thickness obtained using Rhie model, which is 65±5 km.

Pollitz et al. (2006) and Panet et al. (2010) analyzed postseismic GPS time series data in the Sundaland block to estimate a rheology model (see Chapter 2.3). Both reached a similar

conclusion that the asthenosphere (depth of 60~220km) is characterized by the Burgers rheology. According to Panet et al. (2010), the asthenospheric rheology is described by a transient Kelvin viscosity of 4.0 x 10^{17} Pa s and a steady state Maxwell viscosity of 8.0 x 10^{18} Pa s. Their conclusion regarding the transient viscosity is different from the result of the current study. Since our study is based on GPS data in northern Sumatra, different data sets to those used by previous studies, it is worthwhile comparing these models and discussing why we obtained a different conclusion. For Thailand region, we use the GPS data of Satirapod et al. (2008), which were obtained from campaign observations (see Chapter 3.2.2). Time series comparison between GPS data, our best-fit rheology model and calculated viscoelastic model of Panet et al. (2010) for Thailand shows in Figure 5.1.

As shown in Figure 5.1, our rheology model reproduces the long-term features of the GPS time series in Thailand. This result is reasonable since the Maxwell viscosity estimated in this study is similar to the steady state Maxwell viscosity of Panet et al. (2010). In our model, the remaining short-term transient feature is attributed to the afterslip. In Figure 5.2 we show the time series of GPS data in northern Sumatra, our model, and viscoelatic calculation with models of Panet et al. (2010) and Paul et al. (2012). From the comparison based on GPS data in northern Sumatra, we show that the Burgers rheology model of Panet et al. (2010) underpredicts the horizontal displacement but overpredicts the vertical displacement in northern Sumatra (see Chapter 4.3.1). That is, the short-term deformation caused by transient rheology is not consistent with the GPS data in northern Sumatra. On the other hand, our best-fit rheology from Rhie model in addition to afterslip explains the GPS data in northern Sumatra very well. This result clearly indicates that our combined model of Maxwell viscoelastic relaxation and afterslip is more appropriate for GPS data in northern Sumatra than the transient Burgers rheology.

5.2 Postseismic deformation in Andaman Islands

Our analysis indicates the combined model of Maxwell viscoelastic relaxation and afterslip explains GPS data in northern Sumatra very well. The 2004 earthquake rupture, however, is not limited in northern Sumatra region. Instead, the rupture extended northward towards Andaman Islands. Thus we need to examine if our model is applicable to the Andaman region. We use the 20 GPS displacement vectors from January 2005 to February 2006, and 6 vectors from February 2006 to February 2007 of Gahalaut et al. (2008). Along the Sunda trench, the Slab 1.0 model is available until south of Little Andaman. So for the fault parameters in Andaman Islands, we extend the fault parameters at the south of Little Andaman northwards towards Andaman Islands and use these parameters in our calculation. In our calculation, we divide the sub faults into 30 km x 30 km with the down-dip limit of the fault at is 81 km depth, and we fix the rake to 105°, following coseismic fault model in this region (Rhie et al., 2007). The procedure to calculate afterslip in Andaman Islands is similar to the ones used in northern Sumatra (see Chapter 4.3.2).

Our estimated afterslip is located at the down-dip part of the plate boundary as shown in Figure 5.3. Our result of afterslip distribution is generally consistent with previous studies by Gahalaut et al. (2008) and Paul et al. (2012), but the total afterslip moment from January 2005 to February 2006 is 1.1 x 10^{21} N m (M_w 7.9), which is only 29% of the previous estimate 3.8 x 10^{21} N m (M_w 8.3) by Gahalaut et al. (2008). In addition, our afterslip estimate from February 2006 to February 2007 is 0.2 x 10^{21} N m (M_w 7.4), almost one tenth of the previous estimate 1.9 x 10^{21} N m (M_w 8.1) (Gahalaut et al., 2008). In Gahalaut et al. (2008), the whole postseismic displacement was interpreted as a result of afterslip, but our analysis indicates there is significant contribution from viscoelastic relaxation in this region. It should be noted that the interpretation of postseismic deformation is highly sensitive to assumptions.

5.3 Postseismic deformation using all GPS data sets

In this analysis, we investigate postseismic deformation of the 2004 earthquake using all available GPS data sets located in northern Sumatra, Thailand, and Andaman-Nicobar. There is a problem for this integrated analysis that GPS data in each area covers different time period.

Satirapod et al. (2008) fit the GPS data in Thailand using logarithmic function (see equation 2.10). Their fitting parameters obtained under ITRF2000 reference frame. We use these parameters to calculate displacements at GPS sites in Thailand for the time period of 2005.91~2006.90, then we transformed the displacements into Sundaland bock reference frame using equation (3.2) and equation (3.3). In Andaman-Nicobar region, we use 7 sites that have three campaign observations to determine the fitting parameters using equation (2.10). Table 5.1 shows the fitting parameters for GPS data in Thailand and Andaman-Nicobar used in this study. Based on the calculated displacements for all GPS sites between 2005.91~2006.90, we construct a combined postseismic deformation model with Maxwell viscoelasitc relaxation and interplate afterslip.

First, we calculate the displacements due to viscoelastic relaxation, and consider the residual as a result of cumulative afterslip of the 2004 earthquake located from northern Sumatra to Andaman-Nicobar region. Second, using only the “afterslip” displacement for GPS sites in Andaman Islands, we invert the afterslip distribution in this region. Third, we calculate the displacements due to afterslip in northern Sumatra and Andaman Islands for GPS sites in Thailand and Nicobar Islands. By subtracting the cumulative “afterslip” displacements to these displacements, we consider the residual displacements as a result of afterslip in the Nicobar Islands and adjacent region. We invert these “afterslip” displacements, using similar procedure to our inversion analysis (see Chapter 4.3.2). Finally, using the inverted afterslip distribution in northern Sumatra, Andaman Islands and Nicobar Islands, we calculate the “afterslip” displacements for each GPS sites. Figure 5.4 shows our afterslip analysis result along the Sunda

trench in northern Sumatra towards Andaman Islands.

Results show that during 2005.91~2006.90, the seismic moment released by afterslip in northern Sumatra is 1.12 x 10^{21} N m (M_w 8.0), in the Andaman Islands is 0.47 x 10^{21} N m (M_w 7.7), and in Nicobar Islands is 0.64 x 10^{21} N m (M_w 7.8). So the total seismic moment during this period is 2.23 x 10^{21} N m (M_w 8.2). The maximum afterslip calculated in northern Sumatra during this time period is 0.90 m located at 20~40 km depth, in Andaman Islands is 0.75 m located at 40~55 km depth, and in Nicobar Islands is 0.35 m located at 35~50 km depth. Our calculation result also indicates that afterslip distribution located at deeper fault below the main rupture. Finally, calculated "afterslip" displacements obtain from the afterslip distribution show its agreement to the estimated "afterslip" displacements and match the displacement model very well (Figure 5.4). These results clearly indicate our postseismic deformation model is applicable to the GPS datasets in northern Sumatra, Thailand and Andaman-Nicobar.

5.4 Limitation of the current model

In our analysis, we use the continuous data of ACEH and UMLH that were installed two months after the 2004 earthquake (Figure 3.7). Although we did not find any significant contribution due to time-dependent (Burgers transient) rheology, we also note that our analysis does not cover the early two months postseismic period after the 2004 earthquake. In that sense, there is a possibility that such early postseismic data may reflect different rheological properties. However, using the current available data sets in our analysis, we believe that our conclusion of combined model of Maxwell viscoelastic relaxation and afterslip is robust, at least for a time scale longer than 1 year.

The modeling of the postseismic deformation in this study is based on several simplifying assumptions. One such assumption is assuming a layered structure without a subducted slab

(non-slab structure model). The existence of a slab can significantly affect the viscoelastic relaxation pattern, as pointed out by Yoshioka and Suzuki (1999) and Pollitz et al. (2008).

Yoshioka and Suzuki (1999) mentioned that in the structure model with a slab, stress relaxation is limited in the mantle wedge, while in the non-slab structure model, stress relaxation occurs extensively in the top of the asthenosphere (Figure 5.5). Thus for the same rheological structure, the non-slab structure model will have a larger horizontal displacement and a downward surface displacement dominates more than the structure model with slab. They analyzed this discrepancy as the result of different behavior of stress relaxation between the two models. In order to obtain similar displacement with the non-slab model, then the structure model with slab should have a shallower elastic thickness and/or a smaller viscosity value. When the elastic thickness is thinner, the underlying viscoelastic volume will be larger, and will make the asthenospheric flow occurs easily. Underlying the importance of employing a realistic earth structure, investigation of the postseismic deformation using 3-D viscoelastic structure with GPS data in northern Sumatra should be analyzed in the future.

5.5 Summary

Combining all the results of postseismic deformation in northern Sumatra, Thailand, and Andaman invert from GPS datasets, we conclude the same rheology model, consisting of a 65±5 km-thick surface elastic layer overlying Maxwell viscoelastic asthenosphere whose viscosity is 8.0±1.0 x 10^{18} Pa s, is basically applicable to all the GPS datasets of postseismic deformation of the 2004 earthquake. There is also significant contribution of afterslip, which is located at the deeper extension of the coseismic rupture and has a characteristic decay time of about 3 years. We believe this study gives the first-order description of the postseismic deformation of the 2004 earthquake.

Table 5.1. Best-fit logarithmic parameters for GPS sites in (a) Thailand (b) Andaman-Nicobar

(a) Thailand GPS sites

Remarks	PUHK		CHON		BANH		UTHA	
	E	**N**	**E**	**N**	**E**	**N**	**E**	**N**
A(cm)	-15.7	-4.1	-2.9	-2.0	-7.5	-3.2	-2.0	-1.7
T_A	0.624	0.072	0.177	0.183	0.291	0.143	0.166	0.151

(b) Andaman-Nicobar GPS sites

Remarks		A(cm)	T_A(yr)
CBAY	E	-6.93	0.16
	N	-4.04	-0.20
	H	1.00	-2.06
HBAY	E	-9.48	-0.12
	N	1.00	0.00
	H	8.16	-0.06
PORT	E	-5.23	-0.13
	N	1.38	-0.02
	H	2.67	-0.20
SLBY	E	-8.68	-0.08
	N	-2.52	-0.06
	H	2.82	-0.14

Remarks		A(cm)	T_A(yr)
BTNG	E	-7.61	-0.1
	N	-3.14	-0.05
	H	3.08	-0.23
MBDR	E	-2.12	-0.04
	N	1.00	-2.06
	H	1.10	-0.04
DGPR	E	-8.25	-0.06
	N	1.00	-2.09
	H	1.00	-3.55

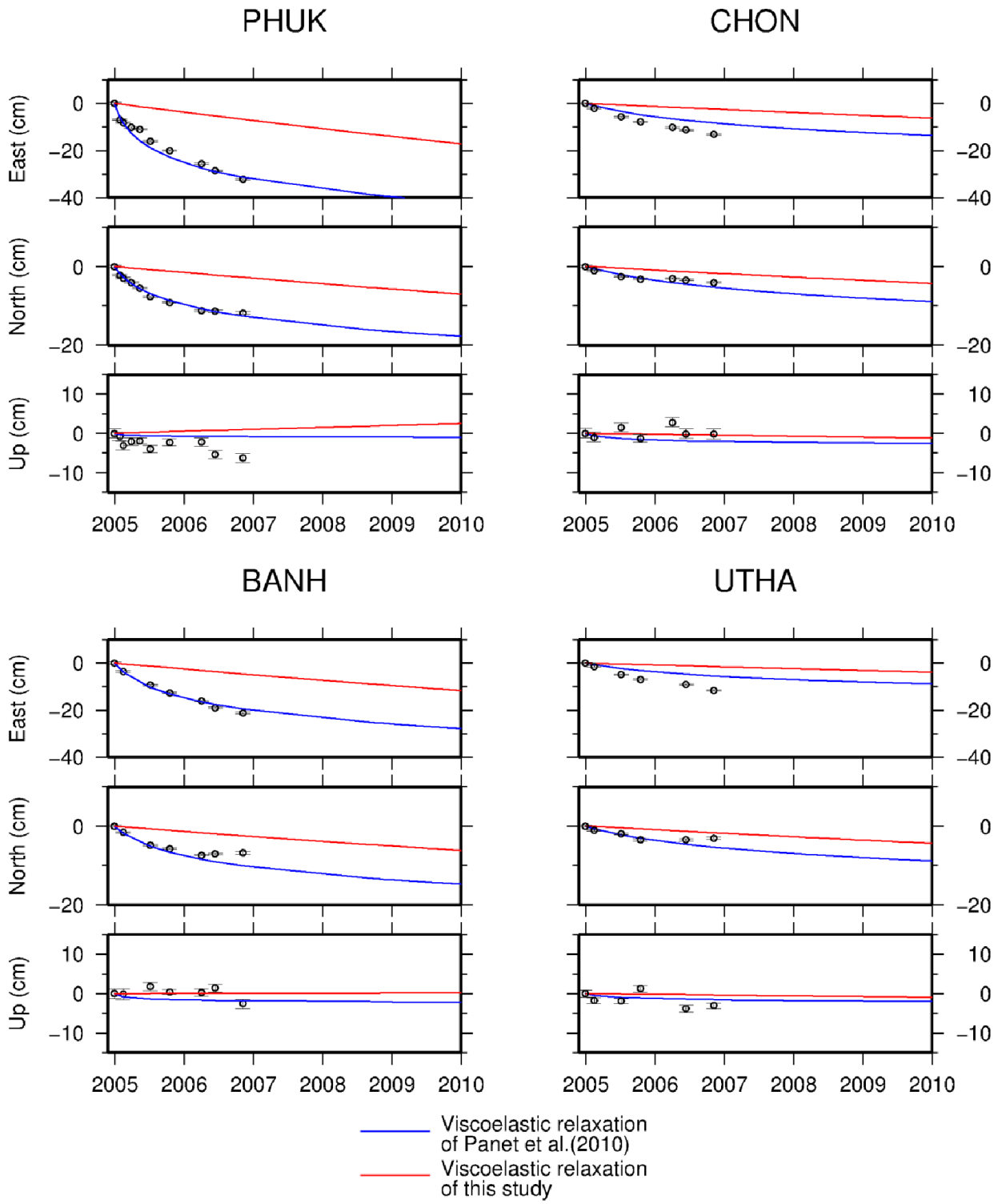

Figure 5.1. Time series comparison of calculated viscoelastic displacement using Panet et al. (2010) model (blue color) and our best-fit model (red color) at four GPS sites in Thailand (PHUK, BANH, CHOM, and UTHA). Time series displacement obtained from Satirapod et al. (2008).

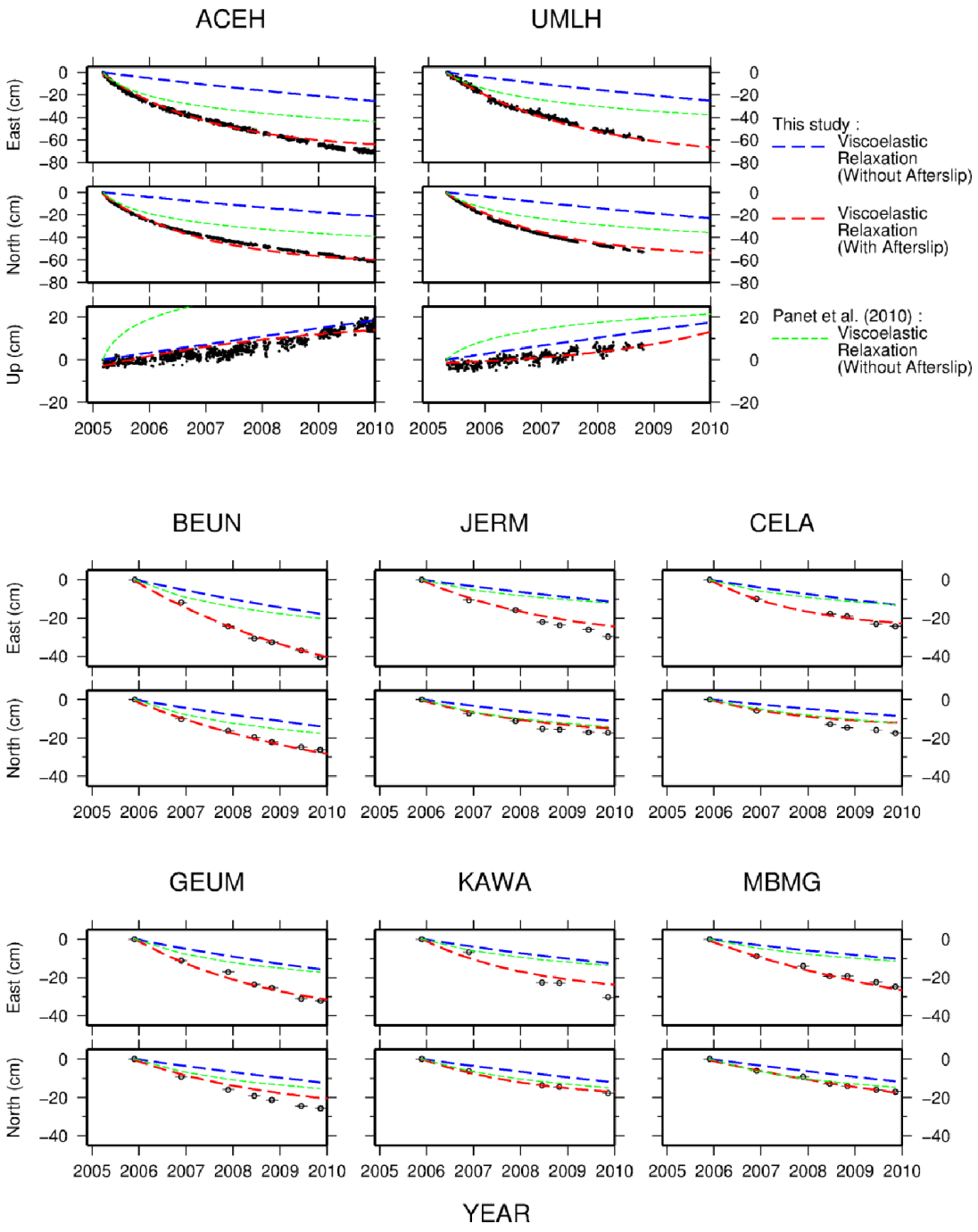

Figure 5.2. Displacement time series of GPS sites located in northern Sumatra (black). Red line indicates surface displacements due to multiple mechanisms of afterslip and viscoelastic relaxation with rheological parameters as follows; $D1$ = 65 km, and η_M = 8.0 x 10^{18} Pa s. Blue dashed line represents surface displacement due to viscoelastic relaxation only. Green dashed line denotes calculated viscoelastic displacement using Panet et al. (2010) model.

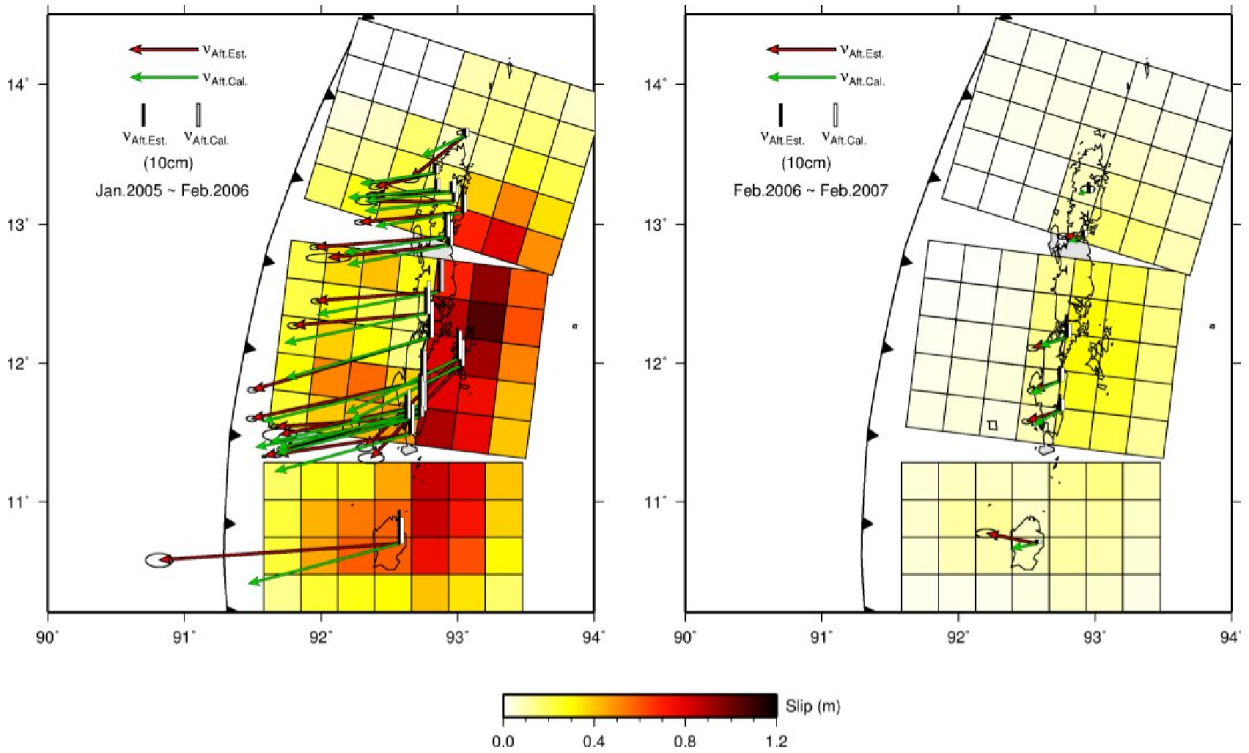

Figure 5.3. Afterslip inversion analysis for Andaman Islands for time period of January 2005 to February 2006 (left figure) and February 2006 to February 2007 (right figure). Red arrows and black bars ($v_{\text{Aft. Est.}}$) denote estimated "afterslip" displacements of horizontal and vertical components with reference to the Sundaland block reference frame, while green arrows and white bars ($v_{\text{Aft. Cal.}}$) indicate calculated "afterslip" displacements of horizontal and vertical components from afterslip inversion.

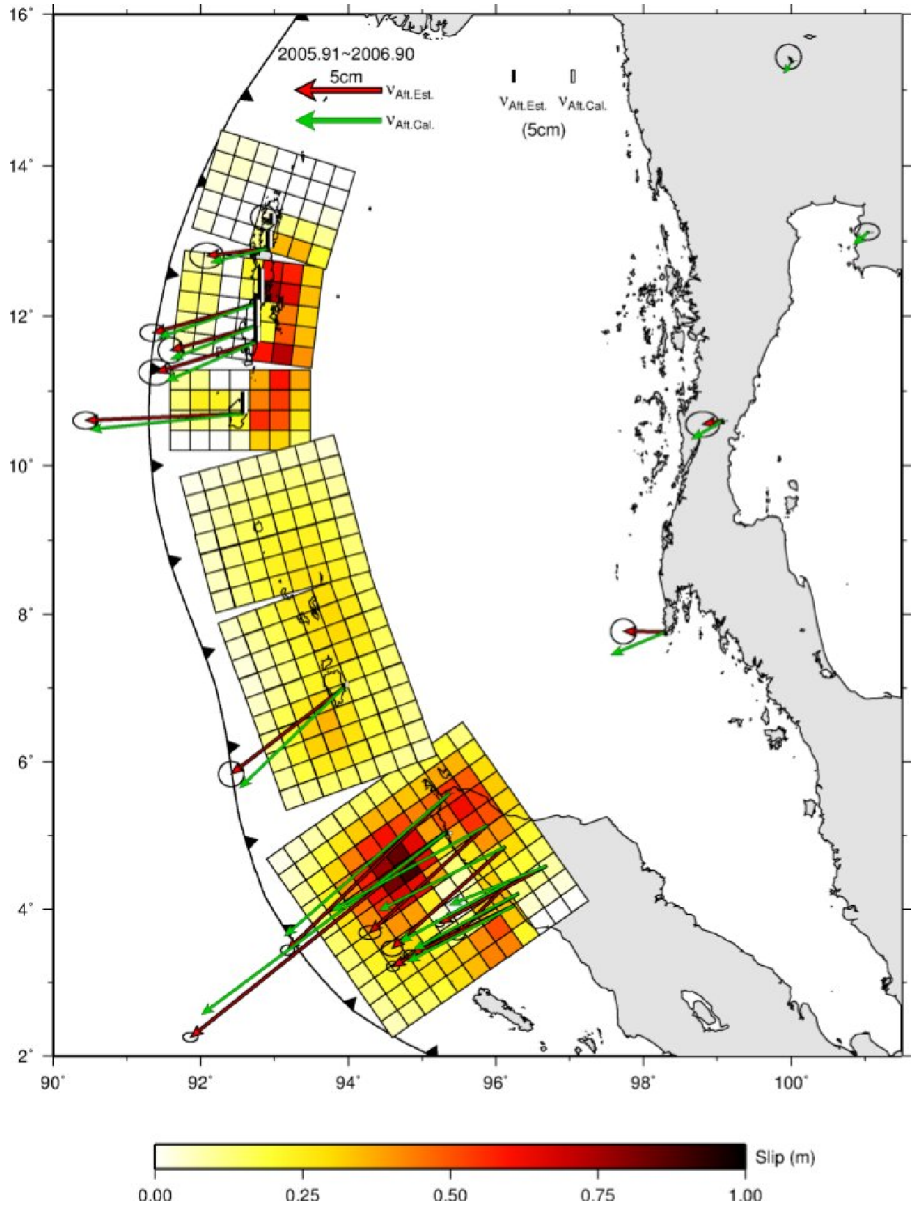

Figure 5.4. Afterslip distribution inverted from GPS data sets in Andaman-Nicobar, northern Sumatra and Thailand for time periods of 2005.91~2006.90. Red arrows ($v_{\text{Aft. Est.}}$) denote estimated "afterslip" displacements of horizontal components, while green arrows ($v_{\text{Aft. Cal.}}$) indicate calculated "afterslip" displacements of horizontal components from afterslip inversion.

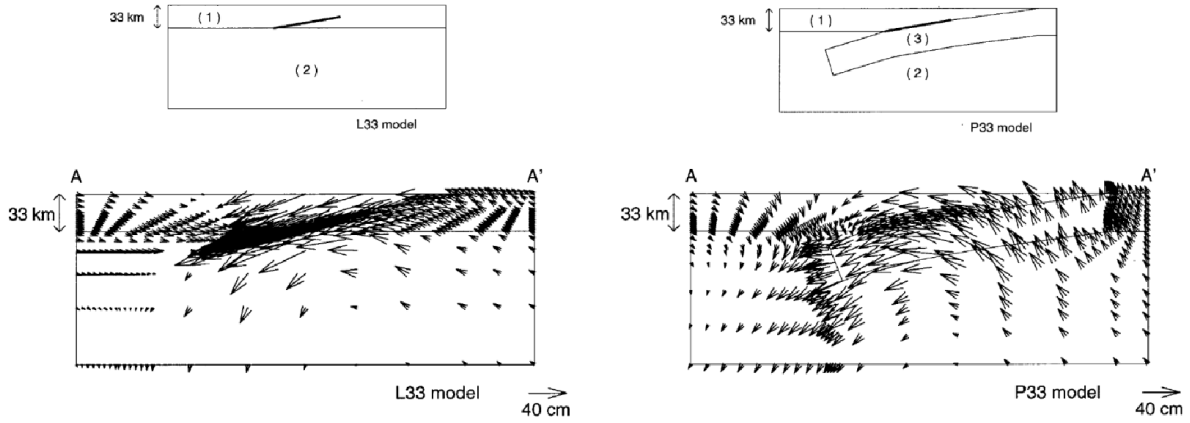

Figure 5.5. Similar to Figure 4 and Figure 7 of Yoshioka and Suzuki, 1999) (Top figures) Models for viscoelastic structures (Bottom figures) Comparisons calculated postseismic displacement between layered structure model without slab (left-hand side panel) and with slab (right-hand side panel).

Chapter 6

Conclusions

The coseismic stress of the M9.2 2004 Sumatra-Andaman earthquake was large and extensive, causing significant postseismic deformation detected by GPS data in various location, such as in Andaman Islands (Gahalaut et al., 2008; Paul et al., 2012), Nicobar Islands (Gahalaut et al., 2008), or even Thailand (Pollitz et al., 2006; Satirapod et al., 2008; Panet et al., 2010). These GPS data displacements are characterized by a trench-ward motion on the continental side of the plate boundary. There have been many studies to explain the postseismic deformation of the 2004 earthquake. These studies are different one another in both in the physical mechanism assumed and observation data analyzed. Some studies assumed only afterslip (Paul et al., 2007; Gahalaut et al., 2008), or viscoelastic (Pollitz et al., 2006; Pollitz et al., 2008; Hoechner et al., 2011), is the main mechanism responsible for the postseismic deformation process, while others argued that combined model of viscoelastic relaxation and afterslip (Panet et al., 2010; Paul et al., 2012; Hu and Wang, 2012) is the main mechanism.

Horizontal GPS data in Andaman-Nicobar and Thailand showed transient deformation that some of the previous studies inferred as a result of afterslip (e.g. Gahalaut et al., 2008), viscoelastic relaxation with the Burgers rheology (e.g. Pollitz et al., 2006), or a steady state Maxwell rheology (Paul et a., 2012). Clearly, the interpretation of this transient deformation is not clear.

Continuous GPS data in northern Sumatra clearly show temporal decays reflecting

postseismic deformation. It is noticeable that horizontal displacements significantly decreased with time, while the vertical component looks almost linear in time. The difference in the temporal changes between horizontal and vertical components implies that multiple physical mechanisms are responsible for the postseismic deformation; we assume that they are viscoelastic relaxation and afterslip. We construct two analysis strategies to investigate the postseismic deformation after the 2004 earthquake. These strategies are (1) Strategy 1 to correlate the shorter relaxation time with viscoelastic relaxation, and the longer relaxation time with afterslip, and (2) Strategy 2 to correlate the longer relaxation time with viscoelastic relaxation, and the shorter relaxation time with afterslip.

Strategy 1, which was used by previous studies, has fatal problems regarding the vertical displacement data. First, using continuous GPS data in northern Sumatra, the calculated vertical displacements of the viscoelastic relaxation and the afterslip are expected to have similar contribution (in an opposite sense), but only viscoelastic relaxation is effective in the horizontal components. Second, in the vertical component, the viscoelastic relaxation and the afterslip have similar time constant as well as similar amplitude just to cancel out each other. These problems simply indicate that the original assumption of using horizontal displacements to construct a viscoelastic relaxation model was wrong.

In order to apply Strategy 2 to the dataset, a new iterative method to estimate both the viscoelatic structure and afterslip distribution is developed. Starting from the estimation of rheological parameters based on vertical GPS data in northern Sumatra, afterslip and the rheological parameters are estimated one after another until the minimum χ^2 is obtained. By applying this method, we can decompose the postseismic deformation into the contribution of viscoelastic relaxation and that of afterslip. We assume a simple rheological model with an elastic lithosphere overlying a Maxwell viscoelastic substratum, in which the lithosphere thickness and the Maxwell viscosity are the rheological parameters. This strategy is applied to the GPS data in northern Sumatra with four different coseismic fault models by Kreemer et al.

(2006), Banerjee et al. (2007), Fujii and Satake (2007), and Rhie et al.(2007). The final solution of rheological structure model of Kreemer model are *D1* of 75±5 km and η_M of 6.0±1.0 x 10^{18} Pa s, those based on Banerjee model are *D1* of 70±5 km and η_M of 1.0±1.0 x 10^{19} Pa s, those based on Fujii model are *D1* of 45±5 km and η_M of 4.0±1.0 x 10^{18} Pa s, and those based on Rhie model are 65±5 km and η_M of 8.0±1.0 x 10^{18} Pa s. We find that the coseismic fault model of Rhie et al. (2007) results in the least χ^2 of 104.22 and that the Maxwell viscoelastic relaxation plus afterslip model successfully explains GPS data in northern Sumatra. For time period between 2005.91~2006.90, the estimated maximum afterslip was 0.90 m located at 20~40 km depth and the total seismic moment released by afterslip was 1.12 x 10^{21} N m (M_w 8.2). During 2005.91~2006.90, the estimated afterslip accounts for only 15% of the observed vertical displacement at ACEH in northern Sumatra, and the contribution is only 1% during 2006.90~2007.90. This result clearly explains why the shorter relaxation time is not evident in the observed vertical displacement at continuous GPS sites in northern Sumatra.

In this study, significance of a time-dependent (Burgers) rheology, suggested by previous studies (Pollitz et al., 2006; Panet et al., 2010), is not supported. The current study suggests that the rapid transient signal at the early postseismic stage was caused mainly by afterslip, not by the viscoelastic relaxation. The vertical component in northern Sumatra is a strong evidence for this result.

This study also demonstrates that the rheology model estimated from GPS data in northern Sumatra is applicable to postseismic deformation of the 2004 Sumatra-Andaman earthquake recorded in other regions such as the Andaman Islands and Thailand. The rheology model can reproduce the long-term trends of GPS data in Thailand while the rapid transient signals in the early postseismic stage can be attributed to the afterslip in Andaman and Nicobar region. Also, it is shown that the postseismic deformation in the Andaman region contains significant contribution of viscoelastic relaxation. Seismic moment release by the afterslip from January 2005 to February 2006 estimated in this study is 1.1 x 10^{21}N m (M_w 7.9), which is 29 %

of the previous estimate by Gahalaut et al. (2008). So it should be noted that the interpretation of postseismic deformation is highly sensitive to assumptions.

This study is based on a simplified layered structure model. So the result may be changed if we take 3-dimensional structure including subducted slab into account. Also, the satellite gravity data analyzed in previous studies are not analyzed in the current study. These problems will be solved in the future.

Through this study, a model of the rheological structure and afterslip distribution is constructed for the postseismic deformation of the 2004 Sumatra-Andaman earthquake. This is a comprehensive model in that it can reproduce main features of all the available GPS data in northern Sumatra, Andaman, and Thailand. This study provides unique as well as important insights into the rheological structure of the asthenosphere and postseismic relaxation processes of great earthquakes.

Bibliography

Akaike, H. (1980). Likelihood and the Bayes procedure, in Bernardo, J. M., DeGroot, M. H.,Lindley, D. V. and Smith, A. F. M.(eds.), *Bayesian Statistics, pp. 143–166*, University Press, Valencia, Spain.

Altamimi, Z., Collilieux, X., Legrand, J., Garayt, B., and Boucher, C. (2007). ITRF2005: A new release of the International Terrestrial Reference Frame based on time series of station positions and Earth Orientation Parameters. *Journal of Geophysical Research: Solid Earth (1978–2012)*, 112(B9).

Altamimi, Z., Collilieux, X., and Métivier, L. (2011). ITRF2008: an improved solution of the international terrestrial reference frame. *Journal of Geodesy,* 85(8), 457-473.

Altamimi, Z., Sillard, P., & Boucher, C. (2002). ITRF2000: A new release of the International Terrestrial Reference Frame for earth science applications. *Journal of Geophysical Research: Solid Earth (1978–2012)*, 107(B10), ETG-2.

Ammon, C. J., Ji, C., Thio, H. K., Robinson, D., Ni, S., Hjorleifsdottir, V., ... and Wald, D. (2005). Rupture process of the 2004 Sumatra-Andaman earthquake. *Science*, 308(5725), 1133-1139.

Árnadóttir, T., Jónsson, S., Pollitz, F. F., Jiang, W., and Feigl, K. L. (2005). Postseismic deformation following the June 2000 earthquake sequence in the south Iceland seismic zone. *Journal of Geophysical Research: Solid Earth (1978–2012)*, 110(B12).

Banerjee, P., Pollitz, F. F., and Bürgmann, R. (2005). The size and duration of the Sumatra-Andaman earthquake from far-field static offsets. *Science*, 308(5729), 1769-1772.

Banerjee, P., Pollitz, F., Nagarajan, B., and Bürgmann, R. (2007). Coseismic slip distributions of the 26 December 2004 Sumatra–Andaman and 28 March 2005 Nias earthquakes from GPS static offsets. *Bulletin of the Seismological Society of America,* 97(1A), S86-S102.

Beavan, J., Motagh, M., Fielding, E. J., Donnelly, N., and Collett, D. (2012). Fault slip models of the 2010–2011 Canterbury, New Zealand, earthquakes from geodetic data and observations of postseismic ground deformation. *New Zealand Journal of Geology and Geophysics*, 55(3), 207-221.

Bedford, J., Moreno, M., Baez, J. C., Lange, D., Tilmann, F., Rosenau, M., ... and Vigny, C. (2013). A high-resolution, time-variable afterslip model for the 2010 Maule Mw= 8.8, Chile megathrust earthquake. *Earth and Planetary Science Letters*, 383, 26-36.

Bock, Y., Prawirodirdjo, L., Genrich, J. F., Stevens, C. W., McCaffrey, R., Subarya, C., ... & Calais, E. (2003). Crustal motion in Indonesia from global positioning system measurements. *Journal of Geophysical Research: Solid Earth (1978–2012)*, 108(B8).

Bruhat, L., Barbot, S., & Avouac, J. P. (2011). Evidence for postseismic deformation of the lower crust following the 2004 Mw6. 0 Parkfield earthquake. *Journal of Geophysical Research: Solid Earth* (1978–2012), 116(B8).

Bürgmann, R., Segall, P., Lisowski, M., and Svarc, J. (1997). Postseismic strain following the

1989 Loma Prieta earthquake from GPS and leveling measurements. *Journal of Geophysical Research: Solid Earth (1978–2012)*,102(B3), 4933-4955.

Bürgmann, R., and G. Dresen, 2008. Rheology of the lower crust andupper mantle: evidence from rock mechanics, geodesy, and field observations. *Annual Review of Earth and Planetary Sciences,* 36, 531-567.

Chen, H. Y., Yu, S. B., Kuo, L. C., and Liu, C. C. (2006). Coseismic and postseismic surface displacements of the 10 December 2003 (M~ w 6.5) Chengkung, eastern Taiwan, earthquake. *Earth, Planets, and Space*, 58(1), 5-21.

Chlieh, M., Avouac, J. P., Hjorleifsdottir, V., Song, T. R. A., Ji, C., Sieh, K., Sladen, A., Hebert, H., Prawirodirdjo, L., Bock, Y., and Galetzka, J. (2007). Coseismic slip and afterslip of the great Mw 9.15 Sumatra–Andaman earthquake of 2004. *Bulletin of the Seismological Society of America,* 97(1A), S152-S173.

Dach, R., Hugentobler, U., Fridez, P., and Meindl, M. (2007). Bernese GPS software version 5.0. Astronomical Institute, University of Bern.

Diao, F., Xiong, X., and Wang, R. (2011). Mechanisms of transient postseismic deformation following the 2001 Mw 7.8 Kunlun (China) earthquake. *Pure and applied geophysics*, 168(5), 767-779.

Dieterich, J. H. (1979). Modeling of rock friction: 1. Experimental results and constitutive equations. *Journal of Geophysical Research: Solid Earth (1978–2012),* 84(B5), 2161-2168.

Dogan, U., Demir, D. Ö., Çakir, Z., Ergintav, S., Ozener, H., Akoğlu, A. M., ... and Reilinger, R. (2014). Postseismic deformation following the Mw 7.2, 23 October 2011 Van

earthquake (Turkey): Evidence for aseismic fault reactivation. *Geophysical Research Letters*, 41(7), 2334-2341.

Dziewonski, A. M., and Anderson, D. L. (1981). Preliminary reference Earth model. *Physics of the Earth and Planetary Interiors,* 25(4), 297-356.

Freed, A. M. (2005). Earthquake triggering by static, dynamic, and postseismic stress transfer. *Annu. Rev. Earth Planet. Sci.*, 33, 335-367.

Freed, A. M. (2007). Afterslip (and only afterslip) following the 2004 Parkfield, California, earthquake. *Geophysical Research Letters*, 34(6).

Freed, A. M., Bürgmann, R., Calais, E., Freymueller, J., & Hreinsdóttir, S. (2006). Implications of deformation following the 2002 Denali, Alaska, earthquake for postseismic relaxation processes and lithospheric rheology. *Journal of Geophysical Research: Solid Earth (1978–2012)*, 111(B1).

Fujii, Y., and Satake, K. (2007). Tsunami source of the 2004 Sumatra–Andaman earthquake inferred from tide gauge and satellite data. *Bulletin of the Seismological Society of America,* 97(1A), S192-S207.

Gahalaut, V. K., Nagarajan, B., Catherine, J. K., and Kumar, S. (2006). Constraints on 2004 Sumatra–Andaman earthquake rupture from GPS measurements in Andaman–Nicobar Islands. *Earth and Planetary Science Letters*, 242(3), 365-374.

Gahalaut, V.K., Jade, S., Catherine, J.K., Gireesh, R., Ananda, M.B., Kumar, P., Narsaiah, M., Jafri, S.S.H., Ambikapathy, A., Bansal, A., Chadha, R.K., Gupta, D.C., Nagarajan, B., and Kumar, S. (2008). GPS measurements of postseismic deformation in the Andaman-Nicobar region following the giant 2004 Sumatra-Andaman earthquake. *Journal*

of Geophysical Research: Solid Earth (1978–2012), 113(B8).

Gudmundsson, Ó., & Sambridge, M. (1998). A regionalized upper mantle (RUM) seismic model. *Journal of Geophysical Research: Solid Earth* (1978–2012), 103(B4), 7121-7136.

Hao, M., Cui, D., Wang, Q., Gan, W., Qin, S., & Wang, W. (2013). Spatial distribution of afterslip for the 2008 Wenchuan earthquake, China. *Geophysical Journal International*, ggt223.

Hashimoto, M., Choosakul, N., Hashizume, M., Takemoto, S., Takiguchi, H., Fukuda, Y., & Fujimori, K. (2006). Crustal deformations associated with the great Sumatra-Andaman earthquake deduced from continuous GPS observation. *Earth Planets Space*, 58, 127-139.

Hayes, G. P., Wald, D. J., and Johnson, R. L. (2012). Slab1.0: a three-dimensional model of global subduction zone geometries. *Journal of Geophysical Research: Solid Earth (1978–2012),* 117(B1).

Heki, K., and Tamura, Y. (1997). Short term afterslip in the 1994 Sanriku-Haruka-Oki Earthquake. *Geophysical research letters*, *24*(24), 3285-3288.

Helmstetter, A., and Shaw, B. E. (2009). Afterslip and aftershocks in the rate-and-state friction law. *Journal of Geophysical Research: Solid Earth (1978–2012),* 114(B1).

Hirata, K., Satake, K., Tanioka, Y., Kuragano, T., Hasegawa, Y., Hayashi, Y., & Hamada, N. (2006). The 2004 Indian Ocean tsunami: Tsunami source model from satellite altimetry. *Earth Planets and Space*, 58(2), 195.

Hirth, G., & Kohlstedt, D. L. (1996). Water in the oceanic upper mantle: implications for rheology, melt extraction and the evolution of the lithosphere. *Earth and Planetary Science Letters*, 144(1), 93-108.

Hoechner, A., Sobolev, S. V., Einarsson, I., and Wang, R.. (2011). Investigation on afterslip and steady state and transient rheology based on postseismic deformation and geoid change caused by the Sumatra 2004 earthquake. *Geochemistry Geophysics Geosystems,* 12(7), Q07010.

Hsu, Y. J., Bechor, N., Segall, P., Yu, S. B., Kuo, L. C., and Ma, K. F. (2002). Rapid afterslip following the 1999 Chi-Chi, Taiwan earthquake. *Geophysical Research Letters*, 29(16), 1-4.

Hsu, Y. J., Simons, M., Avouac, J. P., Galetzka, J., Sieh, K., Chlieh, M., ... & Bock, Y. (2006). Frictional afterslip following the 2005 Nias-Simeulue earthquake, Sumatra. *Science*, 312(5782), 1921-1926.

Hsu, Y. J., Yu, S. B., and Chen, H. Y. (2009). Coseismic and postseismic deformation associated with the 2003 Chengkung, Taiwan, earthquake. *Geophysical Journal International*, 176(2), 420-430.

Hu, Y., Wang, K., He, J., Klotz, J., and Khazaradze, G. (2004). Three-dimensional viscoelastic finite element model for postseismic deformation of the great 1960 Chile earthquake. *Journal of Geophysical Research: Solid Earth (1978–2012)*, 109(B12).

Hu, Y., and Wang, K. (2012). Spherical-Earth finite element model of short-term postseismic deformation following the 2004 Sumatra earthquake. *Journal of Geophysical Research: Solid Earth (1978–2012),* 117(B5).

Ito, T., Gunawan, E., Kimata, F., Tabei, T., Simons, M., Meilano, I., Agustan, Ohta,Y., Nurdin, I., and Sugiyanto, D. (2012). Isolating along-strike variations in the depth extent of shallow creep and fault locking on the northern Great Sumatran Fault. *Journal of Geophysical*

Research: Solid Earth (1978–2012), 117(B6).

Ito, Y., and Nakashima, S. (2002). Water distribution in low-grade siliceous metamorphic rocks by micro-FTIR and its relation to grain size: a case from the Kanto Mountain region, Japan. *Chemical geology, 189(1),* 1-18.

Jade, S., Ananda, M. B., Kumar, P. D., and Banerjee, S. (2005). Co-seismic and post-seismic displacements in Andaman and Nicobar Islands from GPS measurements. *Curr. Sci*, *88*(12), 1980-1984.

Jaeger, J. C., Cook, N. G., and Zimmerman, R. (2009). *Fundamentals of rock mechanics*. John Wiley and Sons.

Johnson, K. M., Hsu, Y. J., Segall, P., & Yu, S. B. (2001). Fault geometry and slip distribution of the 1999 Chi‐Chi, Taiwan Earthquake imaged from inversion of GPS data. *Geophysical Research Letters*, 28(11), 2285-2288.

Jónsson, S., Segall, P., Pedersen, R., and Björnsson, G. (2003). Post-earthquake ground movements correlated to pore-pressure transients. *Nature,* 424(6945), 179-183.

Kanamori, H. (2006). Lessons from the 2004 Sumatra–Andaman earthquake. Philosophical Transactions of the Royal Society A: Mathematical, *Physical and Engineering Sciences,* 364(1845), 1927-1945.

Kessel, R., Schmidt, M. W., Ulmer, P., & Pettke, T. (2005). Trace element signature of subduction-zone fluids, melts and supercritical liquids at 120–180 km depth. *Nature*, 437(7059), 724-727.

Kirby, S. H., and Kronenberg, A. K. (1987). Rheology of the lithosphere: Selected topics. *Reviews of Geophysics*, 25(6), 1219-1244.

Kogan, M. G., Vasilenko, N. F., Frolov, D. I., Freymueller, J. T., Steblov, G. M., Levin, B. W., and Prytkov, A. S. (2011). The mechanism of postseismic deformation triggered by the 2006–2007 great Kuril earthquakes. *Geophysical Research Letters,* 38(6).

Kreemer, C., Blewitt, G., Hammond, W. C., and Plag, H. P. (2006). Global deformation from the great 2004 Sumatra-Andaman earthquake observed by GPS: Implications for rupture process and global reference frame. *Earth Planets and Space,* 58(2), 141.

Langbein, J., Murray, J. R., and Snyder, H. A. (2006). Coseismic and initial postseismic deformation from the 2004 Parkfield, California, earthquake, observed by Global Positioning System, electronic distance meter, creepmeters, and borehole strainmeters. *Bulletin of the Seismological Society of America*, 96(4B), S304-S320.

Larsen, S., Reilinger, R., Neugebauer, H., and Strange, W. (1992). Global Positioning System measurements of deformations associated with the 1987 Superstition Hills earthquake: Evidence for conjugate faulting. *Journal of Geophysical Research: Solid Earth (1978–2012)*, 97(B4), 4885-4902.

Lay, T., Kanamori, H., Ammon, C. J., Nettles, M., Ward, S. N., Aster, R. C., ... & Sipkin, S. (2005). The great Sumatra-Andaman earthquake of 26 december 2004. *Science*, 308(5725), 1127-1133.

Leick, A. (2004). *GPS satellite surveying*. John Wiley & Sons.

Lisowski, M., Prescott, W. H., Savage, J. C., and Johnston, M. J. (1990). Geodetic estimate of coseismic slip during the 1989 Loma Prieta, California, earthquake. *Geophysical Research Letters*, 17(9), 1437-1440.

Liu, Y., & Rice, J. R. (2005). Aseismic slip transients emerge spontaneously in three‐

dimensional rate and state modeling of subduction earthquake sequences. *Journal of Geophysical Research: Solid Earth* (1978‐2012), 110(B8).

Lyard, F., Lefevre, F., Letellier, T., and Francis, O. (2006). Modelling the global ocean tides: modern insights from FES2004. *Ocean Dynamics,* 56(5-6), 394-415.

Marone, C. J., Scholtz, C. H., and Bilham, R. (1991). On the mechanics of earthquake afterslip. *Journal of Geophysical Research: Solid Earth (1978–2012)*, 96(B5), 8441-8452.

Miyazaki, S. I., Segall, P., Fukuda, J., and Kato, T. (2004). Space time distribution of afterslip following the 2003 Tokachi-oki earthquake: implications for variations in fault zone frictional properties. *Geophysical Research Letters,* 31(6), L06623.

Nur, A., & Mavko, G. (1974). Postseismic viscoelastic rebound. *Science*, 183(4121), 204-206.

Ohta, Y., Hino, R., Inazu, D., Ohzono, M., Ito, Y., Mishina, M., ... and Miura, S. (2012). Geodetic constraints on afterslip characteristics following the March 9, 2011, Sanriku-oki earthquake, Japan. *Geophysical Research Letters*, 39(16).

Okada, Y. (1985). Surface deformation due to shear and tensile faults in a half-space. *Bulletin of the Seismological Society of America,* 75(4), 1135-1154.

Ozawa, S., Nishimura, T., Munekane, H., Suito, H., Kobayashi, T., Tobita, M., and Imakiire, T. (2012). Preceding, coseismic, and postseismic slips of the 2011 Tohoku earthquake, Japan. *Journal of Geophysical Research: Solid Earth (1978–2012)*, 117(B7).

Ozawa, S., Nishimura, T., Suito, H., Kobayashi, T., Tobita, M., and Imakiire, T. (2011). Coseismic and postseismic slip of the 2011 magnitude-9 Tohoku-Oki earthquake. *Nature,* 475(7356), 373-376.

Panet, I., Pollitz, F., Mikhailov, V., Diament, M., Banerjee, P., and Grijalva, K. (2010). Upper

mantle rheology from GRACE and GPS postseismic deformation after the 2004 Sumatra-Andaman earthquake. *Geochemistry, Geophysics, Geosystems,* 11(6).

Paul, J., Lowry, A. R., Bilham, R., Sen, S., and Smalley, R. (2007). Postseismic deformation of the Andaman Islands following the 26 December, 2004 Great Sumatra–Andaman earthquake. *Geophysical Research Letters,* 34(19).

Paul, J., Rajendran, C. P., Lowry, A. R., Andrade, V., and Rajendran, K. (2012). Andaman postseismic deformation observations: still slipping after all these years? *Bulletin of the Seismological Society of America,* 102(1), 343-351.

Peltzer, G., Rosen, P., Rogez, F., & Hudnut, K. (1996). Postseismic Rebound in Fault Step-Overs Caused by Pore Fluid Flow. *Science*, 273(5279), 1202-1204.

Peltzer, G., Rosen, P., Rogez, F., & Hudnut, K. (1998). Poroelastic rebound along the Landers 1992 earthquake surface rupture. *Journal of Geophysical Research: Solid Earth* (1978–2012), 103(B12), 30131-30145.

Perfettini, H., & Avouac, J. P. (2007). Modeling afterslip and aftershocks following the 1992 Landers earthquake. *Journal of Geophysical Research: Solid Earth (1978–2012)*, 112(B7).

Piatanesi, A., and Lorito, S. (2007). Rupture process of the 2004 Sumatra–Andaman earthquake from tsunami waveform inversion. *Bulletin of the Seismological Society of America,* 97(1A), S223-S231.

Piombo, A., Martinelli, G., & Dragoni, M. (2005). Post-seismic fluid flow and Coulomb stress changes in a poroelastic medium. *Geophysical Journal International*, 162(2), 507-515.

Poisson, B., Oliveros, C., and Pedreros, R. (2011). Is there a best source model of the Sumatra 2004 earthquake for simulating the consecutive tsunami? *Geophysical Journal*

International, 185(3), 1365-1378.

Pollitz, F. F. (2003). Transient rheology of the uppermost mantle beneath the Mojave Desert, California. *Earth and Planetary Science Letters*, 215(1), 89-104.

Pollitz, F. F., Bürgmann, R., and Banerjee, P. (2006). Post-seismic relaxation following the great 2004 Sumatra-Andaman earthquake on a compressible self-gravitating Earth. *Geophysical Journal International,* 167(1), 397-420.

Pollitz, F. F., Bürgmann, R., and Segall, P. (1998). Joint estimation of afterslip rate and postseismic relaxation following the 1989 Loma Prieta earthquake. *Journal of Geophysical Research: Solid Earth (1978–2012),* 103(B11), 26975-26992.

Pollitz, F. F., Wicks, C., & Thatcher, W. (2001). Mantle flow beneath a continental strike-slip fault: Postseismic deformation after the 1999 Hector Mine earthquake. *Science*, 293(5536), 1814-1818.

Pollitz, F., Banerjee, P., Grijalva, K., Nagarajan, B., and Bürgmann, R. (2008). Effect of 3-D viscoelastic structure on post-seismic relaxation from the 2004 M=9.2 Sumatra earthquake. *Geophysical Journal International,* 173(1), 189-204.

Pollitz, F.F. (1997). Gravitational viscoelastic postseismic relaxation on a layered spherical Earth. *Journal of Geophysical Research: Solid Earth (1978–2012),* 102(B8), 17921-17941.

Reilinger, R. E., Ergintav, S., Bürgmann, R., McClusky, S., Lenk, O., Barka, A., ... and Töksoz, M. N. (2000). Coseismic and postseismic fault slip for the 17 August 1999, M= 7.5, Izmit, Turkey earthquake. *Science*, 289(5484), 1519-1524.

Rhie, J., Dreger, D., Bürgmann, R., and Romanowicz, B. (2007). Slip of the 2004 Sumatra–Andaman earthquake from joint inversion of long-period global seismic

waveforms and GPS static offsets. *Bulletin of the Seismological Society of America,* 97(1A), S115-S127.

Rice, J. R., & Gu, J. C. (1983). Earthquake aftereffects and triggered seismic phenomena. *Pure and Applied Geophysics*, 121(2), 187-219.

Roeloffs, E. A. (1988). Fault stability changes induced beneath a reservoir with cyclic variations in water level. *Journal of Geophysical Research,* 93(B3), 2107-2124.

Ryder, I., Parsons, B., Wright, T. J., and Funning, G. J. (2007). Post-seismic motion following the 1997 Manyi (Tibet) earthquake: InSAR observations and modelling. *Geophysical Journal International,* 169(3), 1009-1027.

Sagiya, T. (2004). A decade of GEONET: 1994-2003-The continuous GPS observation in Japan and its impact on earthquake studies. *Earth Planets and Space*, 56(8), xxix-xlii.

Satirapod, C., Simons, W. J., and Promthong, C. (2008). Monitoring deformation of Thai geodetic network due to the 2004 Sumatra-Andaman and 2005 Nias earthquakes by GPS. *Journal of Surveying Engineering,* 134(3), 83-88.

Savage, J. C., Lisowski, M., and Svarc, J. L. (1994). Postseismic deformation following the 1989 (M= 7.1) Loma Prieta, California, earthquake. *Journal of Geophysical Research: Solid Earth (1978–2012),* 99(B7), 13757-13765.

Savage, J. C., Prescott, W. H., & Lisowski, M. (1987). Deformation along the San Andreas fault 1982–1986 as indicated by frequent Geodolite measurements. *Journal of Geophysical Research: Solid Earth* (1978–2012), 92(B6), 4785-4797.

Savage, J. C., and Svarc, J. L. (1997). Postseismic deformation associated with the 1992 M ω= 7.3 Landers earthquake, southern California. *Journal of Geophysical Research: Solid*

Earth (1978–2012), 102(B4), 7565-7577.

Scholz, C. H. (1998). Earthquakes and friction laws. *Nature*, 391(6662), 37-42.

Segall, P., and Davis, J. L. (1997). GPS applications for geodynamics and earthquake studies. *Annual Review of Earth and Planetary Sciences,* 25(1), 301-336.

Shen, Z. K., Jackson, D. D., Feng, Y., Cline, M., Kim, M., Fang, P., and Bock, Y. (1994). Postseismic deformation following the Landers earthquake, California, 28 June 1992. *Bulletin of the Seismological Society of America*,84(3), 780-791.

Sheu, S. Y., and Shieh, C. F., 2004. Viscoelastic–afterslip concurrence: a possible mechanism in the early post-seismic deformation of the Mw 7.6, 1999 Chi-Chi (Taiwan) earthquake. *Geophysical Journal International,* 159(3), 1112-1124.

Simons, W.J.F., Socquet, A., Vigny, C., Ambrosius, B.A.C., Abu, S.H., Promthong, C., Subarya, C., Sarsito, D.A.,S. Matheussen, P. Morgan and W. Spakman (2007). A decade of GPS in Southeast Asia: resolving Sundaland motion and boundaries. *Journal of Geophysical Research: Solid Earth (1978–2012),* 112(B6).

Socquet, A., Vigny, C., Chamot‐Rooke, N., Simons, W., Rangin, C., & Ambrosius, B. (2006). India and Sunda plates motion and deformation along their boundary in Myanmar determined by GPS. *Journal of Geophysical Research: Solid Earth* (1978‐2012), 111(B5).

Subarya, C., Chlieh, M., Prawirodirdjo, L., Avouac, J. P., Bock, Y., Sieh, K., Meltzner, A. J., Natawidjaja, D. H., and McCaffrey, R.. (2006). Plate-boundary deformation associated with the great Sumatra–Andaman earthquake. *Nature,* 440(7080), 46-51.

Suito, H., and Freymueller, J. T. (2009). A viscoelastic and afterslip postseismic deformation model for the 1964 Alaska earthquake. *Journal of Geophysical Research: Solid Earth*

(1978–2012), 114(B11).

Thatcher, W., and J. B. Rundle (1984), A viscoelastic coupling model for the cyclic deformation due to periodically repeated Earthquakes at subduction zones, *J. Geophys. Res.*, 89(B9), 7631–7640, doi:10.1029/JB089iB09p07631.

Tsuji, H., Hatanaka, Y., Sagiya, T., & Hashimoto, M. (1995). Coseismic crustal deformation from the 1994 Hokkaido‐Toho‐Oki earthquake monitored by a nationwide continuous GPS array in Japan. *Geophysical Research Letters*, 22(13), 1669-1672.

Vigny, C., Simons, W. J., Abu, S., Bamphenyu, R., Satirapod, C., Choosakul, N., ... and Ambrosius, B. A. C. (2005). Insight into the 2004 Sumatra–Andaman earthquake from GPS measurements in southeast Asia. *Nature*, 436(7048), 201-206.

Wang, K. (2007). Elastic and Viscoelastic Models of Crustal Deformation in Subduction Earthquake Cycles. *The Seismogenic Zone of Subduction Thrust Faults, pp. 540-575.* Columbia University Press, New York.

Wang, K., He, J., Dragert, H., and James, T. S. (2001). Three-dimensional viscoelastic interseismic deformation model for the Cascadia subduction zone. *Earth, Planets and Space,* 53, 295-306.

Wang, K., Hu, Y., and He, J. (2012). Deformation cycles of subduction earthquakes in a viscoelastic Earth. *Nature,* 484(7394), 327-332.

Wang, L., Wang, R., Roth, F., Enescu, B., Hainzl, S., and Ergintav, S. (2009). Afterslip and viscoelastic relaxation following the 1999 M 7.4 Izmit earthquake from GPS measurements. *Geophysical Journal International,* 178(3), 1220-1237.

Wang, R., & Kümpel, H. J. (2003). Poroelasticity: Efficient modeling of strongly coupled, slow

deformation processes in a multilayered half-space. *Geophysics*, 68(2), 705-717.

Wessel, P., and Smith, W. H. (1998). New, improved version of Generic Mapping Tools released. *Eos, Transactions American Geophysical Union,* 79(47), 579-579.

Williams, C. R., Arnadottir, T., and Segall, P. (1993). Coseismic deformation and dislocation models of the 1989 Loma Prieta earthquake derived from Global Positioning System measurements. *Journal of Geophysical Research: Solid Earth (1978–2012)*, 98(B3), 4567-4578.

Wu, H. H., Tsai, Y. B., Lee, T. Y., Lo, C. H., Hsieh, C. H., and Van Toan, D. (2004). 3-D shear wave velocity structure of the crust and upper mantle in South China Sea and its surrounding regions by surface wave dispersion analysis. *Marine Geophysical Researches,* 25(1-2), 5-27.

Yabuki, T., and Matsu'ura, M. (1992). Geodetic data inversion using a Bayesian information criterion for spatial distribution of fault slip. *Geophysical Journal International, 109(2),* 363-375.

Yagi, Y., Kikuchi, M., and Nishimura, T. (2003). Co-seismic slip, post-seismic slip, and largest aftershock associated with the 1994 Sanriku-haruka-oki, Japan, earthquake. *Geophysical Research Letters*, 30(22).

Yoshioka, S., and Suzuki, H. (1999). Effects of three-dimensional inhomogeneous viscoelastic structures on postseismic surface deformations associated with the great 1946 Nankaido earthquake. *Pure and Applied Geophysics,* 154(2), 307-328.

Appendix A

Coseismic Fault Models

Lat. (deg)*	Long. (deg)*	Length (km)	Strike (deg)	Rake (deg)	Slip (cm)	Depth-Lower-Edge(km)	Depth-Upper-Edge(km)	Dip (deg)

*Lat. and Long. of northernmost point on lower edge

1. Kreemer model

8.40	93.30	355.00	343.00	104.00	1130.00	50.00	30.00	35.00
5.51	94.13	350.00	322.00	90.00	590.00	50.00	30.00	35.00
5.35	93.93	350.00	322.00	90.00	590.00	30.00	0.00	11.00
8.33	93.05	355.00	343.00	104.00	1130.00	30.00	0.00	15.00
14.01	93.55	162.50	24.00	90.00	330.00	30.00	0.00	18.00
12.68	92.94	162.50	7.00	90.00	330.00	30.00	0.00	18.00
11.26	92.73	162.50	0.00	90.00	330.00	30.00	0.00	18.00
9.75	92.73	162.50	350.00	90.00	330.00	30.00	0.00	18.00
13.93	93.90	162.50	24.00	90.00	330.00	50.00	30.00	35.00
12.65	93.20	162.50	7.00	90.00	330.00	50.00	30.00	35.00
11.26	92.99	162.50	0.00	90.00	330.00	50.00	30.00	35.00
9.79	92.99	162.50	350.00	90.00	330.00	50.00	30.00	35.00

2. Banerjee model

5.35	93.93	175.00	322.00	90.00	1556.00	30.00	0.00	11.00
4.11	94.90	175.00	322.00	90.00	876.00	30.00	0.00	11.00
8.33	93.05	355.00	343.00	109.90	1904.00	30.00	15.00	15.00
14.01	93.55	162.50	24.00	139.00	656.00	30.00	0.00	18.00
12.68	92.92	162.50	9.00	124.00	581.00	30.00	0.00	18.00
11.26	92.73	162.50	0.00	115.00	807.00	30.00	0.00	18.00
9.75	92.73	162.50	350.00	105.00	1678.00	30.00	0.00	18.00

9.79	92.99	162.50	350.00	105.00	300.00	50.00	30.00	35.00
5.51	94.13	175.00	322.00	90.00	1556.00	50.00	30.00	35.00

3. Fujii model

3.67	94.90	100.00	315.00	95.00	2460.00	20.00	3.00	10.00
4.45	94.32	100.00	325.00	100.00	2460.00	20.00	3.00	10.00
5.23	93.83	100.00	330.00	105.00	1280.00	20.00	3.00	10.00
6.05	93.54	100.00	340.00	105.00	190.00	20.00	3.00	10.00
6.95	93.26	100.00	342.00	100.00	600.00	20.00	3.00	10.00
7.87	92.92	100.00	340.00	95.00	650.00	20.00	3.00	10.00
8.82	92.56	100.00	337.00	85.00	710.00	20.00	3.00	10.00
9.64	92.37	100.00	350.00	99.00	320.00	20.00	3.00	10.00
10.50	92.41	100.00	0.00	106.00	270.00	20.00	3.00	10.00
13.95	93.21	100.00	25.00	130.00	100.00	20.00	3.00	10.00
3.65	96.23	100.00	315.00	95.00	430.00	37.00	20.00	10.00
4.96	95.05	100.00	325.00	100.00	1230.00	37.00	20.00	10.00
5.67	94.60	100.00	330.00	105.00	180.00	37.00	20.00	10.00
6.45	94.34	100.00	340.00	105.00	450.00	37.00	20.00	10.00
7.28	94.08	100.00	342.00	100.00	320.00	37.00	20.00	10.00
9.18	93.38	100.00	337.00	85.00	350.00	37.00	20.00	10.00

4. Rhie model

12.69	92.94	30.00	24.00	117.73	233.00	45.00	35.00	18.00
12.95	93.06	30.00	24.00	140.00	246.00	45.00	35.00	18.00
13.22	93.18	30.00	24.00	140.00	208.00	45.00	35.00	18.00
13.49	93.31	30.00	24.00	140.00	117.00	45.00	35.00	18.00
13.75	93.43	30.00	24.00	140.00	21.00	45.00	35.00	18.00
12.80	92.68	30.00	24.00	126.13	285.00	35.00	25.00	18.00
13.06	92.80	30.00	24.00	140.00	285.00	35.00	25.00	18.00
13.33	92.92	30.00	24.00	140.00	246.00	35.00	25.00	18.00
13.60	93.05	30.00	24.00	140.00	161.00	35.00	25.00	18.00
13.87	93.17	30.00	24.00	140.00	83.00	35.00	25.00	18.00
12.91	92.42	30.00	24.00	136.77	674.00	25.00	15.00	18.00
13.18	92.54	30.00	24.00	140.00	766.00	25.00	15.00	18.00

13.44	92.67	30.00	24.00	140.00	655.00	25.00	15.00	18.00
13.71	92.79	30.00	24.00	140.00	367.00	25.00	15.00	18.00
13.98	92.91	30.00	24.00	140.00	156.00	25.00	15.00	18.00
13.02	92.16	30.00	24.00	140.00	698.00	15.00	5.00	18.00
13.29	92.28	30.00	24.00	140.00	688.00	15.00	5.00	18.00
13.56	92.41	30.00	24.00	140.00	526.00	15.00	5.00	18.00
13.82	92.53	30.00	24.00	140.00	217.00	15.00	5.00	18.00
14.09	92.65	30.00	24.00	50.00	0.00	15.00	5.00	18.00
11.24	92.76	30.00	7.00	97.94	231.00	45.00	35.00	18.00
11.53	92.79	30.00	7.00	105.46	274.00	45.00	35.00	18.00
11.82	92.83	30.00	7.00	114.23	308.00	45.00	35.00	18.00
12.11	92.87	30.00	7.00	117.99	305.00	45.00	35.00	18.00
12.40	92.90	30.00	7.00	108.39	253.00	45.00	35.00	18.00
11.27	92.48	30.00	7.00	96.60	298.00	35.00	25.00	18.00
11.56	92.51	30.00	7.00	103.80	245.00	35.00	25.00	18.00
11.85	92.55	30.00	7.00	113.31	259.00	35.00	25.00	18.00
12.14	92.59	30.00	7.00	120.39	272.00	35.00	25.00	18.00
12.43	92.62	30.00	7.00	113.52	276.00	35.00	25.00	18.00
11.31	92.20	30.00	7.00	100.15	586.00	25.00	15.00	18.00
11.60	92.23	30.00	7.00	107.61	557.00	25.00	15.00	18.00
11.89	92.27	30.00	7.00	118.75	583.00	25.00	15.00	18.00
12.18	92.30	30.00	7.00	128.41	625.00	25.00	15.00	18.00
12.47	92.34	30.00	7.00	126.12	611.00	25.00	15.00	18.00
11.34	91.92	30.00	7.00	102.67	426.00	15.00	5.00	18.00
11.63	91.95	30.00	7.00	114.38	493.00	15.00	5.00	18.00
11.92	91.99	30.00	7.00	126.67	537.00	15.00	5.00	18.00
12.21	92.02	30.00	7.00	136.50	603.00	15.00	5.00	18.00
12.50	92.06	30.00	7.00	140.00	669.00	15.00	5.00	18.00
9.80	92.72	30.00	0.00	103.02	426.00	45.00	35.00	18.00
10.10	92.72	30.00	0.00	117.21	366.00	45.00	35.00	18.00
10.39	92.72	30.00	0.00	124.33	308.00	45.00	35.00	18.00
10.68	92.72	30.00	0.00	120.34	251.00	45.00	35.00	18.00
10.97	92.72	30.00	0.00	105.00	223.00	45.00	35.00	18.00
9.80	92.44	30.00	0.00	105.57	472.00	35.00	25.00	18.00
10.10	92.44	30.00	0.00	117.68	368.00	35.00	25.00	18.00
10.39	92.44	30.00	0.00	124.19	308.00	35.00	25.00	18.00

10.68	92.44	30.00	0.00	120.38	249.00	35.00	25.00	18.00
10.97	92.44	30.00	0.00	104.69	293.00	35.00	25.00	18.00
9.80	92.16	30.00	0.00	112.30	1105.00	25.00	15.00	18.00
10.10	92.16	30.00	0.00	122.11	963.00	25.00	15.00	18.00
10.39	92.16	30.00	0.00	126.32	794.00	25.00	15.00	18.00
10.68	92.16	30.00	0.00	123.97	606.00	25.00	15.00	18.00
10.97	92.16	30.00	0.00	108.38	678.00	25.00	15.00	18.00
9.80	91.88	30.00	0.00	126.55	1126.00	15.00	5.00	18.00
10.10	91.88	30.00	0.00	126.31	983.00	15.00	5.00	18.00
10.39	91.88	30.00	0.00	129.26	789.00	15.00	5.00	18.00
10.68	91.88	30.00	0.00	130.02	578.00	15.00	5.00	18.00
10.97	91.88	30.00	0.00	119.67	417.00	15.00	5.00	18.00
8.32	92.98	30.00	350.00	100.19	501.00	45.00	35.00	18.00
8.61	92.93	30.00	350.00	109.66	494.00	45.00	35.00	18.00
8.89	92.88	30.00	350.00	113.33	507.00	45.00	35.00	18.00
9.18	92.83	30.00	350.00	112.01	502.00	45.00	35.00	18.00
9.47	92.77	30.00	350.00	102.38	453.00	45.00	35.00	18.00
8.27	92.70	30.00	350.00	100.99	602.00	35.00	25.00	18.00
8.56	92.65	30.00	350.00	108.80	523.00	35.00	25.00	18.00
8.85	92.60	30.00	350.00	112.52	531.00	35.00	25.00	18.00
9.13	92.55	30.00	350.00	108.96	521.00	35.00	25.00	18.00
9.42	92.50	30.00	350.00	102.22	529.00	35.00	25.00	18.00
8.22	92.43	30.00	350.00	102.10	1615.00	25.00	15.00	18.00
8.51	92.38	30.00	350.00	110.04	1433.00	25.00	15.00	18.00
8.80	92.33	30.00	350.00	112.88	1450.00	25.00	15.00	18.00
9.08	92.27	30.00	350.00	109.92	1438.00	25.00	15.00	18.00
9.37	92.22	30.00	350.00	105.30	1333.00	25.00	15.00	18.00
8.17	92.15	30.00	350.00	101.77	1494.00	15.00	5.00	18.00
8.46	92.10	30.00	350.00	111.91	1489.00	15.00	5.00	18.00
8.75	92.05	30.00	350.00	114.02	1488.00	15.00	5.00	18.00
9.04	92.00	30.00	350.00	111.83	1493.00	15.00	5.00	18.00
9.32	91.95	30.00	350.00	109.60	1526.00	15.00	5.00	18.00
5.28	93.97	30.00	343.00	94.43	859.00	41.25	33.75	15.00
5.56	93.89	30.00	343.00	95.56	784.00	41.25	33.75	15.00
5.84	93.80	30.00	343.00	99.83	796.00	41.25	33.75	15.00
6.11	93.72	30.00	343.00	105.95	781.00	41.25	33.75	15.00

6.39	93.63	30.00	343.00	110.94	749.00	41.25	33.75	15.00
6.67	93.54	30.00	343.00	113.43	706.00	41.25	33.75	15.00
6.95	93.46	30.00	343.00	112.84	655.00	41.25	33.75	15.00
7.22	93.37	30.00	343.00	110.07	615.00	41.25	33.75	15.00
7.50	93.29	30.00	343.00	104.93	588.00	41.25	33.75	15.00
7.78	93.20	30.00	343.00	101.70	580.00	41.25	33.75	15.00
8.06	93.12	30.00	343.00	99.21	567.00	41.25	33.75	15.00
5.21	93.73	30.00	343.00	94.29	1071.00	33.75	26.25	15.00
5.49	93.64	30.00	343.00	95.91	798.00	33.75	26.25	15.00
5.76	93.56	30.00	343.00	100.86	782.00	33.75	26.25	15.00
6.04	93.47	30.00	343.00	106.89	748.00	33.75	26.25	15.00
6.32	93.39	30.00	343.00	112.56	709.00	33.75	26.25	15.00
6.60	93.30	30.00	343.00	115.75	668.00	33.75	26.25	15.00
6.87	93.22	30.00	343.00	116.63	638.00	33.75	26.25	15.00
7.15	93.13	30.00	343.00	114.22	621.00	33.75	26.25	15.00
7.43	93.05	30.00	343.00	109.69	606.00	33.75	26.25	15.00
7.71	92.96	30.00	343.00	105.89	600.00	33.75	26.25	15.00
7.98	92.88	30.00	343.00	100.70	672.00	33.75	26.25	15.00
5.13	93.49	30.00	343.00	95.34	1378.00	26.25	18.75	15.00
5.41	93.40	30.00	343.00	97.71	1230.00	26.25	18.75	15.00
5.69	93.32	30.00	343.00	102.79	1162.00	26.25	18.75	15.00
5.97	93.23	30.00	343.00	109.72	1069.00	26.25	18.75	15.00
6.24	93.15	30.00	343.00	116.42	986.00	26.25	18.75	15.00
6.52	93.06	30.00	343.00	121.95	937.00	26.25	18.75	15.00
6.80	92.98	30.00	343.00	123.92	922.00	26.25	18.75	15.00
7.08	92.89	30.00	343.00	122.11	932.00	26.25	18.75	15.00
7.35	92.81	30.00	343.00	117.98	955.00	26.25	18.75	15.00
7.63	92.72	30.00	343.00	112.25	974.00	26.25	18.75	15.00
7.91	92.63	30.00	343.00	103.77	1094.00	26.25	18.75	15.00
5.06	93.25	30.00	343.00	98.07	2241.00	18.75	11.25	15.00
5.34	93.16	30.00	343.00	101.49	1942.00	18.75	11.25	15.00
5.62	93.08	30.00	343.00	106.54	1766.00	18.75	11.25	15.00
5.89	92.99	30.00	343.00	114.35	1564.00	18.75	11.25	15.00
6.17	92.90	30.00	343.00	123.47	1425.00	18.75	11.25	15.00
6.45	92.82	30.00	343.00	130.20	1374.00	18.75	11.25	15.00
6.73	92.73	30.00	343.00	132.85	1420.00	18.75	11.25	15.00

7.00	92.65	30.00	343.00	130.83	1521.00	18.75	11.25	15.00
7.28	92.56	30.00	343.00	125.71	1628.00	18.75	11.25	15.00
7.56	92.48	30.00	343.00	118.14	1695.00	18.75	11.25	15.00
7.84	92.39	30.00	343.00	106.76	1894.00	18.75	11.25	15.00
4.99	93.00	30.00	343.00	104.44	1980.00	11.25	3.75	15.00
5.26	92.92	30.00	343.00	105.29	1825.00	11.25	3.75	15.00
5.54	92.83	30.00	343.00	110.69	1606.00	11.25	3.75	15.00
5.82	92.75	30.00	343.00	119.16	1402.00	11.25	3.75	15.00
6.10	92.66	30.00	343.00	129.82	1273.00	11.25	3.75	15.00
6.37	92.58	30.00	343.00	137.49	1266.00	11.25	3.75	15.00
6.65	92.49	30.00	343.00	139.66	1361.00	11.25	3.75	15.00
6.93	92.41	30.00	343.00	136.53	1526.00	11.25	3.75	15.00
7.21	92.32	30.00	343.00	130.26	1689.00	11.25	3.75	15.00
7.48	92.24	30.00	343.00	121.64	1787.00	11.25	3.75	15.00
7.76	92.15	30.00	343.00	110.54	1777.00	11.25	3.75	15.00
2.88	95.87	30.00	322.00	94.39	263.00	39.00	33.00	11.00
3.10	95.69	30.00	322.00	95.92	345.00	39.00	33.00	11.00
3.33	95.52	30.00	322.00	96.55	340.00	39.00	33.00	11.00
3.55	95.34	30.00	322.00	96.69	369.00	39.00	33.00	11.00
3.78	95.16	30.00	322.00	95.78	460.00	39.00	33.00	11.00
4.00	94.99	30.00	322.00	94.66	593.00	39.00	33.00	11.00
4.23	94.81	30.00	322.00	93.91	721.00	39.00	33.00	11.00
4.45	94.63	30.00	322.00	93.58	815.00	39.00	33.00	11.00
4.68	94.46	30.00	322.00	93.74	873.00	39.00	33.00	11.00
4.91	94.28	30.00	322.00	94.13	1096.00	39.00	33.00	11.00
5.13	94.11	30.00	322.00	94.42	1144.00	39.00	33.00	11.00
2.71	95.65	30.00	322.00	94.55	331.00	33.00	27.00	11.00
2.93	95.47	30.00	322.00	96.21	508.00	33.00	27.00	11.00
3.16	95.30	30.00	322.00	96.97	476.00	33.00	27.00	11.00
3.38	95.12	30.00	322.00	96.35	512.00	33.00	27.00	11.00
3.61	94.94	30.00	322.00	95.86	641.00	33.00	27.00	11.00
3.83	94.77	30.00	322.00	95.19	830.00	33.00	27.00	11.00
4.06	94.59	30.00	322.00	94.47	1030.00	33.00	27.00	11.00
4.28	94.42	30.00	322.00	94.19	1191.00	33.00	27.00	11.00
4.51	94.24	30.00	322.00	94.23	1310.00	33.00	27.00	11.00
4.73	94.06	30.00	322.00	94.28	1405.00	33.00	27.00	11.00

4.96	93.89	30.00	322.00	94.51	1487.00	33.00	27.00	11.00
2.53	95.43	30.00	322.00	98.34	412.00	27.00	21.00	11.00
2.76	95.26	30.00	322.00	95.15	613.00	27.00	21.00	11.00
2.99	95.08	30.00	322.00	96.05	560.00	27.00	21.00	11.00
3.21	94.90	30.00	322.00	96.35	608.00	27.00	21.00	11.00
3.44	94.73	30.00	322.00	95.99	795.00	27.00	21.00	11.00
3.66	94.55	30.00	322.00	95.32	1084.00	27.00	21.00	11.00
3.89	94.37	30.00	322.00	94.52	1411.00	27.00	21.00	11.00
4.11	94.20	30.00	322.00	94.15	1702.00	27.00	21.00	11.00
4.34	94.02	30.00	322.00	94.23	1938.00	27.00	21.00	11.00
4.56	93.84	30.00	322.00	94.25	2140.00	27.00	21.00	11.00
4.79	93.67	30.00	322.00	94.40	2303.00	27.00	21.00	11.00
2.36	95.21	30.00	322.00	97.58	276.00	21.00	15.00	11.00
2.59	95.04	30.00	322.00	94.52	403.00	21.00	15.00	11.00
2.81	94.86	30.00	322.00	95.57	354.00	21.00	15.00	11.00
3.04	94.68	30.00	322.00	96.37	405.00	21.00	15.00	11.00
3.27	94.51	30.00	322.00	95.72	594.00	21.00	15.00	11.00
3.49	94.33	30.00	322.00	94.85	890.00	21.00	15.00	11.00
3.72	94.15	30.00	322.00	94.47	1230.00	21.00	15.00	11.00
3.94	93.98	30.00	322.00	94.26	1566.00	21.00	15.00	11.00
4.17	93.80	30.00	322.00	94.28	1869.00	21.00	15.00	11.00
4.39	93.62	30.00	322.00	94.19	2125.00	21.00	15.00	11.00
4.62	93.45	30.00	322.00	94.07	1743.00	21.00	15.00	11.00
2.19	94.99	30.00	322.00	93.03	240.00	15.00	9.00	11.00
2.42	94.82	30.00	322.00	93.98	336.00	15.00	9.00	11.00
2.64	94.64	30.00	322.00	94.11	312.00	15.00	9.00	11.00
2.87	94.46	30.00	322.00	95.37	412.00	15.00	9.00	11.00
3.09	94.29	30.00	322.00	94.34	722.00	15.00	9.00	11.00
3.32	94.11	30.00	322.00	93.96	1216.00	15.00	9.00	11.00
3.55	93.94	30.00	322.00	93.77	1819.00	15.00	9.00	11.00
3.77	93.76	30.00	322.00	94.03	2452.00	15.00	9.00	11.00
4.00	93.58	30.00	322.00	94.11	3064.00	15.00	9.00	11.00
4.22	93.41	30.00	322.00	94.29	3532.00	15.00	9.00	11.00
4.45	93.23	30.00	322.00	94.11	2460.00	15.00	9.00	11.00
2.02	94.77	30.00	322.00	91.05	78.00	9.00	3.00	11.00
2.25	94.60	30.00	322.00	92.30	98.00	9.00	3.00	11.00

2.47	94.42	30.00	322.00	90.44	91.00	9.00	3.00	11.00
2.70	94.25	30.00	322.00	92.48	159.00	9.00	3.00	11.00
2.92	94.07	30.00	322.00	91.59	360.00	9.00	3.00	11.00
3.15	93.89	30.00	322.00	92.65	683.00	9.00	3.00	11.00
3.37	93.72	30.00	322.00	93.18	1096.00	9.00	3.00	11.00
3.60	93.54	30.00	322.00	93.93	1545.00	9.00	3.00	11.00
3.83	93.36	30.00	322.00	94.07	1982.00	9.00	3.00	11.00
4.05	93.19	30.00	322.00	94.26	2325.00	9.00	3.00	11.00
4.28	93.01	30.00	322.00	94.04	1837.00	9.00	3.00	11.00

Appendix B

Best-fit Rheological Structure

1. Kreemer model

94 2 6371.000 2.214

3480.000	3481.000	5.566	44.000	21.910	8.000000E+02
3481.000	3500.000	5.536	44.000	21.910	8.000000E+02
3500.000	3600.000	5.506	44.000	21.910	8.000000E+02
3600.000	3700.000	5.497	44.000	21.910	8.000000E+02
3700.000	3800.000	5.491	44.000	21.910	8.000000E+02
3800.000	3900.000	5.357	44.000	21.910	8.000000E+02
3900.000	4000.000	5.307	44.000	21.910	8.000000E+02
4000.000	4100.000	5.257	44.000	21.910	8.000000E+02
4100.000	4200.000	5.207	44.000	21.910	8.000000E+02
4200.000	4300.000	5.156	44.000	21.910	8.000000E+02
4300.000	4400.000	5.105	44.000	21.910	8.000000E+02
4400.000	4500.000	5.054	44.000	21.910	8.000000E+02
4500.000	4600.000	5.003	44.000	21.910	8.000000E+02
4600.000	4700.000	4.950	44.000	21.910	8.000000E+02
4700.000	4800.000	4.897	44.000	21.910	8.000000E+02
4800.000	4900.000	4.843	44.000	21.910	8.000000E+02
4900.000	5000.000	4.789	44.000	21.910	8.000000E+02
5000.000	5100.000	4.733	44.000	21.910	8.000000E+02
5100.000	5200.000	4.678	44.000	21.910	8.000000E+02
5200.000	5319.100	4.670	44.000	21.910	8.000000E+02
5319.100	5353.700	4.635	44.000	21.910	8.000000E+02
5353.700	5388.300	4.611	44.000	21.910	8.000000E+02
5388.300	5422.900	4.587	44.000	21.910	8.000000E+02
5422.900	5457.600	4.563	44.000	21.910	8.000000E+02
5457.600	5492.200	4.539	44.000	21.910	8.000000E+02
5492.200	5526.800	4.515	44.000	21.910	8.000000E+02

5526.800	5561.500	4.491	44.000	21.910 8.000000E+02
5561.500	5596.100	4.467	44.000	21.910 8.000000E+02
5596.100	5630.700	4.443	44.000	21.910 8.000000E+02
5630.700	5665.400	4.443	44.000	21.910 8.000000E+02
5665.400	5711.000	4.380	44.000	21.910 8.000000E+02
5711.000	5731.300	3.992	19.000	9.800 6.000000E+00
5731.300	5771.000	3.983	19.000	9.800 6.000000E+00
5771.000	5793.800	3.975	19.000	9.800 6.000000E+00
5793.800	5825.000	3.931	19.000	9.800 6.000000E+00
5825.000	5856.300	3.890	19.000	9.800 6.000000E+00
5856.300	5887.500	3.849	19.000	9.800 6.000000E+00
5887.500	5918.700	3.764	19.000	9.800 6.000000E+00
5918.700	5950.000	3.743	19.000	9.800 6.000000E+00
5950.000	5971.000	3.723	19.000	9.800 6.000000E+00
5971.000	6001.200	3.543	19.000	9.800 6.000000E+00
6001.200	6021.200	3.543	19.000	9.800 6.000000E+00
6021.200	6026.900	3.543	19.000	9.800 6.000000E+00
6026.900	6052.500	3.490	19.000	9.800 6.000000E+00
6052.500	6078.100	3.490	19.000	9.800 6.000000E+00
6078.100	6103.800	3.435	19.000	9.800 6.000000E+00
6103.800	6121.000	3.435	19.000	9.800 6.000000E+00
6121.000	6126.000	3.435	19.000	9.800 6.000000E+00
6126.000	6131.000	3.435	19.000	9.800 6.000000E+00
6131.000	6136.000	3.435	19.000	9.800 6.000000E+00
6136.000	6141.000	3.435	19.000	9.800 6.000000E+00
6141.000	6146.000	3.435	19.000	9.800 6.000000E+00
6146.000	6151.000	3.435	19.000	9.800 6.000000E+00
6151.000	6156.000	3.360	13.000	6.700 6.000000E+00
6156.000	6161.000	3.360	13.000	6.700 6.000000E+00
6161.000	6166.000	3.360	13.000	6.700 6.000000E+00
6166.000	6171.000	3.360	13.000	6.700 6.000000E+00
6171.000	6176.000	3.360	13.000	6.700 6.000000E+00
6176.000	6181.000	3.360	13.000	6.700 6.000000E+00
6181.000	6186.000	3.360	13.000	6.700 6.000000E+00
6186.000	6191.000	3.360	13.000	6.700 6.000000E+00
6191.000	6196.000	3.360	13.000	6.700 6.000000E+00

6196.000	6201.000	3.360	13.000	6.700 6.000000E+00
6201.000	6206.000	3.360	13.000	6.700 6.000000E+00
6206.000	6211.000	3.360	13.000	6.700 6.000000E+00
6211.000	6216.000	3.360	13.000	6.700 6.000000E+00
6216.000	6221.000	3.360	13.000	6.700 6.000000E+00
6221.000	6226.000	3.360	13.000	6.700 6.000000E+00
6226.000	6230.000	3.360	13.000	6.700 6.000000E+00
6230.000	6236.000	3.360	13.000	6.700 6.000000E+00
6236.000	6241.000	3.360	13.000	6.700 6.000000E+00
6241.000	6246.000	3.360	13.000	6.700 6.000000E+00
6246.000	6251.000	3.360	13.000	6.700 6.000000E+00
6251.000	6256.000	3.360	13.000	6.700 6.000000E+00
6256.000	6261.000	3.360	13.000	6.700 6.000000E+00
6261.000	6266.000	3.360	13.000	6.700 6.000000E+00
6266.000	6271.000	3.360	13.000	6.700 6.000000E+00
6271.000	6276.000	3.360	13.000	6.700 6.000000E+00
6276.000	6286.000	3.360	13.000	6.700 6.000000E+00
6286.000	6291.000	3.360	13.000	6.700 6.000000E+00
6291.000	6296.000	3.360	13.000	6.700 6.000000E+00
6296.000	6301.000	3.380	13.100	6.820 0.100000E+12
6301.000	6306.000	3.380	13.100	6.820 0.100000E+12
6306.000	6316.000	3.380	13.100	6.820 0.100000E+12
6316.000	6326.000	3.380	13.100	6.820 0.100000E+12
6326.000	6331.000	3.380	13.100	6.820 0.100000E+12
6331.000	6336.000	3.380	13.100	6.820 0.100000E+12
6336.000	6346.600	3.380	13.100	6.820 0.100000E+12
6346.600	6351.000	2.900	7.530	4.410 0.100000E+12
6351.000	6356.000	2.900	7.500	4.410 0.100000E+12
6356.000	6359.000	2.900	5.200	2.660 0.100000E+12
6359.000	6363.000	2.600	5.200	2.660 0.100000E+12
6363.000	6369.000	2.600	4.875	2.490 0.100000E+12
6369.000	6371.000	2.600	4.875	2.490 0.100000E+12

2. Banerjee model

94 2 6371.000 2.214

3480.000	3481.000	5.566	44.000	21.910	8.000000E+02
3481.000	3500.000	5.536	44.000	21.910	8.000000E+02
3500.000	3600.000	5.506	44.000	21.910	8.000000E+02
3600.000	3700.000	5.497	44.000	21.910	8.000000E+02
3700.000	3800.000	5.491	44.000	21.910	8.000000E+02
3800.000	3900.000	5.357	44.000	21.910	8.000000E+02
3900.000	4000.000	5.307	44.000	21.910	8.000000E+02
4000.000	4100.000	5.257	44.000	21.910	8.000000E+02
4100.000	4200.000	5.207	44.000	21.910	8.000000E+02
4200.000	4300.000	5.156	44.000	21.910	8.000000E+02
4300.000	4400.000	5.105	44.000	21.910	8.000000E+02
4400.000	4500.000	5.054	44.000	21.910	8.000000E+02
4500.000	4600.000	5.003	44.000	21.910	8.000000E+02
4600.000	4700.000	4.950	44.000	21.910	8.000000E+02
4700.000	4800.000	4.897	44.000	21.910	8.000000E+02
4800.000	4900.000	4.843	44.000	21.910	8.000000E+02
4900.000	5000.000	4.789	44.000	21.910	8.000000E+02
5000.000	5100.000	4.733	44.000	21.910	8.000000E+02
5100.000	5200.000	4.678	44.000	21.910	8.000000E+02
5200.000	5319.100	4.670	44.000	21.910	8.000000E+02
5319.100	5353.700	4.635	44.000	21.910	8.000000E+02
5353.700	5388.300	4.611	44.000	21.910	8.000000E+02
5388.300	5422.900	4.587	44.000	21.910	8.000000E+02
5422.900	5457.600	4.563	44.000	21.910	8.000000E+02
5457.600	5492.200	4.539	44.000	21.910	8.000000E+02
5492.200	5526.800	4.515	44.000	21.910	8.000000E+02
5526.800	5561.500	4.491	44.000	21.910	8.000000E+02
5561.500	5596.100	4.467	44.000	21.910	8.000000E+02
5596.100	5630.700	4.443	44.000	21.910	8.000000E+02
5630.700	5665.400	4.443	44.000	21.910	8.000000E+02
5665.400	5711.000	4.380	44.000	21.910	8.000000E+02
5711.000	5731.300	3.992	19.000	9.800	1.000000E+01
5731.300	5771.000	3.983	19.000	9.800	1.000000E+01

5771.000	5793.800	3.975	19.000	9.800 1.000000E+01
5793.800	5825.000	3.931	19.000	9.800 1.000000E+01
5825.000	5856.300	3.890	19.000	9.800 1.000000E+01
5856.300	5887.500	3.849	19.000	9.800 1.000000E+01
5887.500	5918.700	3.764	19.000	9.800 1.000000E+01
5918.700	5950.000	3.743	19.000	9.800 1.000000E+01
5950.000	5971.000	3.723	19.000	9.800 1.000000E+01
5971.000	6001.200	3.543	19.000	9.800 1.000000E+01
6001.200	6021.200	3.543	19.000	9.800 1.000000E+01
6021.200	6026.900	3.543	19.000	9.800 1.000000E+01
6026.900	6052.500	3.490	19.000	9.800 1.000000E+01
6052.500	6078.100	3.490	19.000	9.800 1.000000E+01
6078.100	6103.800	3.435	19.000	9.800 1.000000E+01
6103.800	6121.000	3.435	19.000	9.800 1.000000E+01
6121.000	6126.000	3.435	19.000	9.800 1.000000E+01
6126.000	6131.000	3.435	19.000	9.800 1.000000E+01
6131.000	6136.000	3.435	19.000	9.800 1.000000E+01
6136.000	6141.000	3.435	19.000	9.800 1.000000E+01
6141.000	6146.000	3.435	19.000	9.800 1.000000E+01
6146.000	6151.000	3.435	19.000	9.800 1.000000E+01
6151.000	6156.000	3.360	13.000	6.700 1.000000E+01
6156.000	6161.000	3.360	13.000	6.700 1.000000E+01
6161.000	6166.000	3.360	13.000	6.700 1.000000E+01
6166.000	6171.000	3.360	13.000	6.700 1.000000E+01
6171.000	6176.000	3.360	13.000	6.700 1.000000E+01
6176.000	6181.000	3.360	13.000	6.700 1.000000E+01
6181.000	6186.000	3.360	13.000	6.700 1.000000E+01
6186.000	6191.000	3.360	13.000	6.700 1.000000E+01
6191.000	6196.000	3.360	13.000	6.700 1.000000E+01
6196.000	6201.000	3.360	13.000	6.700 1.000000E+01
6201.000	6206.000	3.360	13.000	6.700 1.000000E+01
6206.000	6211.000	3.360	13.000	6.700 1.000000E+01
6211.000	6216.000	3.360	13.000	6.700 1.000000E+01
6216.000	6221.000	3.360	13.000	6.700 1.000000E+01
6221.000	6226.000	3.360	13.000	6.700 1.000000E+01
6226.000	6230.000	3.360	13.000	6.700 1.000000E+01

6230.000 6236.000	3.360	13.000	6.700	1.000000E+01
6236.000 6241.000	3.360	13.000	6.700	1.000000E+01
6241.000 6246.000	3.360	13.000	6.700	1.000000E+01
6246.000 6251.000	3.360	13.000	6.700	1.000000E+01
6251.000 6256.000	3.360	13.000	6.700	1.000000E+01
6256.000 6261.000	3.360	13.000	6.700	1.000000E+01
6261.000 6266.000	3.360	13.000	6.700	1.000000E+01
6266.000 6271.000	3.360	13.000	6.700	1.000000E+01
6271.000 6276.000	3.360	13.000	6.700	1.000000E+01
6276.000 6286.000	3.360	13.000	6.700	1.000000E+01
6286.000 6291.000	3.360	13.000	6.700	1.000000E+01
6291.000 6296.000	3.360	13.000	6.700	1.000000E+01
6296.000 6301.000	3.360	13.000	6.700	1.000000E+01
6301.000 6306.000	3.380	13.100	6.820	0.100000E+12
6306.000 6316.000	3.380	13.100	6.820	0.100000E+12
6316.000 6326.000	3.380	13.100	6.820	0.100000E+12
6326.000 6331.000	3.380	13.100	6.820	0.100000E+12
6331.000 6336.000	3.380	13.100	6.820	0.100000E+12
6336.000 6346.600	3.380	13.100	6.820	0.100000E+12
6346.600 6351.000	2.900	7.530	4.410	0.100000E+12
6351.000 6356.000	2.900	7.500	4.410	0.100000E+12
6356.000 6359.000	2.900	5.200	2.660	0.100000E+12
6359.000 6363.000	2.600	5.200	2.660	0.100000E+12
6363.000 6369.000	2.600	4.875	2.490	0.100000E+12
6369.000 6371.000	2.600	4.875	2.490	0.100000E+12

3. Fujii model

94 2 6371.000 2.214

3480.000 3481.000	5.566	44.000	21.910	8.000000E+02
3481.000 3500.000	5.536	44.000	21.910	8.000000E+02
3500.000 3600.000	5.506	44.000	21.910	8.000000E+02
3600.000 3700.000	5.497	44.000	21.910	8.000000E+02
3700.000 3800.000	5.491	44.000	21.910	8.000000E+02
3800.000 3900.000	5.357	44.000	21.910	8.000000E+02

3900.000	4000.000	5.307	44.000	21.910 8.000000E+02
4000.000	4100.000	5.257	44.000	21.910 8.000000E+02
4100.000	4200.000	5.207	44.000	21.910 8.000000E+02
4200.000	4300.000	5.156	44.000	21.910 8.000000E+02
4300.000	4400.000	5.105	44.000	21.910 8.000000E+02
4400.000	4500.000	5.054	44.000	21.910 8.000000E+02
4500.000	4600.000	5.003	44.000	21.910 8.000000E+02
4600.000	4700.000	4.950	44.000	21.910 8.000000E+02
4700.000	4800.000	4.897	44.000	21.910 8.000000E+02
4800.000	4900.000	4.843	44.000	21.910 8.000000E+02
4900.000	5000.000	4.789	44.000	21.910 8.000000E+02
5000.000	5100.000	4.733	44.000	21.910 8.000000E+02
5100.000	5200.000	4.678	44.000	21.910 8.000000E+02
5200.000	5319.100	4.670	44.000	21.910 8.000000E+02
5319.100	5353.700	4.635	44.000	21.910 8.000000E+02
5353.700	5388.300	4.611	44.000	21.910 8.000000E+02
5388.300	5422.900	4.587	44.000	21.910 8.000000E+02
5422.900	5457.600	4.563	44.000	21.910 8.000000E+02
5457.600	5492.200	4.539	44.000	21.910 8.000000E+02
5492.200	5526.800	4.515	44.000	21.910 8.000000E+02
5526.800	5561.500	4.491	44.000	21.910 8.000000E+02
5561.500	5596.100	4.467	44.000	21.910 8.000000E+02
5596.100	5630.700	4.443	44.000	21.910 8.000000E+02
5630.700	5665.400	4.443	44.000	21.910 8.000000E+02
5665.400	5711.000	4.380	44.000	21.910 8.000000E+02
5711.000	5731.300	3.992	19.000	9.800 4.000000E+00
5731.300	5771.000	3.983	19.000	9.800 4.000000E+00
5771.000	5793.800	3.975	19.000	9.800 4.000000E+00
5793.800	5825.000	3.931	19.000	9.800 4.000000E+00
5825.000	5856.300	3.890	19.000	9.800 4.000000E+00
5856.300	5887.500	3.849	19.000	9.800 4.000000E+00
5887.500	5918.700	3.764	19.000	9.800 4.000000E+00
5918.700	5950.000	3.743	19.000	9.800 4.000000E+00
5950.000	5971.000	3.723	19.000	9.800 4.000000E+00
5971.000	6001.200	3.543	19.000	9.800 4.000000E+00
6001.200	6021.200	3.543	19.000	9.800 4.000000E+00

6021.200	6026.900	3.543	19.000	9.800 4.000000E+00
6026.900	6052.500	3.490	19.000	9.800 4.000000E+00
6052.500	6078.100	3.490	19.000	9.800 4.000000E+00
6078.100	6103.800	3.435	19.000	9.800 4.000000E+00
6103.800	6121.000	3.435	19.000	9.800 4.000000E+00
6121.000	6126.000	3.435	19.000	9.800 4.000000E+00
6126.000	6131.000	3.435	19.000	9.800 4.000000E+00
6131.000	6136.000	3.435	19.000	9.800 4.000000E+00
6136.000	6141.000	3.435	19.000	9.800 4.000000E+00
6141.000	6146.000	3.435	19.000	9.800 4.000000E+00
6146.000	6151.000	3.435	19.000	9.800 4.000000E+00
6151.000	6156.000	3.360	13.000	6.700 4.000000E+00
6156.000	6161.000	3.360	13.000	6.700 4.000000E+00
6161.000	6166.000	3.360	13.000	6.700 4.000000E+00
6166.000	6171.000	3.360	13.000	6.700 4.000000E+00
6171.000	6176.000	3.360	13.000	6.700 4.000000E+00
6176.000	6181.000	3.360	13.000	6.700 4.000000E+00
6181.000	6186.000	3.360	13.000	6.700 4.000000E+00
6186.000	6191.000	3.360	13.000	6.700 4.000000E+00
6191.000	6196.000	3.360	13.000	6.700 4.000000E+00
6196.000	6201.000	3.360	13.000	6.700 4.000000E+00
6201.000	6206.000	3.360	13.000	6.700 4.000000E+00
6206.000	6211.000	3.360	13.000	6.700 4.000000E+00
6211.000	6216.000	3.360	13.000	6.700 4.000000E+00
6216.000	6221.000	3.360	13.000	6.700 4.000000E+00
6221.000	6226.000	3.360	13.000	6.700 4.000000E+00
6226.000	6230.000	3.360	13.000	6.700 4.000000E+00
6230.000	6236.000	3.360	13.000	6.700 4.000000E+00
6236.000	6241.000	3.360	13.000	6.700 4.000000E+00
6241.000	6246.000	3.360	13.000	6.700 4.000000E+00
6246.000	6251.000	3.360	13.000	6.700 4.000000E+00
6251.000	6256.000	3.360	13.000	6.700 4.000000E+00
6256.000	6261.000	3.360	13.000	6.700 4.000000E+00
6261.000	6266.000	3.360	13.000	6.700 4.000000E+00
6266.000	6271.000	3.360	13.000	6.700 4.000000E+00
6271.000	6276.000	3.360	13.000	6.700 4.000000E+00

6276.000	6286.000	3.360	13.000	6.700	4.000000E+00
6286.000	6291.000	3.360	13.000	6.700	4.000000E+00
6291.000	6296.000	3.360	13.000	6.700	4.000000E+00
6296.000	6301.000	3.360	13.000	6.700	4.000000E+00
6301.000	6311.000	3.360	13.000	6.700	4.000000E+00
6311.000	6316.000	3.360	13.000	6.700	4.000000E+00
6316.000	6326.000	3.360	13.000	6.700	4.000000E+00
6326.000	6331.000	3.380	13.100	6.820	0.100000E+12
6331.000	6336.000	3.380	13.100	6.820	0.100000E+12
6336.000	6346.600	3.380	13.100	6.820	0.100000E+12
6346.600	6351.000	2.900	7.530	4.410	0.100000E+12
6351.000	6356.000	2.900	7.500	4.410	0.100000E+12
6356.000	6359.000	2.900	5.200	2.660	0.100000E+12
6359.000	6363.000	2.600	5.200	2.660	0.100000E+12
6363.000	6369.000	2.600	4.875	2.490	0.100000E+12
6369.000	6371.000	2.600	4.875	2.490	0.100000E+12

4. Rhie model

94 2 6371.000 2.214

3480.000	3481.000	5.566	44.000	21.910	8.000000E+02
3481.000	3500.000	5.536	44.000	21.910	8.000000E+02
3500.000	3600.000	5.506	44.000	21.910	8.000000E+02
3600.000	3700.000	5.497	44.000	21.910	8.000000E+02
3700.000	3800.000	5.491	44.000	21.910	8.000000E+02
3800.000	3900.000	5.357	44.000	21.910	8.000000E+02
3900.000	4000.000	5.307	44.000	21.910	8.000000E+02
4000.000	4100.000	5.257	44.000	21.910	8.000000E+02
4100.000	4200.000	5.207	44.000	21.910	8.000000E+02
4200.000	4300.000	5.156	44.000	21.910	8.000000E+02
4300.000	4400.000	5.105	44.000	21.910	8.000000E+02
4400.000	4500.000	5.054	44.000	21.910	8.000000E+02
4500.000	4600.000	5.003	44.000	21.910	8.000000E+02
4600.000	4700.000	4.950	44.000	21.910	8.000000E+02
4700.000	4800.000	4.897	44.000	21.910	8.000000E+02

4800.000	4900.000	4.843	44.000	21.910 8.000000E+02
4900.000	5000.000	4.789	44.000	21.910 8.000000E+02
5000.000	5100.000	4.733	44.000	21.910 8.000000E+02
5100.000	5200.000	4.678	44.000	21.910 8.000000E+02
5200.000	5319.100	4.670	44.000	21.910 8.000000E+02
5319.100	5353.700	4.635	44.000	21.910 8.000000E+02
5353.700	5388.300	4.611	44.000	21.910 8.000000E+02
5388.300	5422.900	4.587	44.000	21.910 8.000000E+02
5422.900	5457.600	4.563	44.000	21.910 8.000000E+02
5457.600	5492.200	4.539	44.000	21.910 8.000000E+02
5492.200	5526.800	4.515	44.000	21.910 8.000000E+02
5526.800	5561.500	4.491	44.000	21.910 8.000000E+02
5561.500	5596.100	4.467	44.000	21.910 8.000000E+02
5596.100	5630.700	4.443	44.000	21.910 8.000000E+02
5630.700	5665.400	4.443	44.000	21.910 8.000000E+02
5665.400	5711.000	4.380	44.000	21.910 8.000000E+02
5711.000	5731.300	3.992	19.000	9.800 8.000000E+00
5731.300	5771.000	3.983	19.000	9.800 8.000000E+00
5771.000	5793.800	3.975	19.000	9.800 8.000000E+00
5793.800	5825.000	3.931	19.000	9.800 8.000000E+00
5825.000	5856.300	3.890	19.000	9.800 8.000000E+00
5856.300	5887.500	3.849	19.000	9.800 8.000000E+00
5887.500	5918.700	3.764	19.000	9.800 8.000000E+00
5918.700	5950.000	3.743	19.000	9.800 8.000000E+00
5950.000	5971.000	3.723	19.000	9.800 8.000000E+00
5971.000	6001.200	3.543	19.000	9.800 8.000000E+00
6001.200	6021.200	3.543	19.000	9.800 8.000000E+00
6021.200	6026.900	3.543	19.000	9.800 8.000000E+00
6026.900	6052.500	3.490	19.000	9.800 8.000000E+00
6052.500	6078.100	3.490	19.000	9.800 8.000000E+00
6078.100	6103.800	3.435	19.000	9.800 8.000000E+00
6103.800	6121.000	3.435	19.000	9.800 8.000000E+00
6121.000	6126.000	3.435	19.000	9.800 8.000000E+00
6126.000	6131.000	3.435	19.000	9.800 8.000000E+00
6131.000	6136.000	3.435	19.000	9.800 8.000000E+00
6136.000	6141.000	3.435	19.000	9.800 8.000000E+00

6141.000	6146.000	3.435	19.000	9.800 8.000000E+00
6146.000	6151.000	3.435	19.000	9.800 8.000000E+00
6151.000	6156.000	3.360	13.000	6.700 8.000000E+00
6156.000	6161.000	3.360	13.000	6.700 8.000000E+00
6161.000	6166.000	3.360	13.000	6.700 8.000000E+00
6166.000	6171.000	3.360	13.000	6.700 8.000000E+00
6171.000	6176.000	3.360	13.000	6.700 8.000000E+00
6176.000	6181.000	3.360	13.000	6.700 8.000000E+00
6181.000	6186.000	3.360	13.000	6.700 8.000000E+00
6186.000	6191.000	3.360	13.000	6.700 8.000000E+00
6191.000	6196.000	3.360	13.000	6.700 8.000000E+00
6196.000	6201.000	3.360	13.000	6.700 8.000000E+00
6201.000	6206.000	3.360	13.000	6.700 8.000000E+00
6206.000	6211.000	3.360	13.000	6.700 8.000000E+00
6211.000	6216.000	3.360	13.000	6.700 8.000000E+00
6216.000	6221.000	3.360	13.000	6.700 8.000000E+00
6221.000	6226.000	3.360	13.000	6.700 8.000000E+00
6226.000	6230.000	3.360	13.000	6.700 8.000000E+00
6230.000	6236.000	3.360	13.000	6.700 8.000000E+00
6236.000	6241.000	3.360	13.000	6.700 8.000000E+00
6241.000	6246.000	3.360	13.000	6.700 8.000000E+00
6246.000	6251.000	3.360	13.000	6.700 8.000000E+00
6251.000	6256.000	3.360	13.000	6.700 8.000000E+00
6256.000	6261.000	3.360	13.000	6.700 8.000000E+00
6261.000	6266.000	3.360	13.000	6.700 8.000000E+00
6266.000	6271.000	3.360	13.000	6.700 8.000000E+00
6271.000	6276.000	3.360	13.000	6.700 8.000000E+00
6276.000	6286.000	3.360	13.000	6.700 8.000000E+00
6286.000	6291.000	3.360	13.000	6.700 8.000000E+00
6291.000	6296.000	3.360	13.000	6.700 8.000000E+00
6296.000	6301.000	3.360	13.000	6.700 8.000000E+00
6301.000	6306.000	3.360	13.000	6.700 8.000000E+00
6306.000	6316.000	3.380	13.100	6.820 0.100000E+12
6316.000	6326.000	3.380	13.100	6.820 0.100000E+12
6326.000	6331.000	3.380	13.100	6.820 0.100000E+12
6331.000	6336.000	3.380	13.100	6.820 0.100000E+12

6336.000	6346.600	3.380	13.100	6.820 0.100000E+12
6346.600	6351.000	2.900	7.530	4.410 0.100000E+12
6351.000	6356.000	2.900	7.500	4.410 0.100000E+12
6356.000	6359.000	2.900	5.200	2.660 0.100000E+12
6359.000	6363.000	2.600	5.200	2.660 0.100000E+12
6363.000	6369.000	2.600	4.875	2.490 0.100000E+12
6369.000	6371.000	2.600	4.875	2.490 0.100000E+12

Appendix C

Chi-square Distribution Table

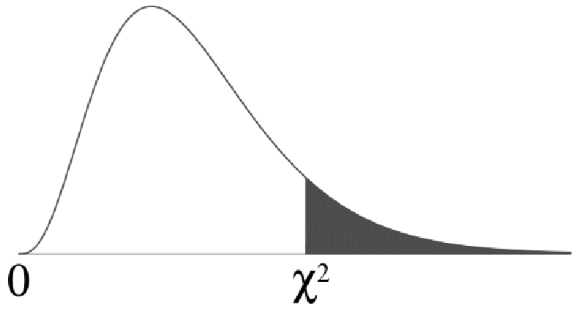

The shaded area is the right tail probability, that is the area under chi-square distribution from the chi-square value to positive infinity (χ^2_α).

dof	$\chi^2_{.010}$
1	6.635
10	23.209
20	37.566
30	50.892
40	63.691
50	76.154
60	88.379

dof	$\chi^2_{.010}$
70	100.425
71	101.621
72	102.816
73	104.009
74	105.202
75	106.393
76	107.582

dof	$\chi^2_{.010}$
77	108.771
78	109.958
79	111.144
80	112.329
90	124.116
100	135.807